MOLECULAR LASERS IN E-BEAM STABILIZED DISCHARGES

S. R. Byron, et al

Mathematical Sciences Northwest, Incorporated

Prepared for:

Office of Naval Research
Advanced Research Projects Agency

February 1975

SECURITY CLASSIFICATION OF THIS PAGE (When Data Entered)

REPORT DOCUMENTATION PAGE

READ INSTRUCTIONS BEFORE COMPLETING FORM

1. REPORT NUMBER: 75-105-4	2. GOVT ACCESSION NO.
3. RECIPIENT'S CATALOG NUMBER: AD-A007 577	
4. TITLE (and Subtitle): MOLECULAR LASERS IN E-BEAM STABILIZED DISCHARGES	5. TYPE OF REPORT & PERIOD COVERED: Final Report 15 March 1972- 30 June 1974
	6. PERFORMING ORG. REPORT NUMBER
7. AUTHOR(s): S. R. Byron, L. Y. Nelson, C. H. Fisher, G. J. Mullaney, and A. L. Pindroh	8. CONTRACT OR GRANT NUMBER(s): N00014-72-C-0430
9. PERFORMING ORGANIZATION NAME AND ADDRESS: Mathematical Sciences Northwest, Inc. P. O. Box 1887 Bellevue, Washington, 98009	10. PROGRAM ELEMENT, PROJECT, TASK AREA & WORK UNIT NUMBERS
11. CONTROLLING OFFICE NAME AND ADDRESS: Office of Naval Research 800 North Quinch Street Arlington, VA 22217	12. REPORT DATE: February 1975
	13. NUMBER OF PAGES: 182
14. MONITORING AGENCY NAME & ADDRESS (if different from Controlling Office)	15. SECURITY CLASS (of this report): UNCLASSIFIED
	15a. DECLASSIFICATION/DOWNGRADING SCHEDULE

16. DISTRIBUTION STATEMENT (of this Report)

17. DISTRIBUTION STATEMENT (of the abstract entered in Block 20, if different from Report)

18. SUPPLEMENTARY NOTES

19. KEY WORDS (Continue on reverse side if necessary and identify by block number)

HF/DF Lasers
Electron Beam
Electronic State Lasers
N_2 Visible Lasers

20. ABSTRACT (Continue on reverse side if necessary and identify by block number)

This report describes the results of a 2-year program directed toward the development of new lasers in the infrared and visible regions of the spectrum, utilizing electron-beam-stabilized electric discharge excitation. The program covered two major areas of investigation:

1. Direct electric discharge excitation of the vibrational levels of HF and DF to provide laser emission over the spectral range from 2.8 to 3.1 μm and 3.8 to 4.1 μm, respectively.

DD FORM 1 JAN 73 1473 EDITION OF 1 NOV 65 IS OBSOLETE

UNCLASSIFIED

SECURITY CLASSIFICATION OF THIS PAGE (When Data Entered)

Block 20. Abstract (continued)

2. Direct electric discharge excitation of electronic states of stable molecules such as N_2 to produce long pulse, visible or ultraviolet laser emission.

An additional task was carried out early in this program to evaluate the possibility of generating long duration, high energy density infrared laser pulses on various molecules, particularly CO_2.

Under this program, the first laboratory observations of laser emission from HF and DF excited directly by an electric discharge were made. The effectiveness of vibrational transfer from H_2 and D_2 to HF and DF, respectively, was also verified experimentally. A quantitative model of the kinetics of the electric discharge and the vibrational populations of H_2 and HF was formulated for $Ar/H_2/HF$ mixtures and found to predict a laser power output that is a factor of 10 to 100 greater than the observed output. The discrepancy indicates that some aspects of the kinetics of this molecular system have not yet been determined, such as intermolecular V-V processes, rotational non-equilibrium, and superelastic collisions with electrons.

During this program a model for long pulse visible laser emission from electronically excited molecules was formulated that involves rapid collisional quenching of the vibrational energy of the electronic states. The application of this approach to N_2 electric discharge lasers was explored through fluorecence emission studies of the $N_2(C^3\pi_u)$ and $N_2(B^3\pi_g)$ states. In these measurements the effect of the energy pooling reaction, $2\ N_2(A^3\Sigma_u^+) \rightarrow N_2(X^1\Sigma_g^+) + N_2(\text{upper excited state})$ was studied. The effect of various additives such as He, Ar, SF_6, and C_2H_6 on the populations of several vibrational levels of each of these excited states was investigated.

MSNW Report No. 75-105-4

MOLECULAR LASERS IN E-BEAM STABILIZED DISCHARGES

Final Report

Covering Work Performed During the Period
15 March 1972 through 30 June 1974

By

S. R. Byron, L. Y. Nelson, C. H. Fisher,
G. J. Mullaney, and A. L. Pindroh

Mathematical Sciences Northwest, Inc.
P. O. Box 1887
Bellevue, Washington 98009

February 1975

Contract N00014-72-C-0430

Sponsored by

Advanced Research Projects Agency
ARPA Order No. 1807

Monitored by

Office of Naval Research
Code 421

ARPA ORDER NO.:	1807
PROGRAM CODE:	2E90
NAME OF CONTRACTOR:	Mathematical Sciences Northwest, Inc.
EFFECTIVE DATE OF CONTRACT:	15 March 1972 through 2 March 1975
CONTRACT AMOUNT:	$535,567
CONTRACT NUMBER:	N00014-72-C-0430
PRINCIPAL INVESTIGATOR:	Dr. S. R. Byron (206)827-0460
SCIENTIFIC OFFICER:	Director, Physics Programs Physical Sciences Division Office of Naval Research Department of the Navy 800 North Quincy Street Arlington, Virginia 22217
DISCLAIMER:	The views and conclusions contained in this document are those of the authors and should not be interpreted as necessarily representing the official policies, either expressed or implied, of the Advanced Research Projects Agency or the U. S. Government.

ABSTRACT

This report describes the results of a 2-year program directed toward the development of new lasers in the infrared and visible regions of the spectrum, utilizing electron-beam-stabilized electric discharge excitation. The program covered two major areas of investigation:

1. Direct electric discharge excitation of the vibrational levels of HF and DF to provide laser emission over the spectral range from 2.8 to 3.1 μm and 3.8 to 4.1 μm, respectively.
2. Direct electric discharge excitation of electronic states of stable molecules such as N_2 to produce long pulse, visible or ultraviolet laser emission.

An additional task was carried out early in this program to evaluate the possibility of generating long duration, high energy density infrared laser pulses on various molecules, particularly CO_2.

Under this program, the first laboratory observations of laser emission from HF and DF excited directly by an electric discharge were made. The effectiveness of vibrational transfer from H_2 and D_2 to HF and DF, respectively, was also verified experimentally. A quantitative model of the kinetics of the electric discharge and the vibrational populations of H_2 and HF was formulated for $Ar/H_2/HF$ mixtures and found to predict a laser power output that is a factor of 10 to 100 greater than the observed output. The discrepancy indicates that some aspects of the kinetics of this molecular system have not yet been determined, such as

intermolecular V-V processes, rotational non-equilibrium, and super-elastic collisions with electrons.

During this program a model for long pulse visible laser emission from electronically excited molecules was formulated that involves rapid collisional quenching of the vibrational energy of the electronic states. The application of this approach to N_2 electric discharge lasers was explored through fluorescence emission studies of the $N_2(C^3\pi_u)$ and $N_2(B^3\pi_g)$ states. In these measurements the effect of the energy pooling reaction, $2\ N_2(A^3\Sigma_u^+) \rightarrow N_2(X^1\Sigma_g^+) + N_2$(upper excited state) was studied. The effect of various additives such as He, Ar, SF_6, and C_2H_6 on the populations of several vibrational levels of each of these excited states was investigated.

TABLE OF CONTENTS

SECTION		PAGE
I	INTRODUCTION	1
II	HF AND DF ELECTRIC DISCHARGE LASER TECHNOLOGY	5
	2.1. Laser Concept	5
	2.2. Analytical Model of Electrical Excitation Processes	11
	2.3. Analytical Model of Molecular Transfer and Loss Processes	23
	2.4. HF and DF Laser Emission Measurements	42
	2.5. HF Probe Laser Absorption and Gain Measurements	75
	2.6. Comparison of Computer Model with HF Laser Measurements	87
III	ELECTRONIC STATES LASER TECHNOLOGY	103
	3.1. Summary	103
	3.2. Electronic State Kinetic Processes	106
	3.3. Electronic State Fluorescence Measurements	112
	3.4. Laser Cavity Studies	143
IV	CONCLUSIONS AND RECOMMENDATIONS	147
	4.1. HF and DF Electric Discharge Lasers	147
	4.2. Molecular Electronic State Lasers	148
APPENDIX		
A	E-BEAM STABILIZED ELECTRIC DISCHARGE FACILITIES	150
	A.1. Thermionic Cathode Electron Gun	150
	A.2. Five-Tube Plasma Diode Electron Gun	150
	A.3. Ceramic Plasma Diode Electron Gun	157
	REFERENCES	165

LIST OF TABLES

TABLE		PAGE
I	Spectroscopic Constants for Several Candidate Partial Inversion Infrared Laser Molecules	6
II	Summary of H_2/HF V-V, V-T, and R-T Rate Data from the Literature	28
III	Summary of Additional, Assumed Rates for the H_2/HF Kinetic Model	29
IV	Frequency Shift of HF Lines by HF and Ar Collisions	31
V	Electron Attachment Rate Coefficients Obtained from Discharge Current Measurements in HF Gas Mixtures at 200 Torr	51
VI	Spectroscopic Measurements of Chemical Laser Emission in Ar/H_2/SF_6 Mixtures	56
VII	Time Resolved Spectroscopic Measurements of the Vibration Rotation Lines Observed in HF and DF Electric Discharge Lasers	58
VIII	Time Resolved Spectroscopic Measurements of the Vibration Rotation Lines Observed in HF Electric Discharges in the New Ceramic Plasma Diode Electron Gun	69
IX	Summary of Collisional Quenching Data (cm^3/sec) for N_2 and CO Electronic States by Various Molecules	111
X	Locations of Peak Superfluorescence in N_2 and H_2	116

LIST OF FIGURES

FIGURE		PAGE
1	Inelastic Cross-Sections for Electron Impact with Hydrogen	9
2	Momentum Transfer Cross Sections for H_2 and Argon	13
3	Inelastic Cross Sections for H_2 and Ar	14
4	Comparison of Analytical and Experimental Dependence of Electron Transport Properties on E/N for Pure H_2	16
5	Comparison of Analytical and Experimental Dependence of Electron Transport Properties on E/N for Pure Argon	17
6	Computed Electron Distribution Function	18
7	Comparison of Analytical and Experimental Dependence of Electron Transport Properties on E/N for a 10/90 H_2/Ar Mixture	20
8	Distribution of Electrical Power in 10/90 Hydrogen/Argon Mixtures	21
9	Vibrational Dependence of V-T and V-V Rates of HF in HF/HF Collisions	27
10	HF Lorentz Broadening	30
11	Effect on Probe Laser Measurements Caused by HF Line Shift Due to Argon Collisions	33
12	Computed HF Optical Gain Versus Time During a 20 μsec Electric Discharge Excitation Pulse	34
13	Computed Populations of HF Vibrational Levels Versus Time During a 20 μsec Electric Discharge Excitation Pulse	36

FIGURE		PAGE
14	Computed HF Optical Gain Versus Time During a 20 μsec Electric Discharge Excitation Pulse in a 0.15 Percent HF Mixture	37
15	Computed HF Optical Gain Versus Time During a 20 μsec Electric Discharge Excitation Pulse in a 0.4 Percent HF Mixture	38
16	Computed HF Optical Gain Versus Time as a Function of Direct Electron Impact Excitation of HF Vibration	40
17	Computed Peak Laser Power Output Versus Power Input for Several HF Laser Gas Mixtures	41
18	Computed Peak Laser Efficiency Versus Power Input	43
19	Schematic of Plasma Diode Electron-Beam Stabilized Electric Discharge Cell and Laser Cavity	44
20	Schematic Diagram of Gas Handling System as First Used on the Thermionic E-Beam Facility	46
21	Block Diagram of the Electric Circuitry Used with the Plasma Diode Electron-Gun and Electrical Discharge Cell	49
22	HF Laser Emission on All Lines from $Ar/H_2/SF_6$ Gas Mixtures at 200 Torr Pumped Directly by External Electron Beam Excitation Alone (Time Scale - 20 μsec/div)	55
23	Electric Discharge Excitation of HF Laser Emission in Mixtures of (a) 0.99 Ar and 0.004 HF, and (b) 0.89 Ar, 0.10 H_2, and 0.004 HF. The Discharge Voltage Sensitivity is 700 V/Div and the Discharge Current Sensitivity is 1380 A/Div	60
24	Range of Population Ratios for $v = 1 \rightarrow 0$ Gain to be at a Maximum on P(9)	62
25	HF Laser Cavity Intensity in Ar/N_2 and $Ar/He/N_2$ Mixtures at 200 Torr, Using 0.4 Percent HF	64

FIGURE		PAGE
26	Effect of Helium Diluent on HF Laser Emission at 200 Torr and E/N = 0.7 to 1.0 x 10^{-16} V-cm^2	65
27	Time Sequence of Laser Emission from Ar/D_2/DF Mixtures at 200 Torr. The Discharge Voltage Sensitivity is 700 V/Div and the Discharge Current Sensitivity is 1380 A/Div	67
28	Output Power Measured in the Five-Tube and Ceramic Plasma Diode Devices for Ar/H_2/HF (94.8/5/0.15) Mixtures at 200 Torr Pressure	72
29	Output Power Measured for an Ar/H_2/HF (89.8/10/0.15) Mixture in the Continuous, Ceramic Plasma Diode Apparatus	73
30	Output Power Measured for Ar/N_2/HF (89.8/10/0.2) Mixtures in the Five-Tube Plasma Diode Apparatus	74
31	Optical Arrangement Used for HF Probe Laser Absorption and Gain Measurements	76
32	Optical Arrangement Used for the Gain and Absorption Measurements Made with the Continuous, Ceramic Plasma Diode Electron Beam. Two Infrared Detectors Provide a Reference and Signal Channel which Eliminates Problems Encountered in Single Channel Experiments Due to Fluctuations in the Pin Laser Output	78
33	Probe Laser Measurements of HF Absorption in the 5-Tube Plasma Diode Facility for 89/10/0.3 Ar/H_2/HF Mixtures at 200 Torr, using a Power Input of 1.6 kW/cm^3 for 30 μsec at an E/N of 0.43 x 10^{-16} V-cm^2	82
34	Comparison of Probe Laser Measurements on the 2 → 1 P(6) Line Through Gas Samples With and Without HF	84
35	Probe Laser Measurements of HF Absorption in the Ceramic Plasma Diode Facility	86

FIGURE		PAGE
36	Probe Laser Measurements for a 50 μsec Discharge Pulse in 89/10/0.4 $Ar/N_2/HF$ Mixtures at 200 Torr and a Power Input of 2 kW/cm^3 and an E/N of 0.36×10^{-16} V-cm^2	89
37	Measured HF Fraction in v = 1 and v = 2 in 89/10/0.4 $Ar/N_2/HF$ Mixtures at 200 Torr for a Power Input of 2 kW/cm^3, a Pulse Duration of 30 μsec, and an E/N of 0.36×10^{-16} V-cm^2	90
38	Computer Model Calculations of Optical Gain or Absorption on the 2 → 1 P(7) Transition of HF in 89/10/0.4 Mixtures of $Ar/N_2/HF$ at 200 Torr for a Power Input of 3 kW/cm^3	92
39	Comparison of Probe Laser Absorption Measurements with Computer Model Results in 89/10/0.3 $Ar/H_2/HF$ Mixtures at 200 Torr and a Power Input of 1.6 kW/cm^3 for 30 μsec at an E/N of 0.43×10^{-16} V-cm^2	94
40	Comparison of Probe Laser Absorption Measurements in the Ceramic Electron Gun Facility with the Computer Model in an 89.85/10/0.15 $Ar/H_2/HF$ Mixture at 200 Torr	97
41	Experimentally Observed Laser Onset Time as a Function of Output Coupling, Compared with Computed Low Signal Gain Versus Time	99
42	Comparison of Theoretical and Experimental Dependence of Maximum Laser Power Output on Power Input	101
43	Collision Dominated Visible Electronic State Laser Concept	105
44	Competing Rate Processes for Collision Dominated Visible Electronic State Molecular Laser	108
45	Superfluorescent Pulses at 3370 Å in a Mixture of 10% N_2, 89% Ar, and 1% HF at 200 Torr Pressure	114
46	Optical-Cavity Emission in the IR from a 10% N_2, 89% Ar, 1% HF Mixture at 200 Torr Pressure	117

FIGURE		PAGE
47	Fluorescence in 10% N_2, 90% Argon with Trace HF.	71
48	Time History of the Nitrogen C → B (3370 Å) and B → A (1.04 μm) Fluorescense Produced a) by the E-Beam and b) by the E-Beam Stabilized Electric Discharge in an 85/15 Ar/N_2 Mixture at 200 Torr Total Pressure	125
49	Time Decay of the 3370 Å and 1μ Emission After the Discharge is Terminated for an 85% Ar/15% N_2 Mixture at 200 Torr Total Pressure	127
50	Plot of the Reciprocal of the Square Root of the N_2 First and Second Positive Intensities Versus Time After the Discharge Crowbar	129
51	Effect of Approximately 0.1% SF_6 Addition on the Discharge Voltage, Discharge Current, and 3370 Å Emission for an 85/15 Ar/N_2 Mixture	132
52	Fluorescence Emission from the v=0 Level of the N_2 $C^3\pi_u$ State.	
53	Comparison of Fluorescence Emission from the v = 0 and v = 1 Levels of the $N_2(C^3\pi_u)$ State in 20/80 N_2/Ar Mixture at 200 Torr	138
54	Comparison of Fluorescence Emission from the v = 0 and v = 1 Levels of the N_2 $C^3\pi_u$ State in a 5:1 He/N_2 Mixture at 200 Torr	140
55	Fluorescence Emission from the v = 0 and v = 1 Levels of the $B^3\pi_g$ State in a 5:1 Ar/N_2 Mixture at 200 Torr	142
A-1	Thermionic Cathode Electron Gun and 0.7 Liter Teflon Discharge Chamber Used for Initial Fluorescence Studies in HF and N_2 and H_2	151
A-2	Schematic of Five Tube Plasma Diode Electron-Beam-Stabilized Electric Discharge Cell and Laser Cavity	153

FIGURE

PAGE

A-3 Typical Electron Beam Voltage and Current Versus Time; Peak Electron Beam Voltage 110 kV; Peak Electron Beam Current Density 100 ma/cm^2 Measured 2 cm from the 0.012-mm Thick Titanium Foil; Helium Pressure was 95 Microns 154

A-4 Peak Electron Beam Current Density at a Distance 2 cm from a 0.012-mm Thick Titanium Foil 155

A-5 Electron Beam Nonuniformities Measured Below the Foil and Screen of the 5-Tube Plasma Diode Electron Gun 158

A-6 Schematic of Single Electrode Ceramic Plasma Diode and Electric Discharge Cell 159

A-7 Oscilloscope Trace Showing Ceramic Plasma Diode Performance 161

A-8 Transverse Current Density Profile in Ceramic Plasma Diode Electron Gun 163

A-9 Current Density Profile in Air Versus Distance from the Foil 164

SECTION I

INTRODUCTION

A major advance in high energy density pulsed gas lasers resulted from the development of large area, high voltage electron beams to stabilize high pressure, large volume electrical discharges (Refs. 1 and 2). This approach was first applied to CO_2 lasers and soon thereafter was extended to cryogenic CO lasers (Ref. 3). At the same time considerable attention was directed toward the development of high power chemical lasers which have been based primarily on reactions that produce HF or DF (Refs. 4 and 5). It was recognized at Mathematical Sciences Northwest that HF and DF molecules could be pumped in an electron-beam-stabilized electrical discharge in much the same way that CO_2 and CO have been and could yield high energy density laser pulses at 2.8 to 3.0 microns and at 3.8 to 4.1 microns. This program was therefore initiated to explore this possibility and led to the first successful demonstration of HF and DF electric discharge lasers, reported in Applied Physics Letters, 23, 565 (1973), (Ref. 6).

There are several advantages of utilizing HF or DF rather than CO_2 or CO as the laser molecule in an electrical discharge laser; there are also several disadvantages. The principal advantage of DF is the high transmission characteristics of the atmosphere at 3.7 to 4.1 microns. In addition, the HF and DF lasers (like the CO laser) are based on a partial inversion and thus have a much higher quantum efficiency limit than CO_2. Furthermore, it should be possible to achieve good laser

than CO_2. Furthermore, it should be possible to achieve good laser performance with DF initially at room temperature because of its large anharmonicity and large rotational spacing; CO on the other hand must be operated at cryogenic temperatures (< 100 °K). The principal disadvantage of HF and DF is the high collisional decay rate of the vibrational energy. A second disadvantage of HF and DF is the possibility of a high electron attachment rate which would require the use of a very high e-beam current. Both of these disadvantages can be overcome in principle by utilizing V-V transfer from H_2 to HF or D_2 to DF in gas mixtures that contain only a few percent HF or DF.

The investigation of HF and DF in this program has centered heavily on the HF molecule for two reasons. First, there are very few suppliers of DF, and the cost is high. Second, the vibrational relaxation processes of HF and H_2 have been investigated much more thoroughly in recent years than have those of DF and D_2. Thus a good correlation between theory and experiment will be achieved earlier with HF and will lead most rapidly to a thorough understanding of the principles involved. However, some exploratory experiments were conducted with DF and are reported here. The results of the analytical and experimental studies of HF and DF electrical discharge laser technology are presented in Section II.

To carry out this program a cooperative effort was established between Mathematical Sciences Northwest, Inc. (MSNW) and Physics International (PI). The laser technology was provided by MSNW, while

PI supplied the thermionic electron gun and power supply, and the electrical discharge power supply and timing circuity (described in Appendix A). The program included a joint effort between MSNW and PI to study the characteristics of electron-beam-stabilized electric discharges, with particular emphasis on high pressure and long pulse duration. The results of the small scale experimental study of high pressure, long duration e-beam stabilized discharges was described in the First Semi-Annual Report (Ref. 7). Late in 1972 the collaboration between MSNW and PI was terminated, and the electron gun and power supplies were purchased by MSNW. The subsequent development of higher current density electron guns based on low pressure, high voltage, plasma diode technology was carried out by MSNW and is described in Appendix A.

Unexpectedly, during the initial experimental studies of HF fluorescence, a series of repetitive pulses was observed in the near infrared region of the spectrum when H_2 or N_2 was present in the gas. Through spectral analysis, it was found that these emission pulses originate from excited electronic states of H_2 or N_2. In the case of N_2 these pulses were identified with the N_2 first positive band, and in the ultraviolet, with the N_2 second positive band. The appearance, magnitude, duration, and repetition rate of these pulses were found to depend critically on the amount of HF in the gas mixture, although only 0.5 to 3 percent HF was used. These results were described in Applied Physics Letters 22, 79 (1973) (Ref. 8). As yet there is no definite explanation of these observations; several possible interpretations are included in Section III of this report.

These initial observations of electronic state emission pulses led to a more detailed investigation of electronic state laser possibilities in e-beam-stabilized electric discharges. This included the formation of a new laser concept which offers good prospects for developing high efficiency, high energy density, visible gas lasers. The concept is based on the use of preferential collisional processes to provide a two temperature system, a high temperature among electronic states, and a low vibrational temperature within each electronic state. The laser inversion is then achieved between a low vibrational level of an upper electronic state and a high vibrational level of a lower electronic state. The application of this new laser concept was first directed toward molecules such as N_2 and CO which have already produced electronic state laser emission. In this connection the possibility of making use of the energy pooling process in N_2 was also investigated. The results of these studies are described in Section III of this report.

SECTION II

HF AND DF ELECTRIC DISCHARGE LASER TECHNOLOGY

2.1. Laser Concept

This program is directed toward an investigation of the properties of V-V pumped, infrared active diatomic molecules for use in electric discharge lasers. Previous work (Ref.9) has shown that V-V pumping is effective in producing a partial inversion of CO, and leads to high efficiency conversion of electrical energy to laser energy (Ref. 10). In some cases the CO vibrational temperature is increased and laser efficiency is improved by including a significant fraction of N_2 in the gas mixture.

In the investigation described here this laser principle is extended to other diatomic molecule pairs such as HF and H_2, DF and D_2, HCl with D_2, and DCl with N_2 or CO. In each case the pair of diatomic molecules is composed of an infrared inactive molecule and an infrared active molecule which have reasonably close coincidence of vibrational energies. The vibrational mode of the infrared inactive molecule is excited by electron impact in an electrical discharge that is controlled and stabilized by an external ionization source. The vibrational energy of the inactive molecule is transferred by V-V collisions to the infrared active molecule and a partial inversion may be produced in the upper vibrational levels of the infrared active molecule.

The spectroscopic constants of a number of candidate molecule pairs are given in Table I, along with the VT decay time of the laser molecule. The H_2-HF system has the favorable characteristics of large anharmonicity, $\Delta\theta_v$, and large rotational energy level spacing, θ_R, but

Table I

Spectroscopic Constants for Several Candidate Partial Inversion Infrared Laser Molecules

Pump Molecule	θ_v, °K	$\Delta\theta_v$, °K	Laser Molecule	θ_v, °K	$\Delta\theta_v$, °K	θ_r, °K	Emission Region, μ	VT Decay (300 °K) μsec-atm
N_2	3353	41.5	CO	3076	38.6	2.76	4.8 - 6	$> 10^6$ (Ref. 11)
H_2	5985	342.0	HF	5697	256.0	30.0	2.7 - 3	0.024 (Ref. 12)
D_2	4300	184.0	DF	4180	131.0	15.8	3.7 - 4	0.055 (Ref. 13)
D_2	4300	184.0	HCl	4150	117.0	15.0	3.7 - 4	1.6 (Ref. 14)
N_2	3353	41.5	DCl	3010	78.0	7.8	5.0 - 6	6.0 (Ref. 15)

HF has the unfavorable characteristic of short VT decay time, τ_{VT}. The D_2-DF and D_2-HCl systems have smaller values of θ_V and θ_R, but larger values of τ_{VT}. By comparison the N_2-CO system has very small values of θ_V and θ_R, but very large values of τ_{VT}.

The effect of these parameters is illustrated by an approximate criterion for a partial inversion in the laser molecule, given by

$$T_V' > \theta_V' (T_R/4\theta_R)^{1/2} \qquad (1)$$

where T_V' represents the effective vibrational temperature based on the population of the lasing level, V', relative to the next lower vibrational level, $V'-1$. The value of T_V' required by Equation (1) for CO at 100 °K is about the same as that required for HF, DF, HCl, or DCl at 300 °K. Thus the spectroscopic constants indicate that electric discharge lasers may be achieved at room temperature in the hydrogen and deuterium halides.

In order to reach the required value of T_V' in these gases, it is necessary that the V-V collisional transfer rates must exceed the VT decay rates by a large margin. The ratio for HF of about 25 is much larger than 1, although it is considerably smaller than the value of about 10^5 for CO at room temperature. The effect of the ratio of the VV rate to that of the VT rate in the hydrogen and deuterium halides is one of the key questions being addressed in this program and is discussed in more detail in subsequent portions of Section II of this report.

A second requirement in achieving a high vibrational temperature, T_V', in the gas mixture is efficient transfer of the electric discharge energy to molecular vibration. The cross section for electron impact

excitation of the V=1 level of H_2 (Ref. 16) is compared in Figure 1 with the integrated cross section for the first 8 levels of N_2 (Ref. 17). Excitation of the V=2 level of H_2 is an order of magnitude smaller than that for V=1. It is seen that the peak cross section for H_2 vibration is about one-seventh that for N_2 vibration, although the H_2 cross section covers a wider range of electron energy. The efficiency of vibrational pumping of H_2 in an electric discharge is then dependent on the relative magnitude of the competing energy loss processes. These include elastic collisions, rotational excitation, and electronic excitation. The inelastic cross sections for rotational excitation (Ref. 16) and for excitation of the lowest electronic state, the repulsive $b\,^3\Sigma_u^+$ state of H_2 (Ref. 18) are also shown in Figure 1. It is apparent that very low electron energies or very high electron energies would be inefficient in exciting H_2 vibration. In Section 2.2 a detailed analysis of this problem is described, and it is shown that satisfactory vibrational excitation can be achieved over a range of intermediate electron energies; the maximum vibrational pumping efficiency of H_2 is about 65 percent.

Since the preceding discussion indicates that the basic requirements for producing a partial inversion laser on HF, DF, HCl, or DCl appear (qualitatively) to be met, it is natural to ask why this has not been accomplished previously in the laboratory. There are two principal reasons. The first reason is associated with the low lying, repulsive excited electronic states of these molecules. In self-sustained electric discharges, the electron energy must be sufficiently high to produce the

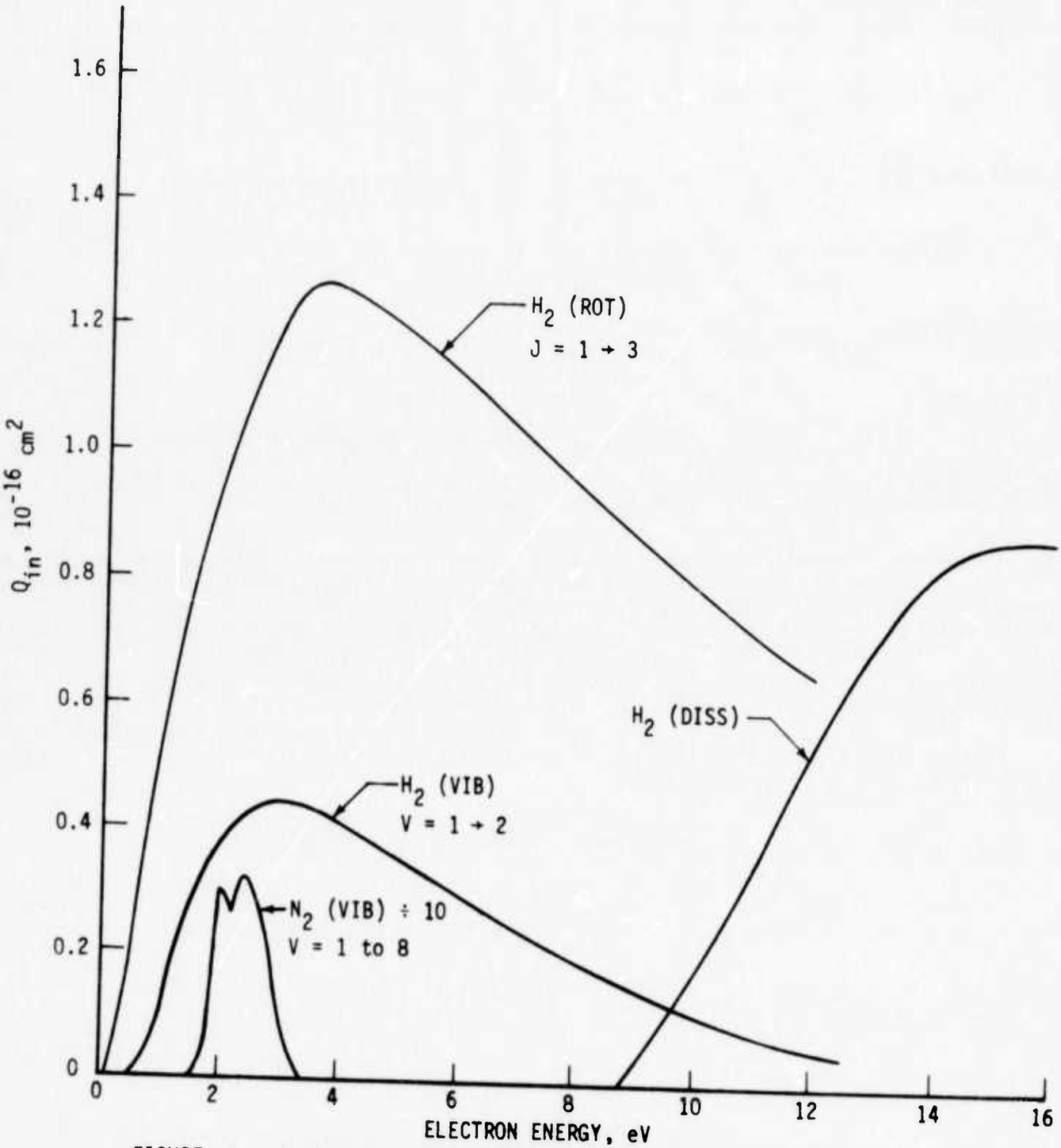

FIGURE 1. Inelastic Cross-sections for Electron Impact with Hydrogen

required rate of ionization. Under these conditions a large fraction of the discharge energy produces molecular dissociation and only a small fraction goes into molecular vibration. In addition, the atoms then add to the already rapid VT decay rate. It is therefore essential to use an external ionizing source and a low electric discharge voltage in order to achieve high vibrational excitation and low dissociation. The second reason is associated with the relatively low electron impact vibrational excitation cross section and the large VT decay rates of these molecules. In order to achieve a vibrational pumping rate that sufficiently exceeds the VT decay rate, it is necessary to provide an electron density of the order of 10^{13} cm^{-3} or more in the electric discharge. Only recently have external ionizing techniques been developed that will provide the required electron density. With this new technology, a new class of molecular laser possibilities may be realized.

One additional physical process plays a key role in the development of these laser possibilities. Since an external ionizing source is necessary, the requirements on this source may be affected strongly by electron attachment losses to HF, DF, HCl, or DCl. For example, the dissociative attachment cross section for HCl is about 2×10^{-18} cm^2 (Ref. 19) at an electron energy of 0.5 to 1 eV. Thus a partial pressure of 2 Torr of HCl in the gas mixture will lead to an electron density decay time of about 10^{-7} sec. This is about a factor of 10 shorter than that due to dissociative recombination (for an electron density of 10^{13} cm^{-3}) and will require a corresponding factor of 10 increase in the electron beam current density used for ionizing the gas.

Due to the greater bond strength of HF and DF, the electron attachment rate should be smaller than for HCl and will have considerably less impact on the requirements of the external ionization source. This has been investigated experimentally as discussed in Section 2.4.

A more detailed analysis of this concept as it applies to H_2-HF mixtures is given in Sections 2.2 and 2.3. A series of laser emission experiments is described in Section 2.4 which serves to confirm the basic principles involved. Probe laser absorption and gain measurements, made on a number of HF vibration-rotation lines, are described in Section 2.5. Finally in Section 2.6 the experimental data are compared with the computer model.

2.2 Analytical Model of Electrical Excitation Processes

The H_2/HF molecular system was selected in this program to be the focal point for development of a detailed analytical model representative of infrared electric discharge vibration transfer lasers. This choice was based on the extensive information already available for H_2 and HF and on the close analogy with the D_2/DF system which provides a good laser emission wavelength range. The analysis is divided into two basic components: first, the electrical discharge excitation of the molecular system as described in this section, and second, the vibrational kinetics and optical inversion and extraction characteristics of the molecular system as described in Section 2.3.

In carrying out the electrical discharge excitation analysis of H_2/HF/diluent mixtures, it was recognized that only a very small fraction of HF would be used (less than 1 percent) and, to first order, HF could be neglected in solving the electron Boltzmann equation; since the electron impact excitation cross sections for HF are not yet known, accurate values could not be included anyway. In addition, because of the need for a high discharge current and the limitations on the e-beam current densities presently available, argon was selected as the best diluent. Thus the electron Boltzmann equation has been solved for argon-hydrogen mixtures using the best currently available experimental data for electron impact cross sections.

2.2.1 Momentum-Transfer and Inelastic Cross Sections

The momentum-transfer cross sections for electron impact on H_2 and Ar are shown in Figure 2. The curve for Ar was used by Engelhardt and Phelps (Ref. 20) in a study of H_2/Ar mixtures, whereas the curve for H_2 is based on the Engelhardt and Phelps study of H_2 (Ref. 21).

The inelastic cross sections for H_2 and Ar are shown in Figure 3. The total rotational excitation cross section of H_2, obtained from Linder and Schmidt (Ref. 16) is for a $j = 1 \rightarrow j = 3$ transition. This is satisfactory at room temperature since most of the H_2 is in the $j = 1$ state. The value of this cross section is an order of magnitude larger than that used by Engelhardt and Phelps (Ref. 21). The vibrational excitation cross section of H_2 is for the $v = 1$ state; the cross

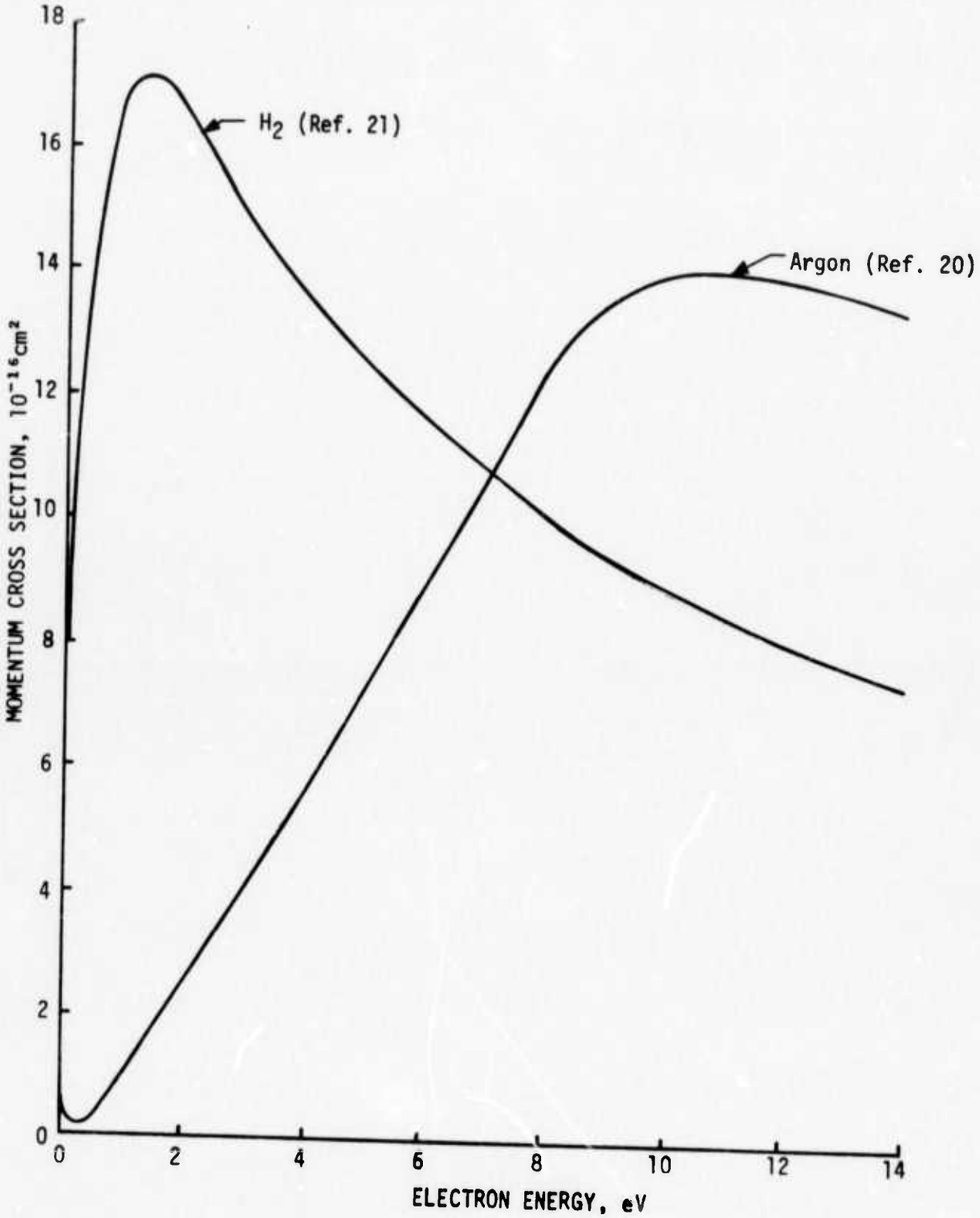

Figure 2. Momentum Transfer Cross Sections for H_2 and Argon

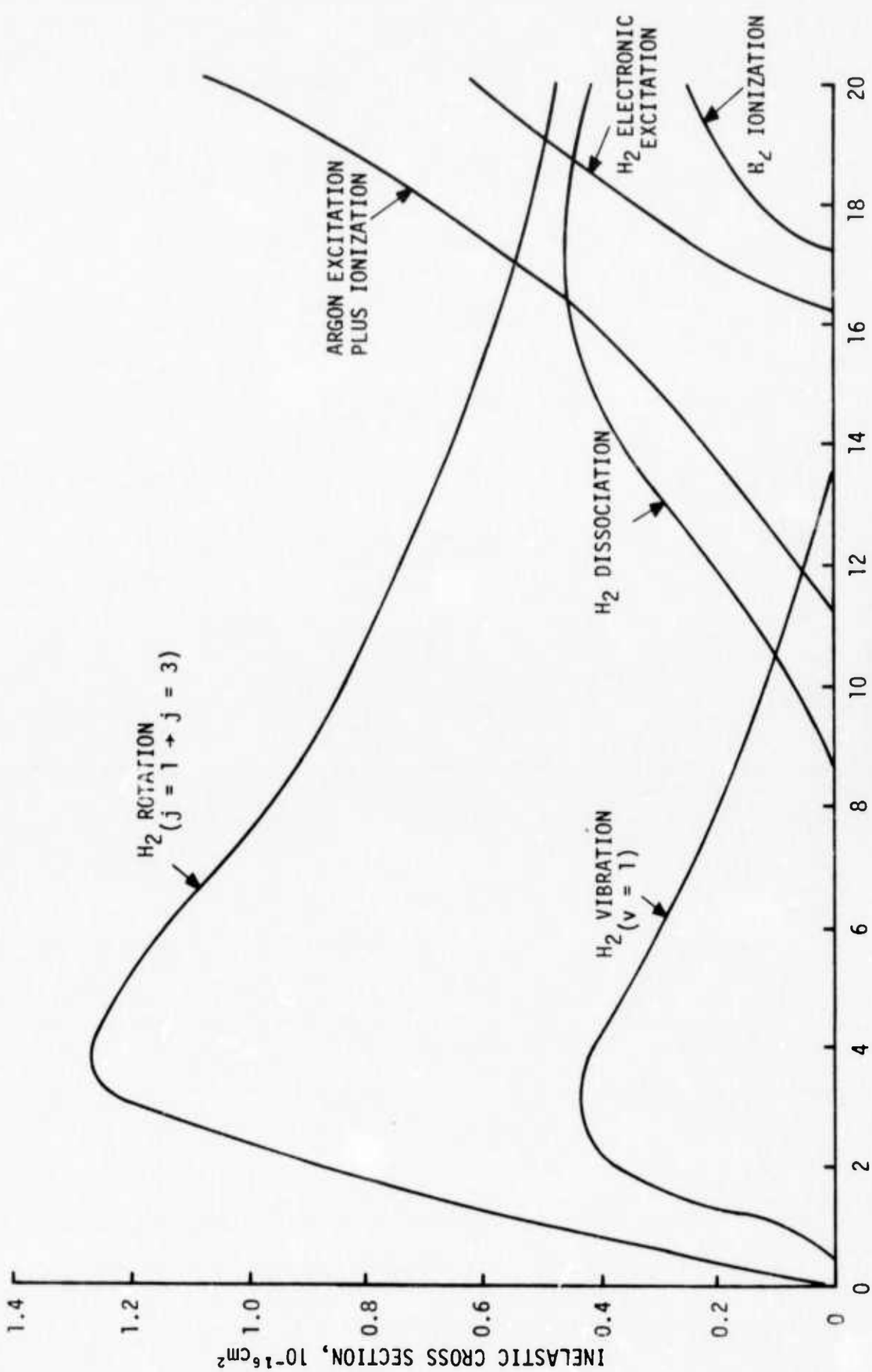

Figure 3. Inelastic Cross Sections for H_2 and Ar

section for excitation of v = 2 is believed to be an order of magnitude smaller than that for v = 1 and is currently being neglected since no experimental data have been found. The electronic excitation cross section of H_2 is for the process $X\,^1\Sigma_g^+ \rightarrow b\,^3\Sigma_u^+$ which leads to dissociation of H_2. A characteristic electron energy loss of 10 eV is assumed. Also shown are cross sections for excitation of upper electronic states of H_2 which lead to UV emission and for direct ionization of H_2, both from Engelhardt and Phelps (Ref. 21).

The inelastic cross sections for H_2 described above have been used together with a computer program that solves the Boltzmann equation to determine electron transport properties in pure H_2. The resulting values of characteristic energy, ε_k = eED/v, agree satisfactorily with experimental data (Ref. 21), but computed values of the drift velocity, v, are low by 2 to 5 percent, as shown in Figure 4. Thus, completely satisfactory values of the cross sections of H_2 have not yet been found.

The inelastic cross section for electronic excitation plus ionization of argon is taken from Engelhardt and Phelps (Ref. 20). A characteristic electron energy loss of 12 eV is assumed for this process. Good agreement is obtained between computed and measured transport coefficients in pure argon as shown in Figure 5. In Figure 6, the close agreement between our electron distribution function for pure argon with that of Engelhardt and Phelps (Ref. 20) is evident at an E/N of 4×10^{-16} V-cm^2.

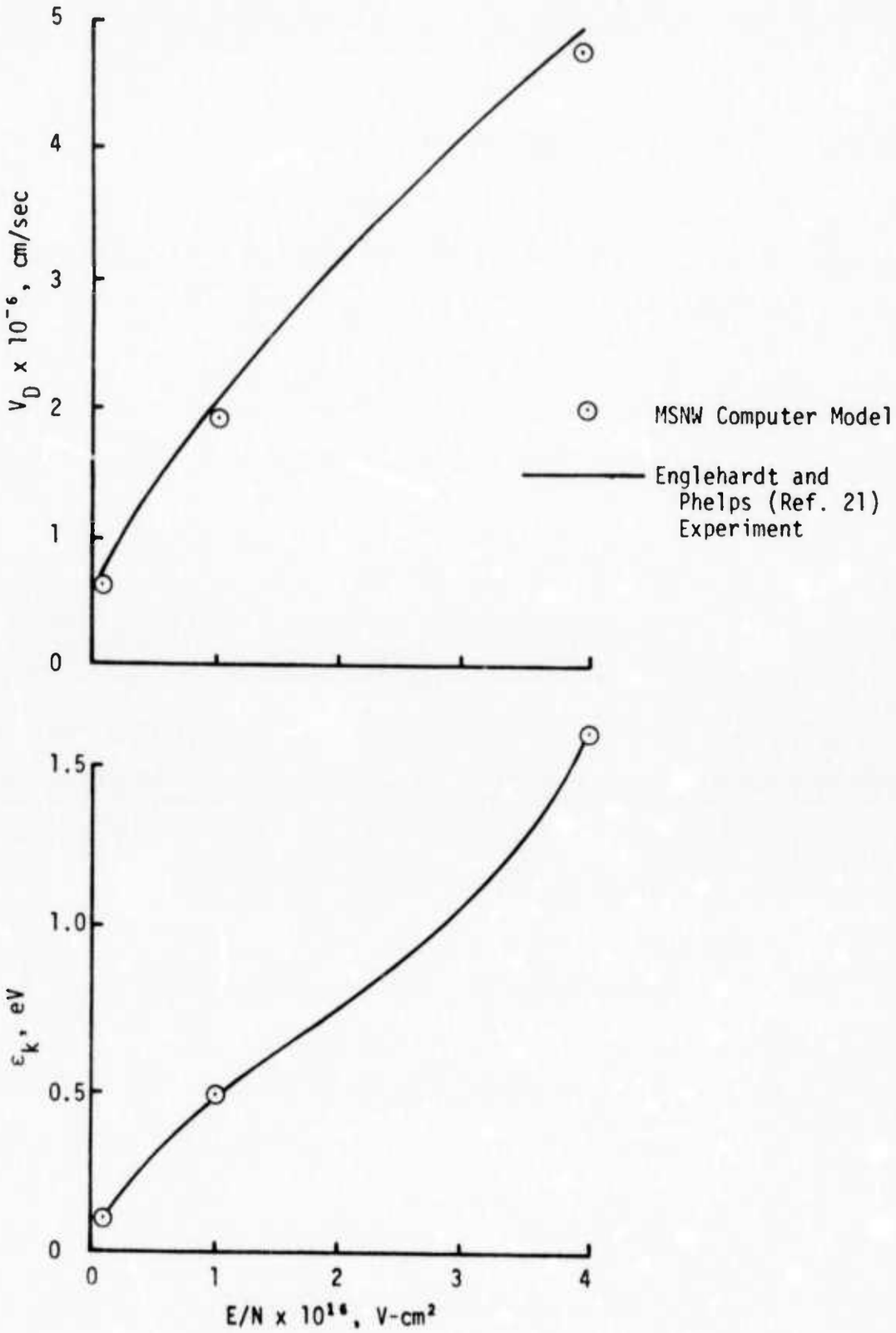

Figure 4. Comparison of Analytical and Experimental Dependence of Electron Transport Properties on E/N for Pure H_2

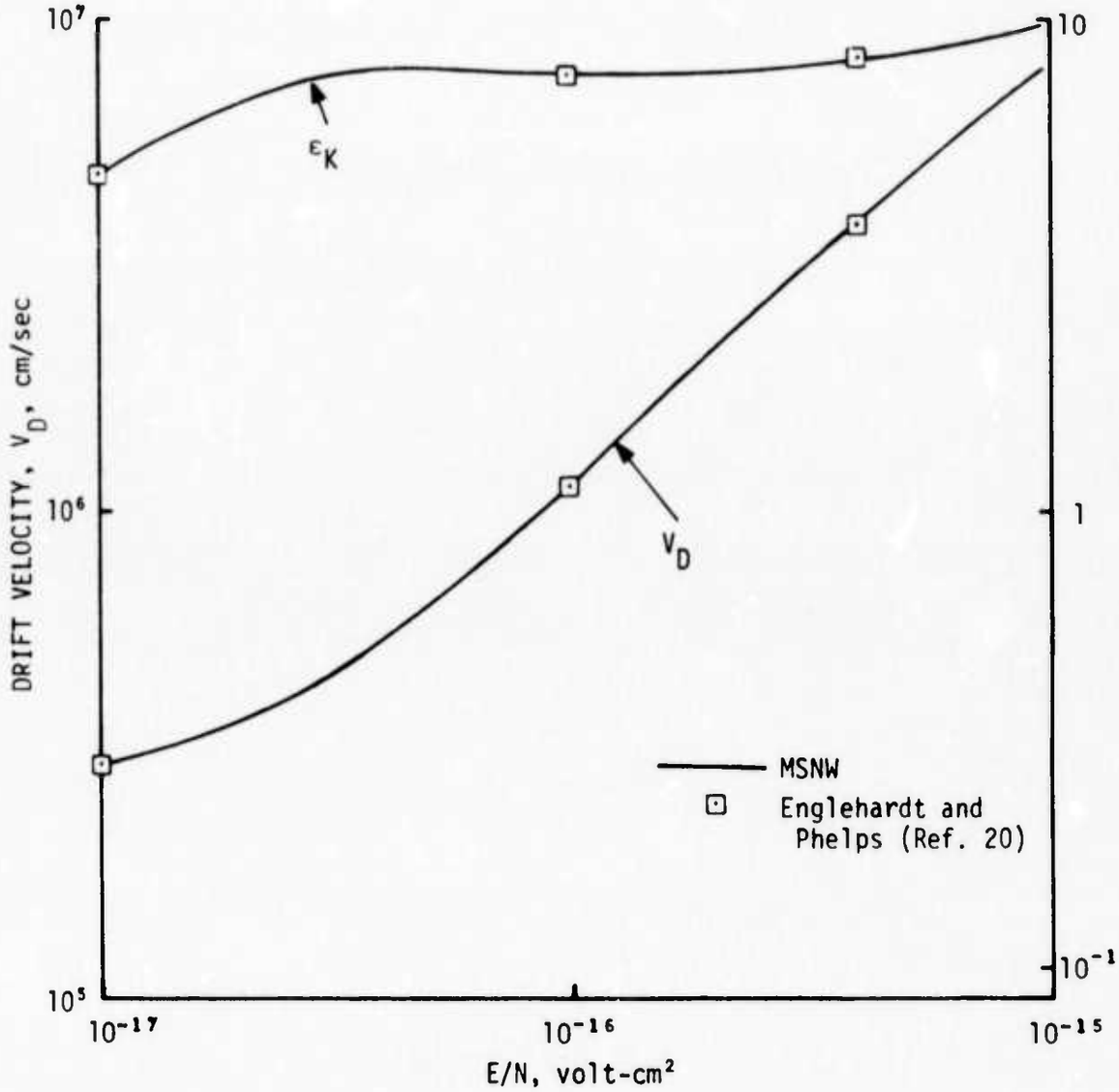

Figure 5. Comparison of Analytical and Experimental Dependence of Electron Transport Properties on E/N for Pure Argon

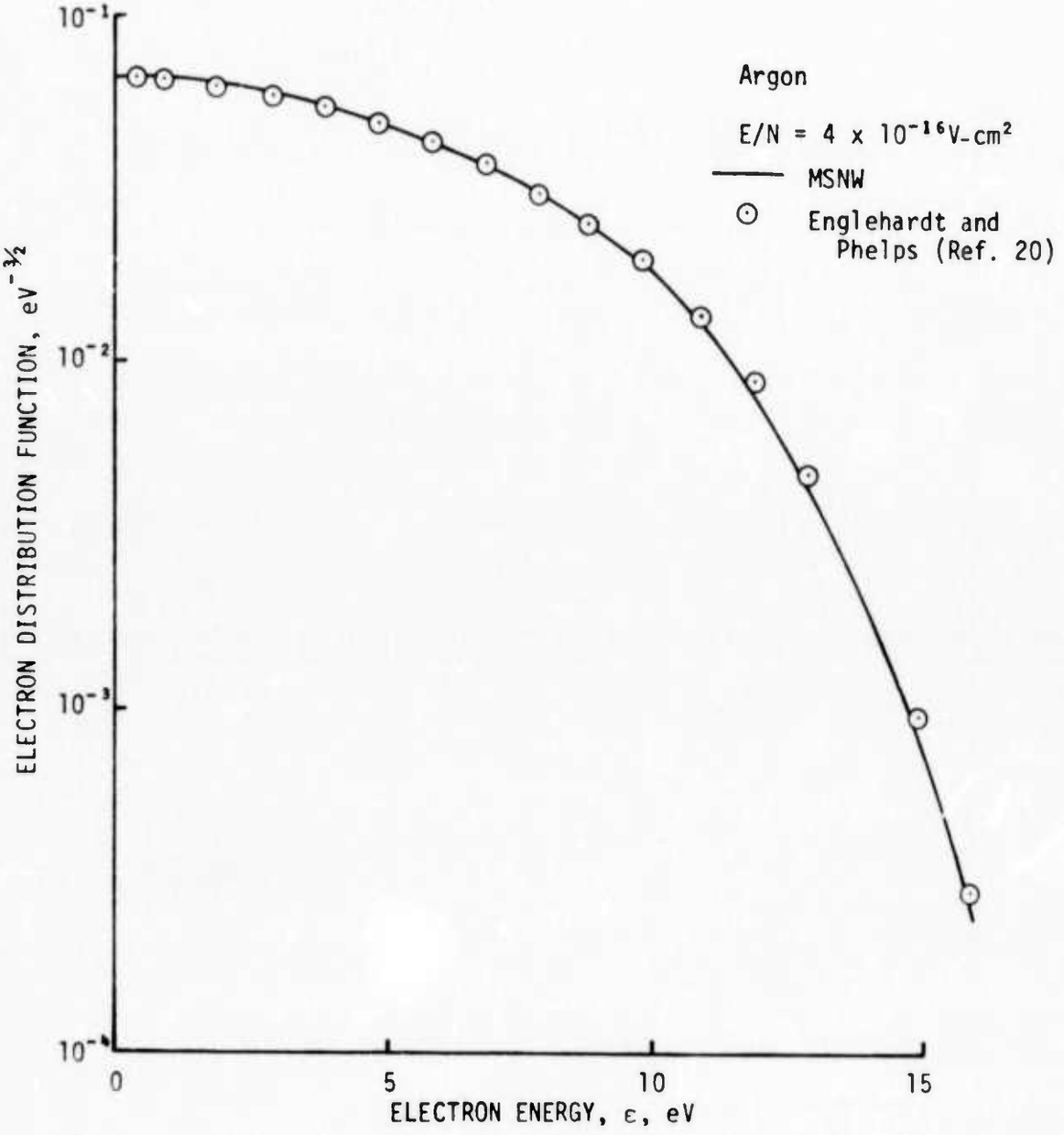

Figure 6. Computed Electron Distribution Function

It is concluded on the basis of these comparisons that the MSNW computer program for solving the electron Boltzmann equation is working satisfactorily and that the cross sections used are in reasonable agreement with existing experimental data. Thus the program can be applied with confidence to the calculation of energy partitioning in H_2/Ar mixtures.

2.2.2 Energy Partition in Electric Discharges in H_2/Ar Mixtures

Using the cross sections for electron impact excitation of rotation, vibration, and dissociation of H_2 described in the previous section, the Boltzmann equation was solved for a 10/90 H_2/Ar mixture. The computed drift velocity and characteristic energy are shown in Figure 7. It is seen that the characteristic energy agrees with the experimental results of Engelhardt and Phelps (Ref. 20), whereas the drift velocities are 2 to 4 percent too low for $E/N < 6 \times 10^{-17}$ V-cm^2.

The fractional power input to the elastic and inelastic processes for a 10/90, H_2/Ar mixture, based on the above Boltzmann solution, is shown in Figure 8. It is seen that the optimum power transfer to the vibrational mode of H_2 occurs for E/N between 0.4 and 0.6×10^{-16} V-cm^2. At these values of E/N it is seen in Figure 8 that the best electrical efficiency expected for pumping H_2 vibration is about 65 percent; rotational heating is seen to be quite significant (about 25 percent). The effect of this distribution of the electric discharge energy is examined in Section 2.3.

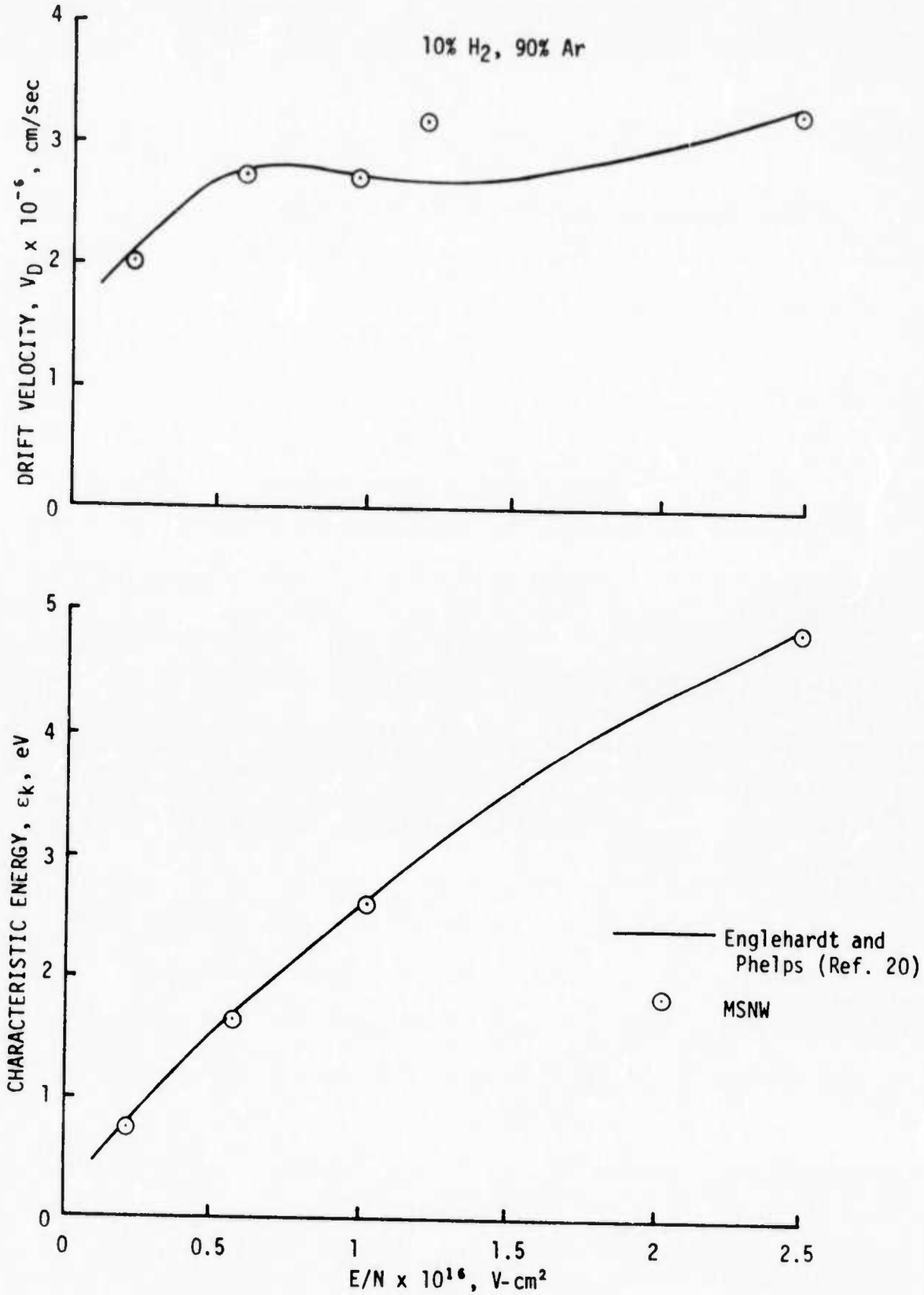

Figure 7. Comparison of Analytical and Experimental Dependence of Electron Transport Properties on E/N for a 10/90 H_2/Ar Mixture

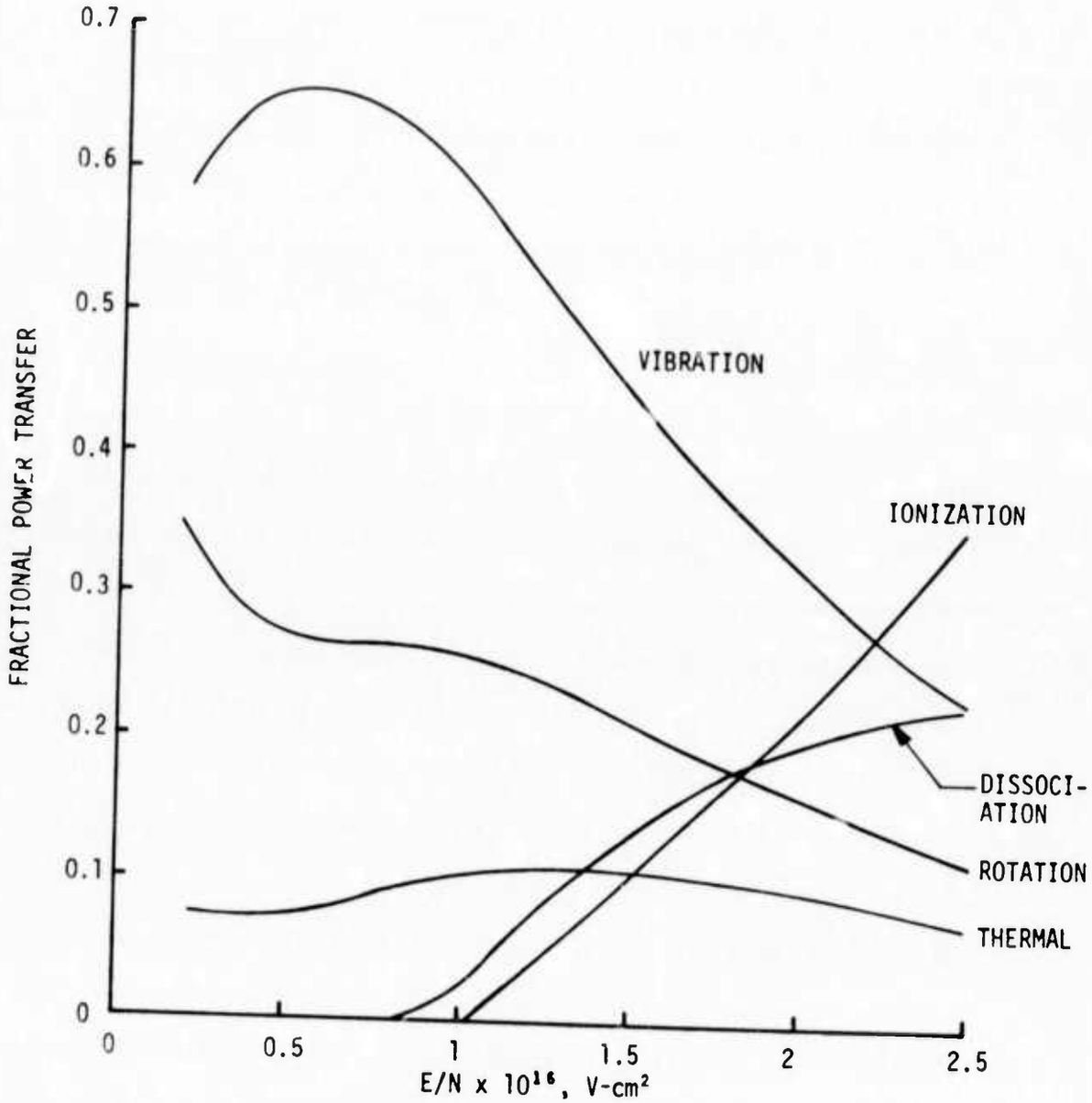

Figure 8. Distribution of Electrical Power in 10/90 Hydrogen/ Argon Mixtures

2.2.3 Processes Omitted in the Present Model

A number of processes that may be significant has been omitted in the present electrical excitation model, of which three are of particular concern. First, direct excitation of HF vibration (and rotation) by electron impact is expected to occur, and apparently is observed in laser experiments as discussed in Section 2.4. However, the cross sections as functions of electron energy are not yet known and therefore can only be incorporated into the computer model in a parametric fashion. Second, further collisional excitation of already excited vibrational (or rotational) states of H_2 by electron impact has not been included because the cross-section information is not available. Since the degree of vibrational excitation of H_2 must be quite high for this laser mechanism to be effective, further excitation of the $v = 1$ or $v = 2$ levels may be significant in the kinetic model. Third, we have not included the effects of superelastic collisions whereby cold electrons collide with excited vibrational states of H_2 and de-excite the molecules, heating the electrons. The effect of this process on the present model was examined for a specific case and found to cause only a few percent change in the fraction of the electric discharge power put into vibration. However, the upper vibrational levels of H_2 may become inverted and superelastic collisions with electrons could then become a very significant depopulation mechanism.

2.3. Analytical Model of Molecular Transfer and Loss Processes

2.3.1. Time Dependent Vibrational Population Rate Equations

A simplified kinetics model has been developed to study the vibrational relaxation of H_2 and HF in the presence of argon. The anharmonic oscillator model was used to describe the vibrational levels of H_2 and HF. Seven vibrational levels were considered in HF, with the seventh level being a reflecting boundary, whereas six levels were considered for H_2, with the top level containing a sink.

Relaxation mechanisms considered were intra- and inter-molecular V-V transfer and V-T decay. In addition, the rotational relaxation of H_2 and HF were considered since the rotational relaxation times are comparable to the time scale of vibrational relaxation, and are important for determining the gain coefficients which are a function of the rotational distribution.

The complete kinetic equations were simplified somewhat by assuming that only the first excited vibrational level of HF or H_2 was responsible for pumping the higher levels by intra-molecular V-V transfer, e.g.,

$$N_i(v = 1) + N_i(v = n) \rightleftarrows N_i(v = 0) + N_i(v = n + 1) \qquad (2)$$

The inter-molecular V-V transfer mechanism was limited to the exchange of one quantum from the first two excited levels of H_2 with all levels of HF, e.g.,

$$H_2(v = 1) + HF(v = n) \rightleftarrows H_2(v = 0) + HF(v = n + 1) \qquad (3)$$

$$H_2(v = 2) + HF(v = n) \rightleftarrows H_2(v = 1) + HF(v = n + 1) \qquad (4)$$

In the case of V-T relaxation, the following mechanisms were included:

$$HF(v) + M \rightleftarrows HF(v - 1) + M \qquad (5)$$

$$H_2(v) + M \rightleftarrows H_2(v - 1) + M \qquad M = HF, H_2, Ar \qquad (6)$$

The kinetics of the rotational energy were treated by assuming a Boltzmann distribution for the rotational energy at one rotational temperature for both H_2 and HF. The relaxation of the H_2 rotational energy included only H_2 as a catalyst, and the HF rotational energy was assumed to be in equilibrium with the H_2 rotational energy.

The electric discharge excitation rates of rotation, vibration, and "elastic" energy transfer were obtained from a solution of the Boltzmann equation for a given E/N and mixture composition, as described previously in Section 2.2.

In the case of a lasing mixture, the radiative relaxation of the HF vibrational states was determined for laser intensities which satisfied the laser cavity boundary conditions.

The system of equations to be solved for constant density cases is

$$\frac{dN_i(v)}{dt} = \left(\frac{dN_i(v)}{dt}\right)_{V\text{-}V} + \left(\frac{dN_i(v)}{dt}\right)_{V\text{-}T} + \left(\frac{dN_i(v)}{dt}\right)_{\substack{\text{electron} \\ \text{pumping}}} + \frac{g_{v+1}\,\Phi_{v+1}}{\Delta\varepsilon_{v+1}} - \frac{g_v \Phi_v}{\Delta\varepsilon_v} \qquad (7)$$

$$\frac{dE_{rot}}{dt} = \frac{1}{\tau_{rot}} [E(T) - E(T_{rot})] + \left(\frac{dE_{rot}}{dt}\right)_{\substack{\text{electron} \\ \text{pumping}}} \tag{8}$$

$$\frac{dT}{dt} = - \frac{1}{NC_v} \left[\sum_{i,v} E_i(v) \frac{dN_i(v)}{dt} + \frac{dE_{rot}}{dt} + \Sigma_v \frac{g_v \Phi_v}{\Delta\varepsilon_v} - P_{in} \right] \tag{9}$$

where

$E_i(v)$ = energy of level v for species i

$\Delta\varepsilon_v$ = energy of radiative transition from level v to v -1

$N_i(v)$ = density of level v of species i

E_{rot} = rotational energy density

T_{rot} = rotational temperature

$P_{thermal}$ = volumetric heating due to "elastic" energy transfer

P_{in} = volumetric power input

2.3.2. V-V and V-R,T Rate Constants

The required rate coefficients for the theoretical modeling for complete calculations of the behavior of HF lasers were compiled from the best available data in the literature. For reactions where no data exist, the rate coefficients were given reasonable estimates.

In the $HF/H_2/Ar$ gas mixture, the most important reactions involve the HF/HF V-V ladder climbing, the HF V-R,T decay, the inter-molecular HF/H_2 V-V exchange, and the H_2 V-R,T decay. The vibrational decay rates for HF/HF reactions were measured recently (Ref. 22) by Osgood, Sackett, and Javan for vibrational quantum numbers up to 4. However, their decay rates involved the sum of the V-V and V-T decay rates and therefore

required an assumed variation of the V-T decay rate with vibrational quantum number, with the v = 1 V-T decay rate being known from measurement. The V-T rate for higher levels was assumed to be proportional to the square of the quantum number; the resulting rate coefficients (K_{VV}^{*}) for the production of quantum levels 3 and 4 were then just below the gas kinetic limit. The results of this assumption are shown in Figure 9.

A summary of the rate data extracted from the literature is given in Table II, and the additional, assumed rates are given in Table III.

2.3.3. Optical Constants

The small signal gain, g_o, at the line center for a P(J) transition ($v \rightarrow v - 1$; $J - 1 \rightarrow J$) is given by

$$g_o = \frac{\lambda_o^2}{8\pi} A \frac{B_v}{T_r} (2J-1) \exp\left[\frac{-J(J-1)B_v}{T_r}\right] x \qquad (10)$$

$$\left[1 - \frac{n(v-1)}{n(v)} \left(\frac{B_{v-1}}{B_v}\right) x \exp\left(\frac{-J(J+1)B_{v-1} + J(J-1)B_v}{T_r}\right)\right] n(v) G(\nu_o)$$

where

$G(\nu_o)$ = line shape function = $\frac{2\sqrt{\ell n 2}}{\sqrt{\pi}\ \nu_p} \exp(a^2)\ \mathrm{erfc}(a)$

$a = \frac{\Delta\nu_c}{\Delta\nu_p} \sqrt{\ell n 2}$

$\Delta\nu_p = \left[\frac{8kT\ell n 2}{m}\right]^{\frac{1}{2}} \frac{1}{\lambda_o}$, Doppler full width at half-maximum, sec^{-1}

$\Delta\nu_c = \frac{\nu_c}{\pi}$, Lorentz full width at half-maximum, sec^{-1}

ν_c = optical broadening collision frequency, sec^{-1}

A = transition probability for radiation (Ref. 26)

n(v) = molecular density of vibrational level v

T_r = rotational temperature

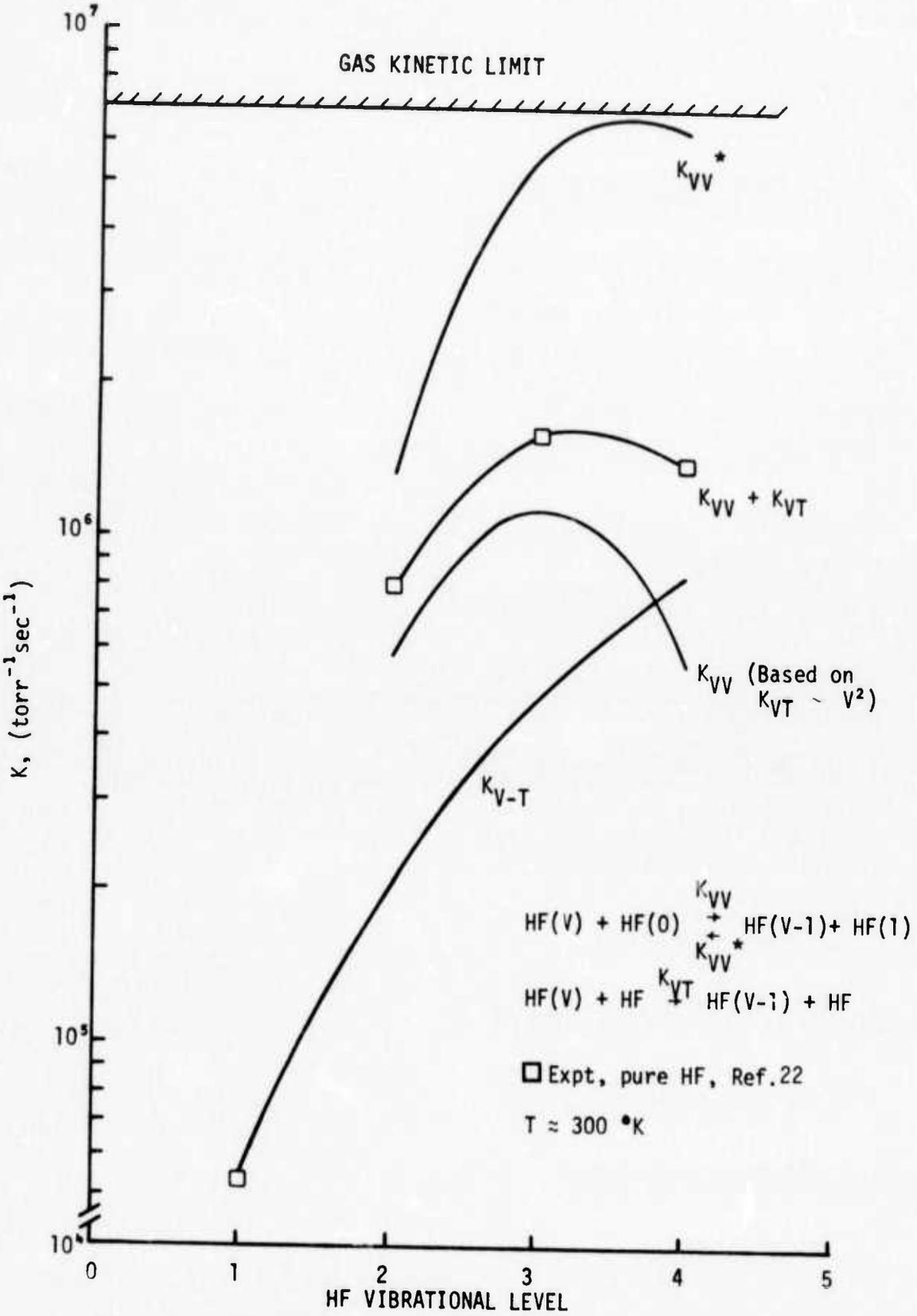

Figure 9. Vibrational Dependence of V-T and V-V Rates of HF in HF/HF Collisions

Table II

Summary of H_2/HF V-V, V-T, and R-T Rate Data from the Literature

Reaction	Rate Constant[a] (sec^{-1} $torr^{-1}$)	Reference
$HF(1) + HF \rightarrow 2HF(0)$ (in argon)	8.7×10^4 (b)	23
$HF(1) + HF \rightarrow 2HF(0)$ (in pure HF)	5.6×10^4 (b)	22
$HF(1) + Ar \rightarrow Ar + HF(0)$	60 (b)	23
$HF(1) + H_2 \xrightarrow{k_{12}} HF(0) + H_2$	$\leq 1 \times 10^3$ (b)	23
$H_2(1) + HF \xrightarrow{k_{21}} H_2(0) + HF$	$\leq 2 \times 10^3$ (b)	23
$H_2(1) + H_2 \rightarrow 2H_2(0)$	4.5 (b)	24
$H_2(1) + HF(0) \rightarrow HF(1) + H_2(0)$	6.3×10^4 (c)	23
$HF(2) + HF(0) \rightarrow HF(1) + HF(1)$	8×10^5	22
$HF(3) + HF(0) \rightarrow HF(2) + HF(1)$	1.6×10^6	22
$HF(4) + HF(0) \rightarrow HF(3) + HF(1)$	1.4×10^6	22
$HF(1) + N_2 \rightarrow HF(0) + N_2$	1.25×10^2	23
$H_2(J=3) + H_2 \rightarrow H_2(J=1) + H_2$ (rotational relaxation)	6.1×10^4 (d)	25

(a) Rate = $K_{V\text{-}R,T} + K_{V\text{-}V}$, unless otherwise noted.

(b) Rate = $K_{V\text{-}R,T}$

(c) Rate = $K_{V\text{-}V}$

(d) Rate = $K_{R,T}$

Table III

Summary of Additional, Assumed Rates for the H_2/HF Kinetic Model

REACTION	RATE CONSTANT (sec^{-1} $torr^{-1}$)
$HF(4) + HF(1) \rightarrow HF(5) + HF(0)$	6×10^6
$HF(5) + HF(1) \rightarrow HF(6) + HF(0)$	6×10^6
	$\simeq$ gas kinetic limit
$HF(v) + \quad \rightarrow HF(v-1) + M \quad (v \neq 1)$	$K_{V-T} \propto V^2$
$H_2(1) + H_2(1) \rightarrow H_2(2) + H_2(0)$	2.14×10^4
$H_2(v) + H_2(1) \rightarrow H_2(v+1) + H_2(0)$	$K_{V-V} \propto V$
$H_2(2) + HF(0) \rightarrow H_2(1) + HF(1)$	$K_{V-V} \propto V$

B_v = rotational constant for vibrational level v

The Lorentz broadening due to the collisions of HF with itself and other species present in the mixture (H_2 and Ar) is given by

$$\Delta\nu_c = \frac{1}{\pi} \Sigma_i \nu_c (HF,i) \qquad (11)$$

In Figure 10, experimentally determined half-widths (1/2 of the full width at half-maximum) for HF self-broadening, H_2 broadening, and Ar broadening are plotted versus |m|, where |m| = J for P-branch transitions, and |m| = J + 1 for R-branch transitions. It is seen that the HF self-broadening has the character of the resonant dipole interaction model, although the theory over-estimates the broadening for low |m| values.

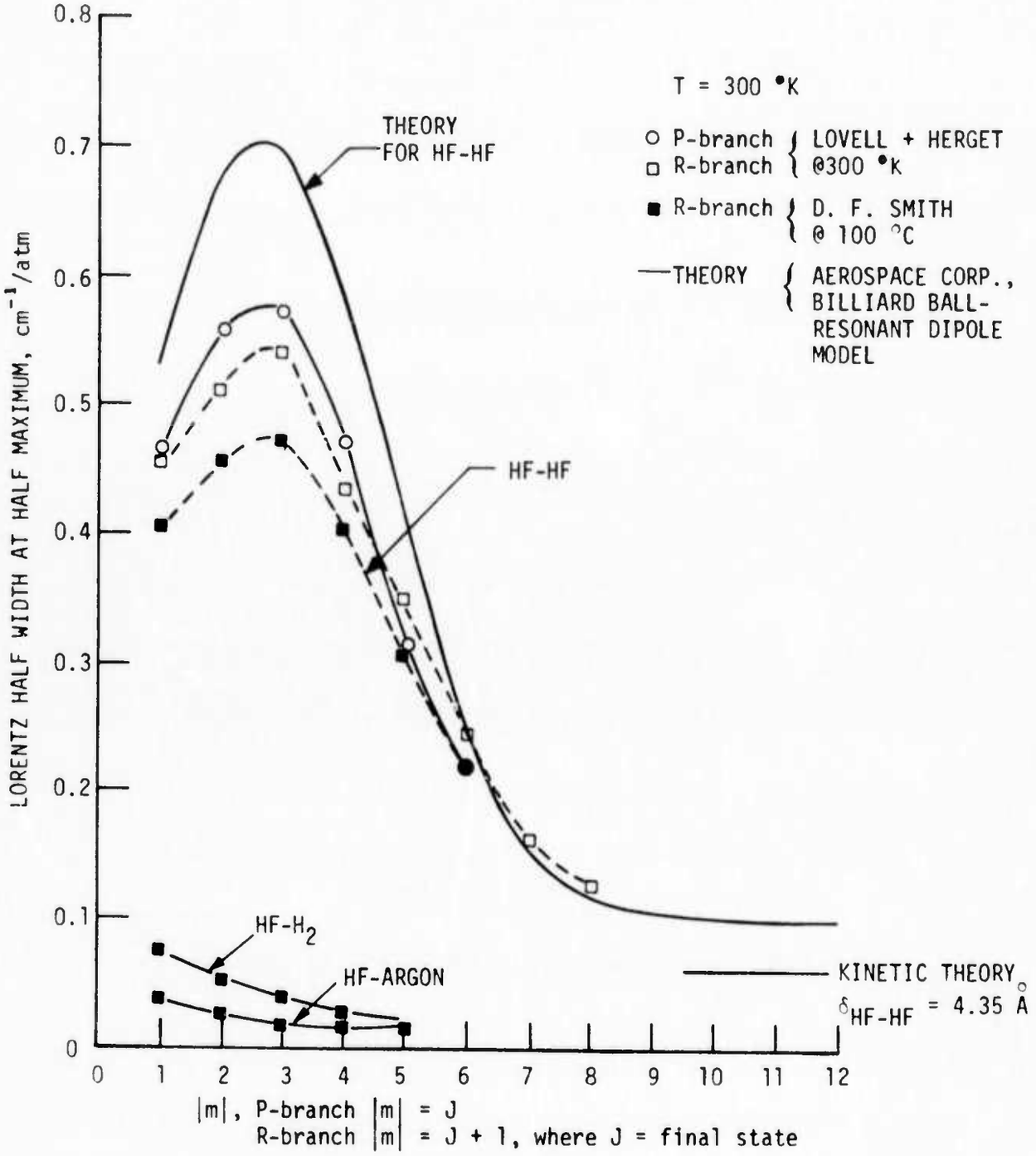

Figure 10. HF Lorentz Broadening

The room temperature data of Lovell and Herget (Ref. 27) were used for the self-broadening of HF, with the temperature dependence determined by the theoretical resonant dipole-billiard ball model fitted to their data. Collision broadening by H_2 and argon was based on the data of D.F. Smith (Ref. 28) at 100 °C, with the temperature scaled by $T^{-\frac{1}{2}}$, which assumes constant broadening cross sections. This scaling was verified by comparison with the HF/Ar cross sections at 293 °K obtained by Oksengorn (Ref. 29).

In the measurement of the gain (absorption) of HF mixtures containing argon, the effect of the line shift due to argon must be considered since the line center of the mixture may not coincide with the line center of the probe laser. This line shift is comparable to the Lorentz half-width. The line shifts due to the presence of Ar and HF are given in Table IV. These line shifts were scaled with a $T^{-0.85}$ dependence based on the data of Reference 29.

Table IV

Frequency Shift of HF Lines by HF and Ar Collisions

Line	Line Shift (cm^{-1}/atm)	
	(a)	(b)
R(0)	HF/Ar (Ref. 29)	HF/HF (Ref. 27)
R(0)	+ 0.0128	+ 0.036
R(1)	- 0.0198	not measured
R(2)	- 0.0222	- 0.012
R(3)	- 0.0259	not measured
R(4)	- 0.0280	- 0.018
R(5)	- 0.0289	- 0.014

(a) T = 20 °C. (b) T = 100 °C.

The effect of this shift on the probe laser measurements is shown graphically in Figure 11. It is seen that by using a low pressure probe laser ($w_{probe} = w_o$ vacuum) to study an HF mixture at 200 torr the measured gain or absorption would be only 50 percent of the value at line center. By operating the probe laser with helium as the buffer gas the measured gain is estimated to be 78 percent of the peak gain. This approximation is based upon comparisons of 1-0 P(8) absorption data with a calibrated-volume-flow measurement of the HF concentration (see Sect. 2.5.1). All of the data was reduced in this manner, using a factor of 0.78 to correct for the effect of line shift.

2.3.4. Small Signal Gain Calculations

The gain coefficients for various mixtures of $HF/H_2/Ar$ at 200 torr pressure were obtained for energy input rates from 1.5 to 4.6 kW/cm^3 and for 20 μsec duration. This energy was distributed among the various internal energy modes for an E/N of 0.7×10^{-16} V-cm^2, which resulted in the maximum amount of energy (65%) going into the H_2 vibrational excitation.

It is seen in Figure 12 that the highest gain, for a 0.15% HF mixture, was achieved for the high power input (4.6 kW/cm^3) although this resulted in the shortest duration for a positive gain coefficient. The duration of positive gain is essentially determined by the amount

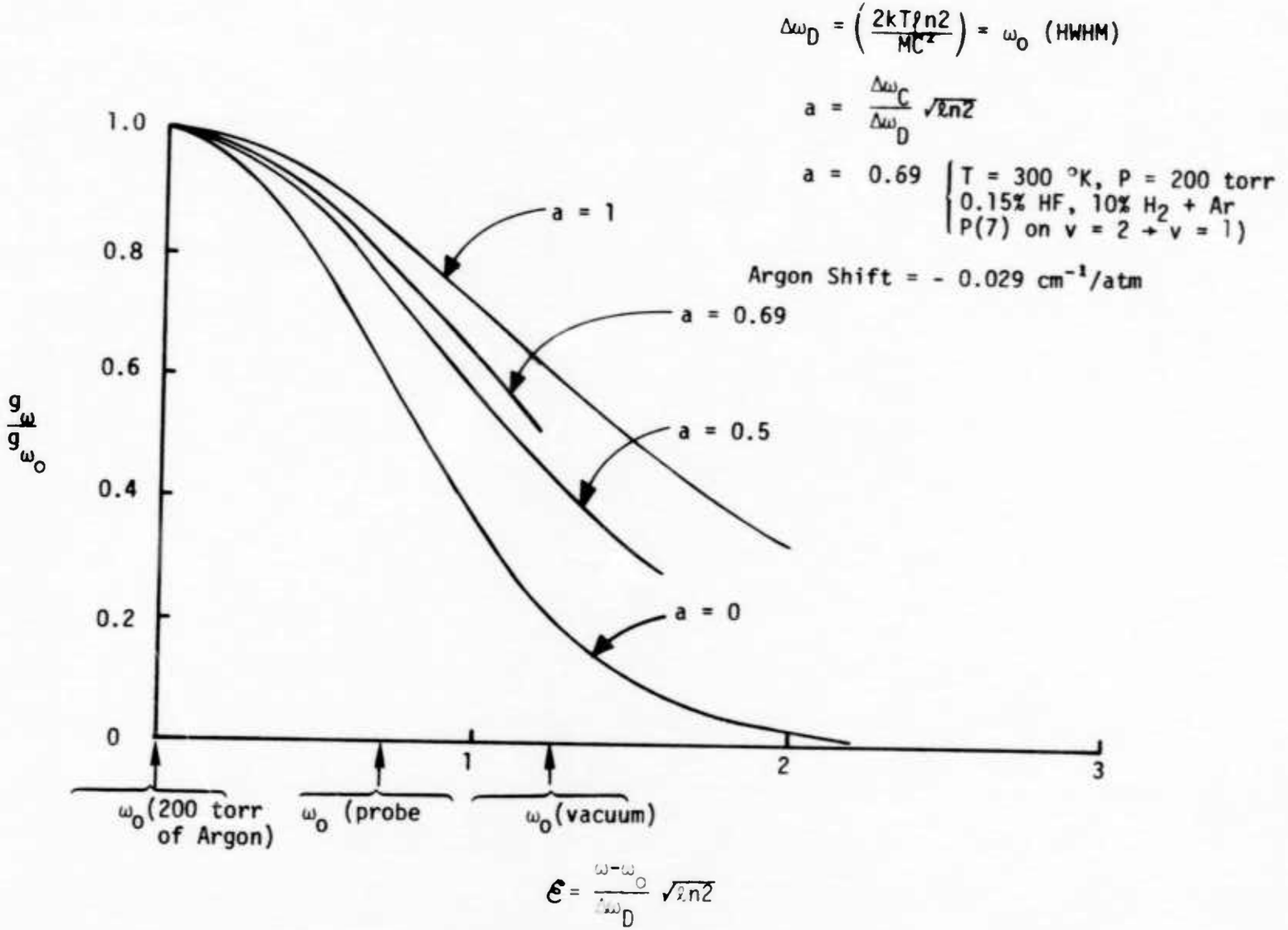

Figure 11. Effect on Probe Laser Measurements Caused by HF Line Shift Due to Argon Collisions

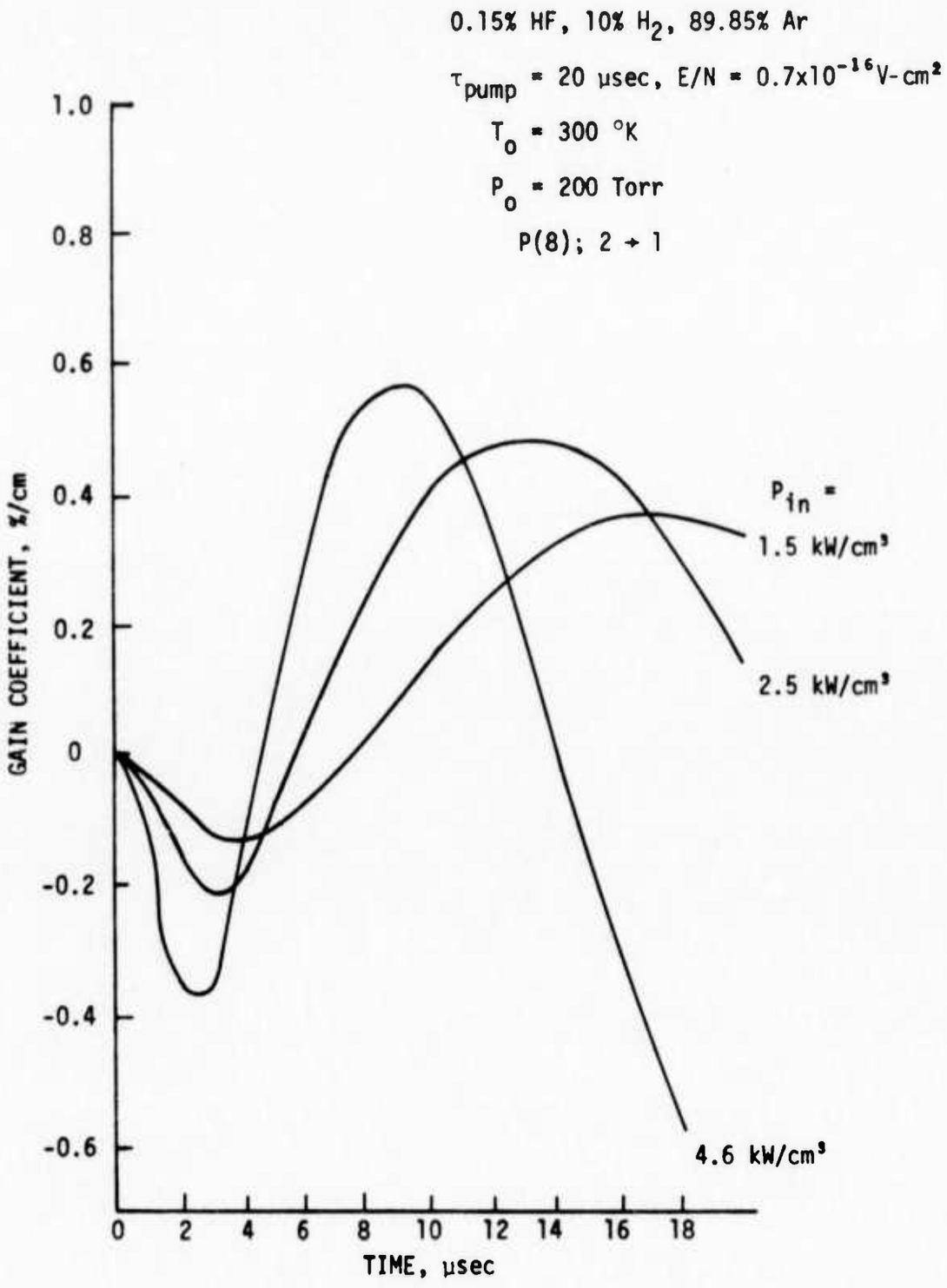

Figure 12. Computed HF Optical Gain Versus Time During a 20 μsec Electric Discharge Excitation Pulse

of gas heating, which, in the case of the high power input, amounted to about 240 °K temperature rise by the time (14 μsec) the gain coefficient became negative on the 2 → 1 P(8) line.

Figure 13 shows the time history of the population of vibrational levels for v = 1 to v = 3 at two power levels, 1.5 and 4.6 kW/cm^3. It is seen that after the initial rapid rise, the populations reach quasi-steady levels, with the values at low power input being 60 to 80% of the values at high power input, although the pumping rates differ by a factor of three.

The effect of concentration of HF for a given power input is seen by comparing the maximum gain coefficients for the v = 3 → v = 2 and v = 2 → v = 1 transitions for 0.15 percent HF (Figure 14) with those for 0.4 percent HF (Figure 15). For the 0.4 percent HF concentration the gain coefficient reached a maximum on the P(9) lines whereas P(8) was the maximum at 0.15% HF. Since the rotational and translational temperature history of both cases were essentially the same, the higher rotational quantum number required for the maximum gain on the 0.4% HF was due to the smaller ratio of the upper to lower vibrational level concentrations (N_v/N_{v-1}), when compared to the 0.15% HF case. Except for the shift in rotational line, it is seen that the maximum gain and the time dependence of the gain coefficient are computed to be roughly the same for the two different values of HF concentration.

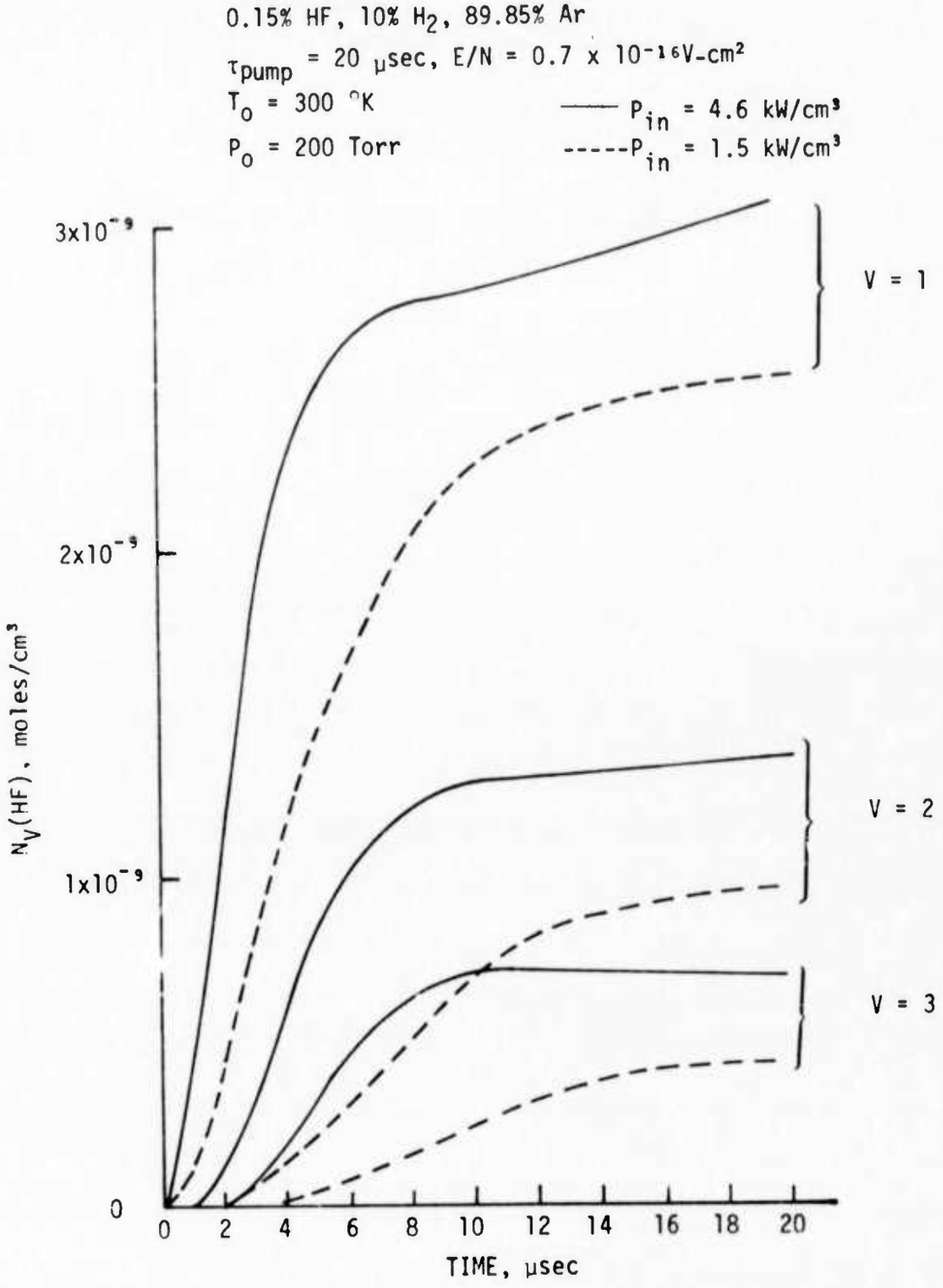

Figure 13. Computed Populations of HF Vibrational Levels Versus Time During a 20 μsec Electric Discharge Excitation Pulse

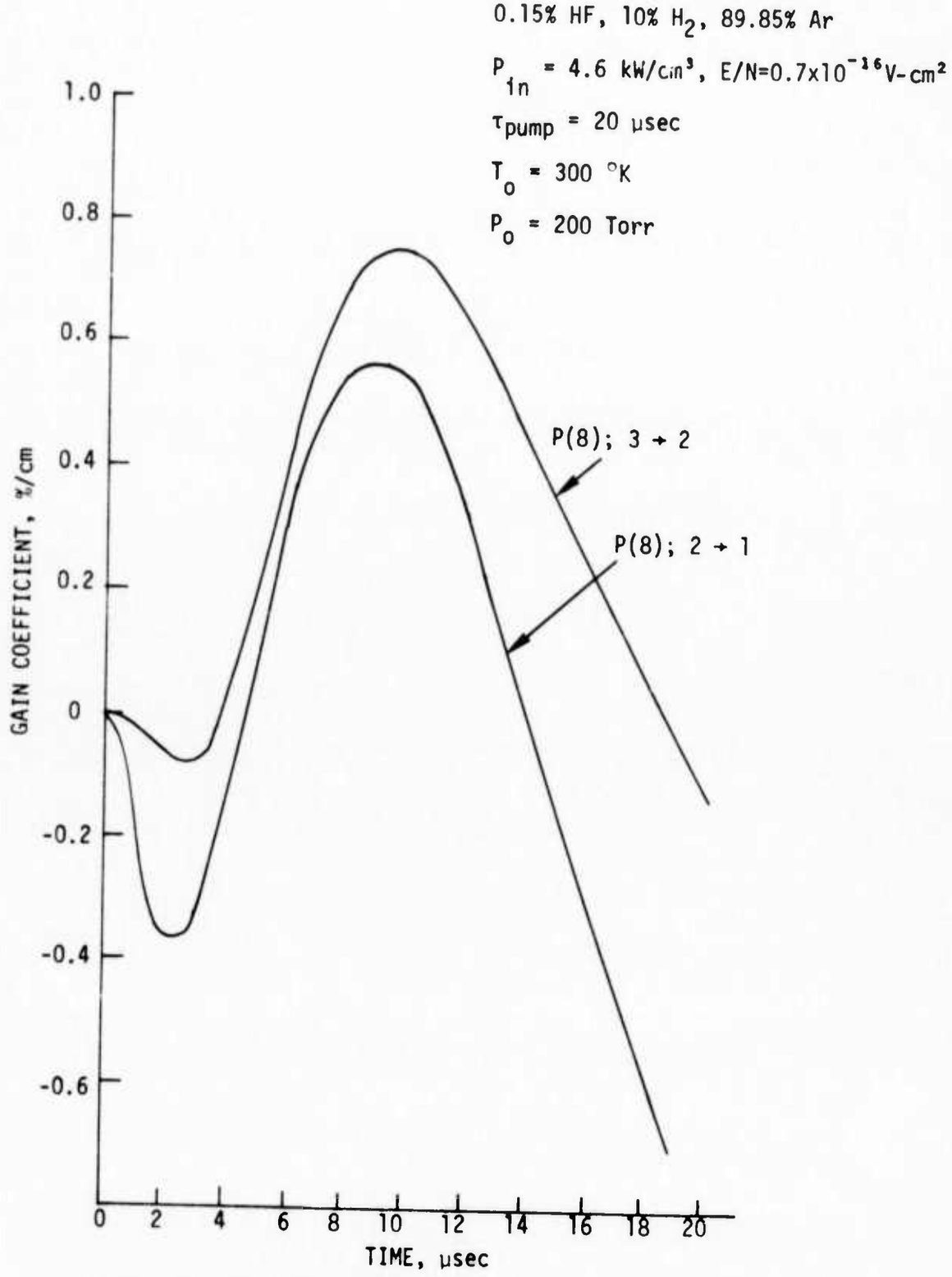

Figure 14. Computed HF Optical Gain Versus Time During a 20 μsec Electric Discharge Excitation Pulse in a 0.15 Percent HF Mixture

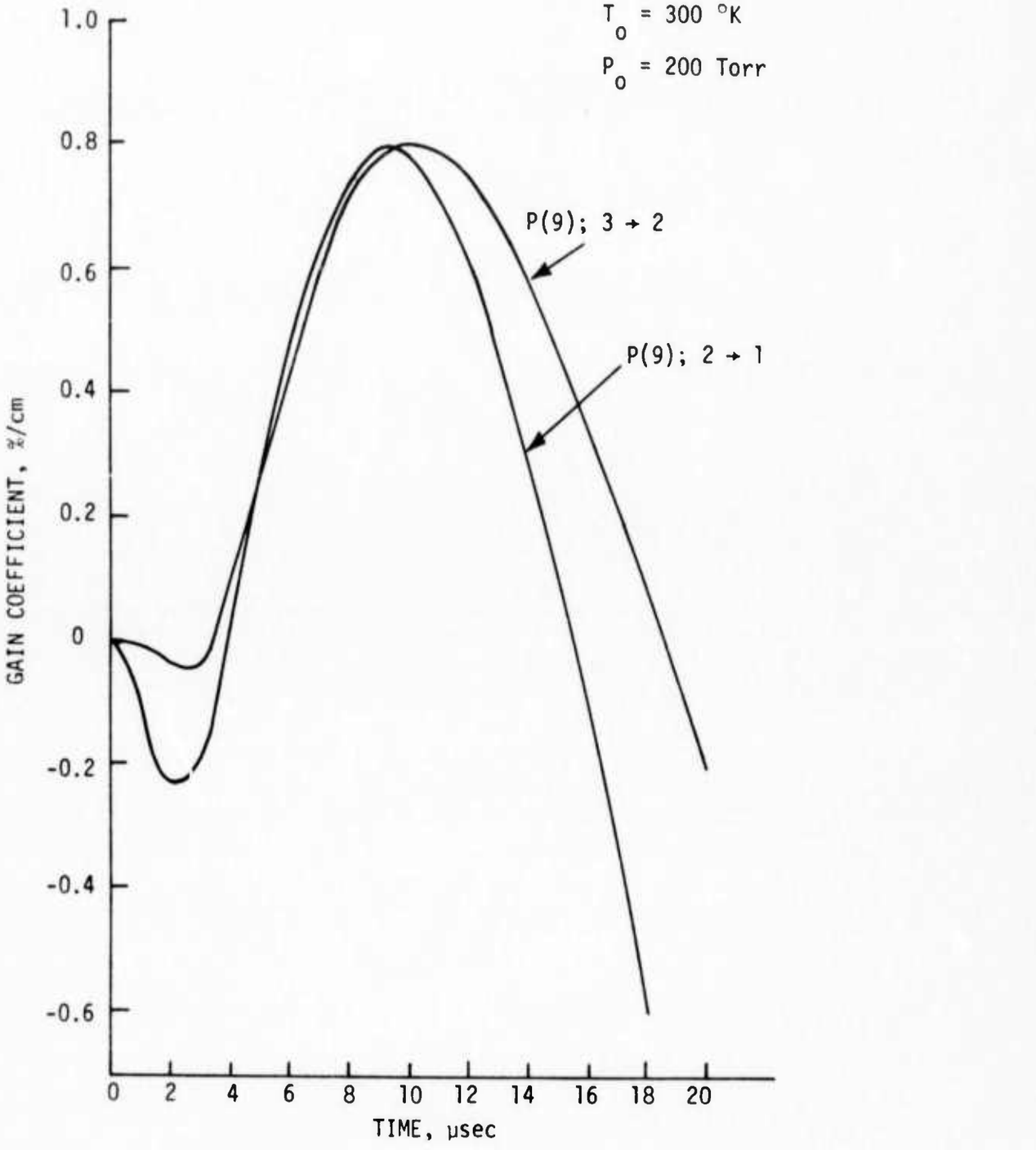

Figure 15. Computed HF Optical Gain Versus Time During a 20 μsec Electric Discharge Excitation Pulse in a 0.4 Percent HF Mixture

Effect of Direct HF Pumping

In order to study the effect of direct electron impact pumping of HF on the temporal behavior of the HF gain coefficient, a fractional power ranging from 0.5% to 3% was assumed to be added directly to HF vibration by the electric discharge. This energy input was distributed to the first and second vibrational levels of HF. The results of this analysis are shown in Figure 16. It is seen that the 0.5% energy input into HF(v = 1), which implies that the inelastic collision frequency of electrons with HF is about 1/2 of that for H_2, only slightly alters the gain history. However higher input rates, including pumping of the first two HF vibrational levels, lead to much higher peak gain coefficients and earlier crossover times (crossover from negative to positive gain coefficient). At the highest direct pumping rate, 1.5% of the total power into each of the first two HF vibrational levels, the gain coefficient becomes positive after less than 0.1 μsec of pumping. These results, together with the experimental observation that the laser onset time was 5.5 μsec for a high Q cavity ($g_{threshold} \simeq 0.1\%/cm$), suggest that less than one percent of the electrical discharge power goes into direct HF vibrational pumping. However, this conclusion is quite tenuous because many effects were not included, for example the effects of superelastic collisions of electrons with HF and the effects of direct rotational excitation of HF.

2.3.5. Laser Emission Calculations

The maximum laser power output on two adjacent vibrational transitions as a function of power input was analyzed for a 50-cm length optical cavity and 10 percent output coupling. It is seen in Figure 17

0.15% HF, 10% H_2, 89.85% Ar
P_{in} = 4.6 kW/cm^3, E/N = 0.7 x 10^{-16} V cm^2
P = 200 Torr, T_o = 300 °K

Direct Pumping of HF, % of P_{in}

	HF(1)	HF(2)	$\nu_c(HF)/\nu_c(H_2)$
I	0	0	-
II	0.5	0	0.54
III	0.5	0.25	0.68
IV	0.5	0.5	0.81
V	1.5	1.5	2.44

P(8), 2 → 1

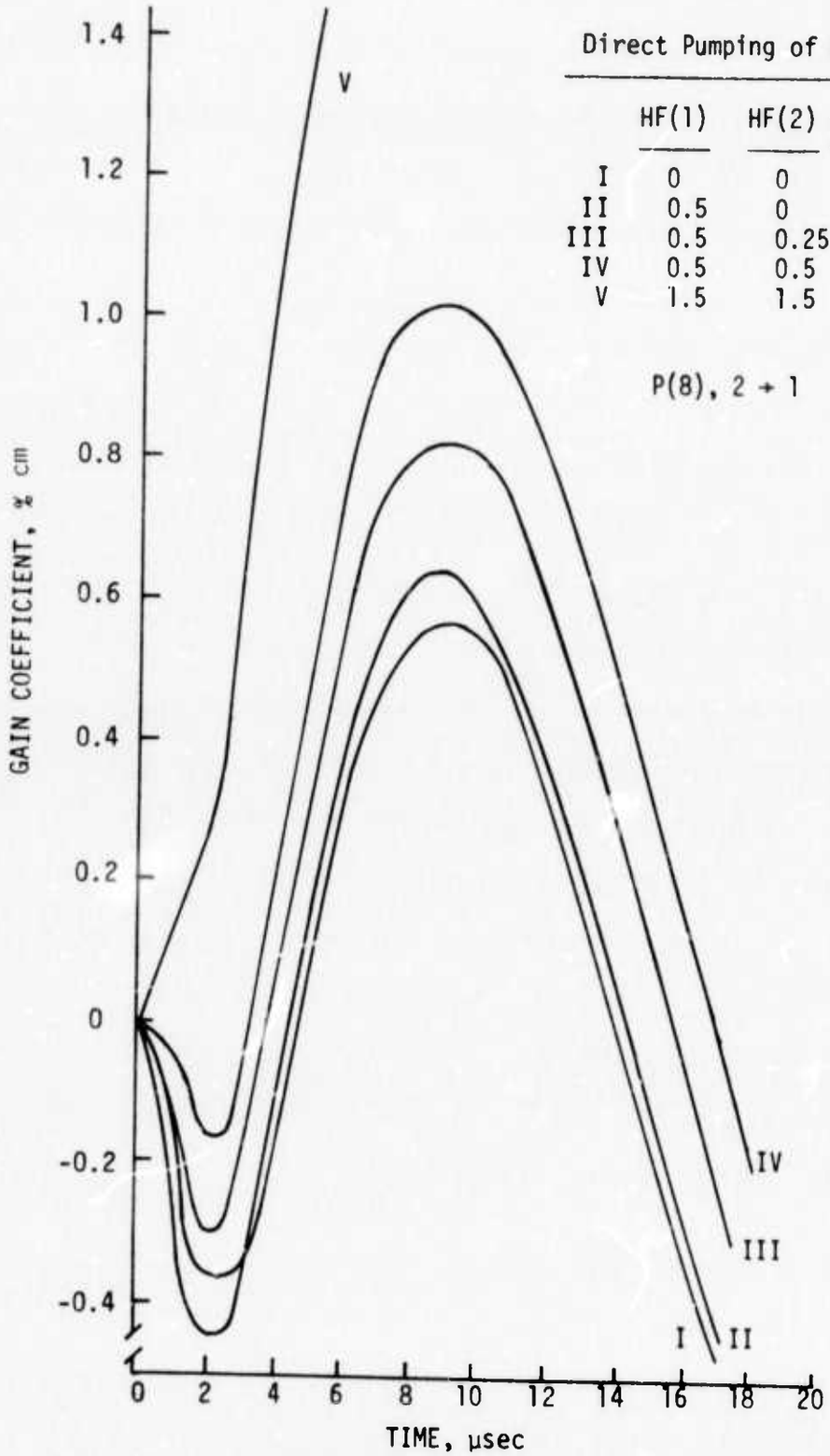

Figure 16. Computed HF Optical Gain Versus Time as a Function of Direct Electron Impact Excitation of HF Vibration

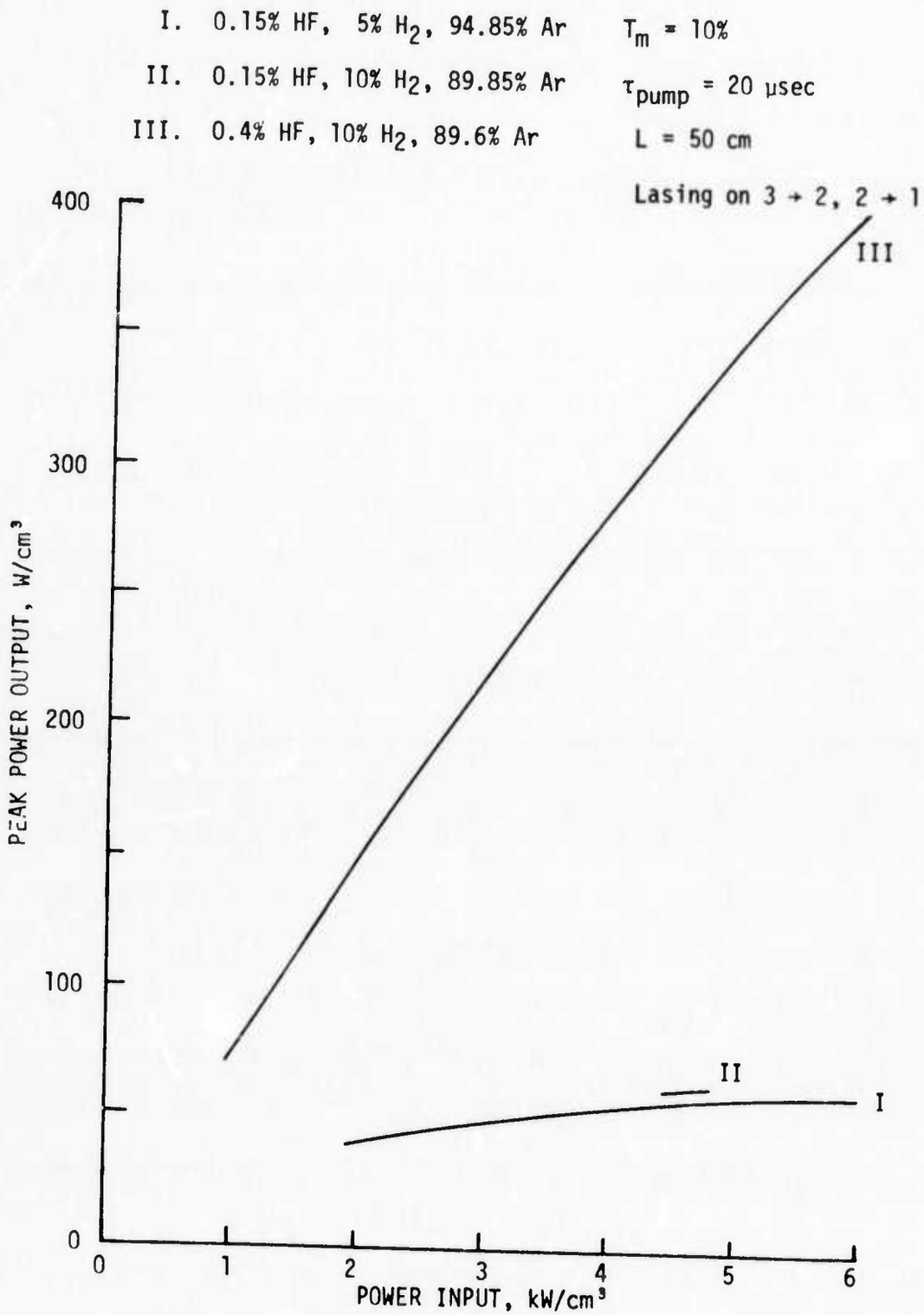

Figure 17. Computed Peak Laser Power Output Versus Power Input for Several HF Laser Gas Mixtures

that the peak power output for the 0.4% HF mixture is 4 to 6 times more than that for a 0.15% HF mixture at equivalent power input levels, even though the low intensity gain coefficients are within 30% for the two mixtures.

The computed efficiency of power extraction for the 0.4% HF is about 7%, whereas for the 0.15% HF the efficiency varies from 2% at low power levels to 1% at high power levels, as seen in Figure 18. This efficiency is representative of the power output at peak power; however the overall efficiency is lower since the laser turn-on time varies from 5 μsec at high power input levels to 9 μsec at low power input levels.

2.4. HF and DF Laser Emission Measurements

2.4.1. Experimental Arrangement

Laser cavity tests were conducted using all three of the electron beam configurations described in Appendix A. No laser emission was observed using the short (14 cm) optical path thermionic cathode electron gun, as described in the first semi-annual report (Ref. 7). Laser emission was first observed in HF and DF electric discharges using the 5-tube plasma diode electron gun. Following this, laser output measurements were also made using the uniform, rectangular (10 cm x 50 cm) plasma diode electron gun. The optical arrangements for both of the 50 cm long devices were the same and are discussed here as applied to the 5-tube plasma diode.

In Figure 19 a schematic is shown of the electron-beam-stabilized electric discharge chamber together with the optical arrangement used for

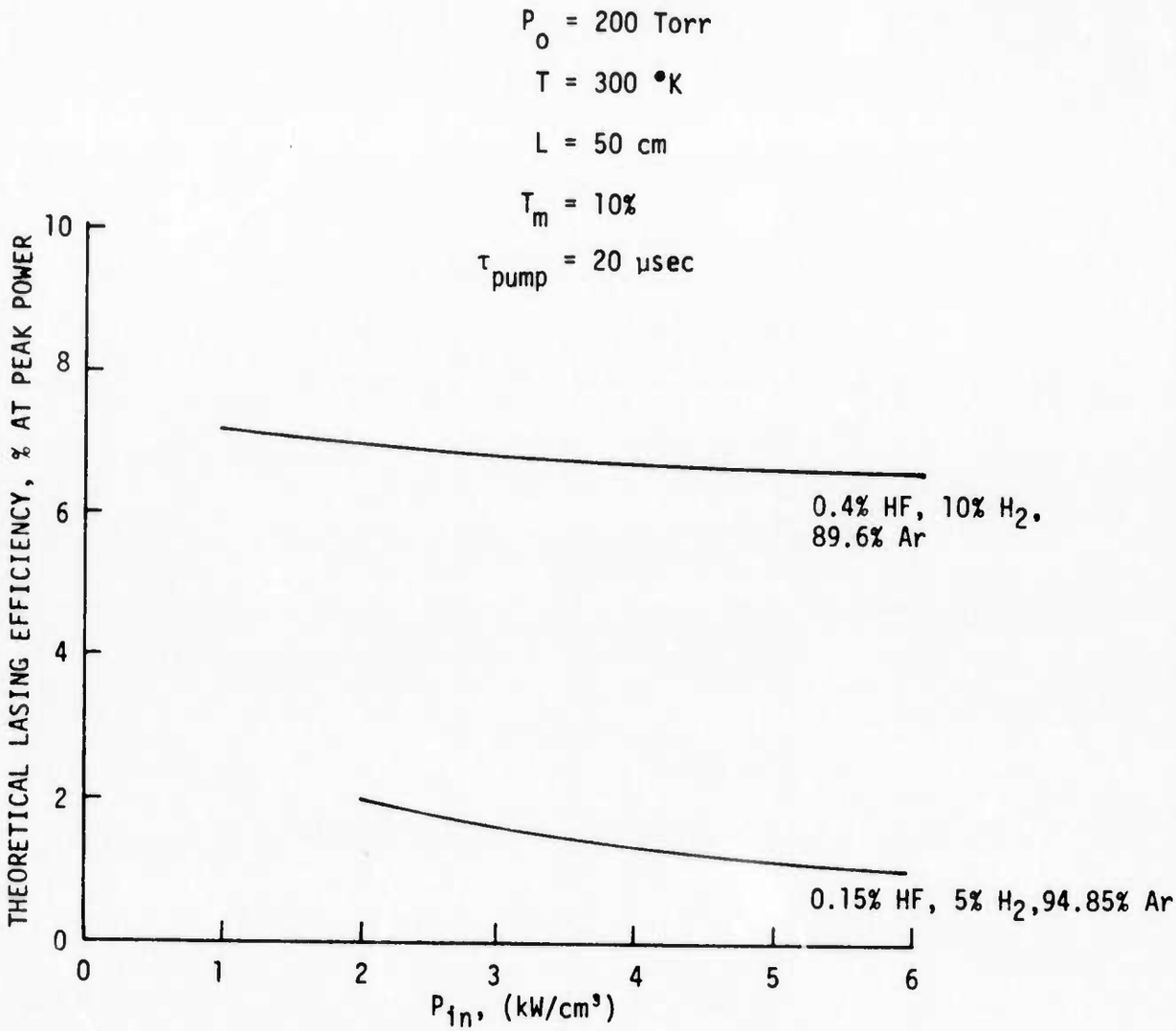

Figure 18. Computed Peak Laser Efficiency Versus Power Input

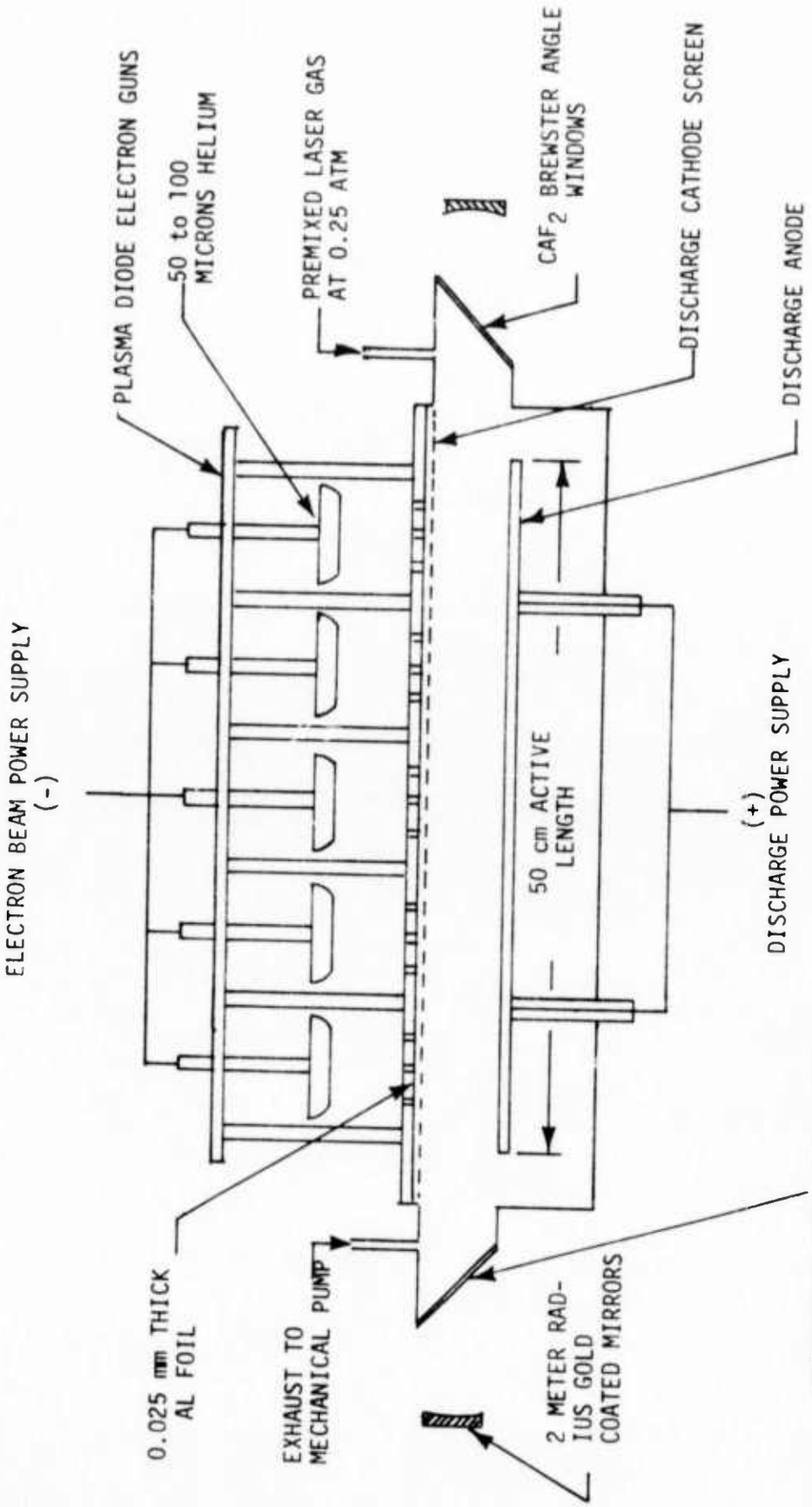

Figure 19. Schematic of Plasma Diode Electron-Beam Stabilized Electric Discharge Cell and Laser Cavity

high-Q laser cavity tests. A flat aluminum screen was located adjacent to the e-beam foil window and served as the discharge cathode. A rounded, 5-cm x 50-cm aluminum anode was supported by insulating feed throughs mounted on the rectangular aluminum discharge chamber. An electrode spacing of 2.5 cm was generally used. A premixed laser gas mixture was introduced at one end of the discharge chamber and removed at the opposite end. With a chamber pressure of about 200 torr the gas flow provided a time interval of about 2 minutes to replace the gas volume in the chamber.

The optical arrangement included two 5-cm diameter CaF_2 windows at the Brewster angle (55 degrees) and two 2.5-cm diameter gold-coated mirrors spaced 1.5 meters apart and each having a 2-meter radius of curvature. The clear aperture was about 2.0 cm in diameter. This provided a stable, high-Q resonator that covers a broad wavelength range. The laser cavity intensity was monitored by directing the light scattered by one of the CaF_2 windows into a 1/4-m Jarrell-Ash monochromator with a spectral resolution of 0.002 μm. The monochromator signal at the exit slit was monitored by a cooled (77 °K) gold-doped germanium detector.

Gas Handling System

The gas handling system is shown schematically in Figure 20. The hydrogen fluoride purification system was constructed out of monel tubing and cylinders; however, brass and steel valves were used for controls. Prior to use, the entire vacuum system for HF handling was passivated using ClF_3 at 1 atmosphere pressure. A small oil diffusion pump provided a 10^{-3} torr vacuum in the entire purification section. Heating tape was wrapped around the monel tubing sections, and dewars with boiling water were used to bake out the monel storage bottles in order to speed the pump

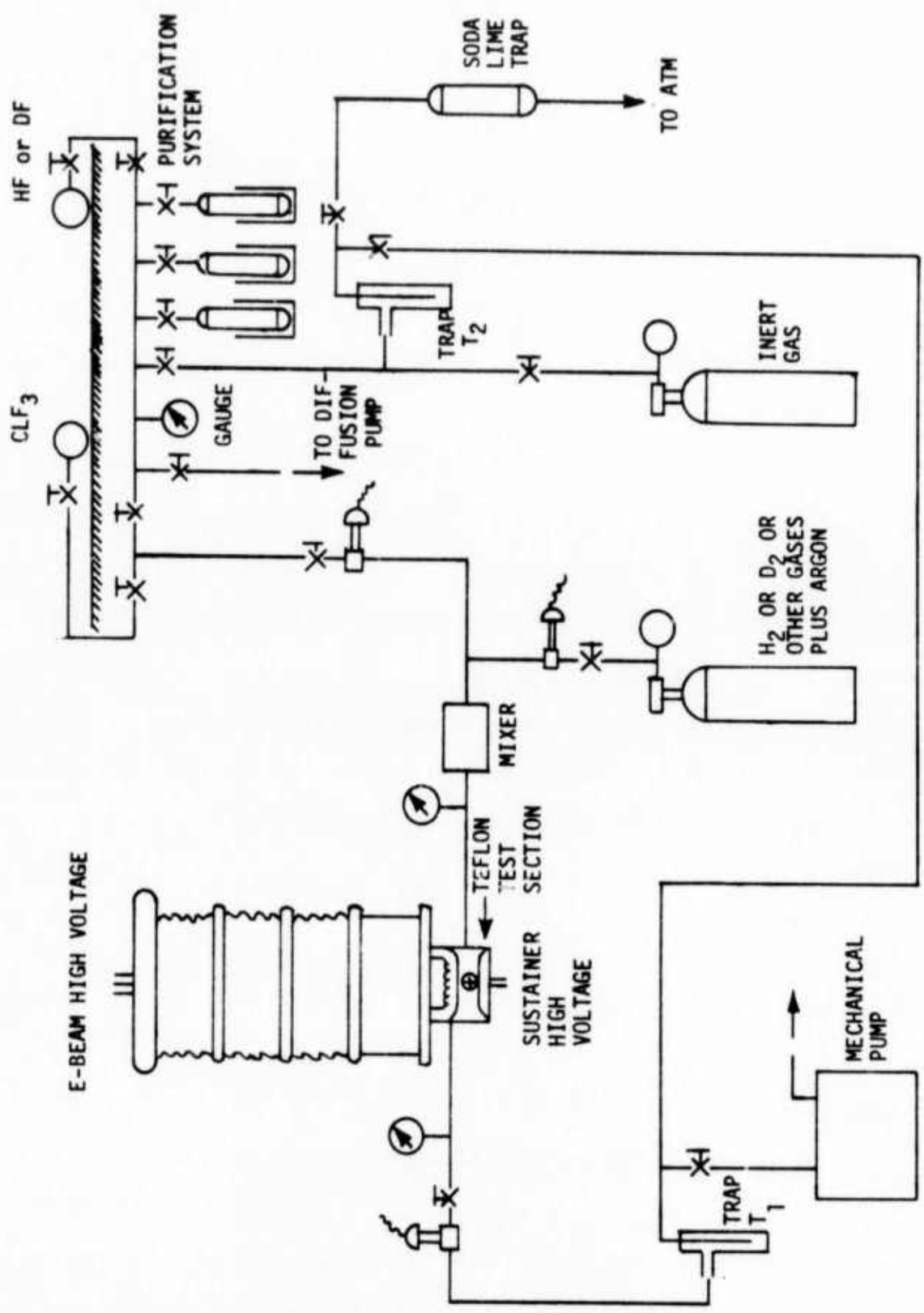

Figure 20. Schematic Diagram of Gas Handling System as First Used on the **Thermionic E-Beam Facility**

down operation. An NRC thermocouple gauge was used to monitor pressures below 1 torr, and a Marsh Instrument Co. Type 100 M, monel gauge could be used from 10 torr up to a pressure of 30 psig.

For safety reasons, the chlorine trifluoride and hydrogen fluoride supply tanks (Matheson Gas Co.) were installed outside the building, but adjacent to the fume hood used for gas handling. Hydrogen fluoride was withdrawn from the storage tank and frozen down at liquid nitrogen temperatures into one of the monel storage tanks. All non-condensible gases were pumped away by the diffusion pump to a pressure (measured by the NRC gauge) of 10^{-3} torr. By replacing the nitrogen coolant with a dewar filled with a chloroform slush, the HF could be brought up to its equilibrium vapor pressure (approximately 12 torr) at the chloroform melting point (-63.5 °C). Liquid nitrogen was gradually mixed with the chloroform to maintain it at this temperature. Approximately 2-3 percent of the HF was discarded once it had reached 15-25 torr vapor pressure, and a bottom fraction of 5-10 percent also was not used at the completion of the distillation from chloroform slush temperature to another monel tank held at liquid nitrogen temperature. Occasionally a second distillation was performed, but no significant change in discharge behavior or light emission characteristics was observed when this was done.

Any HF gas to be disposed of was collected and frozen in a trap (T_2, Figure 20) and was then removed by warming the trap to room temperature. Dry nitrogen or helium was used to flush the HF through a soda lime reactor and was exhausted to the atmosphere. After 5 to 10 minutes of this gas purge, the trap was evacuated by the mechanical pump.

Argon (Airco 99.995 percent), hydrogen (Airco, 99.999 percent), and nitrogen (Airco, 99.99 percent) gases were used without further purification. The HF was used from the monel storage vessel at an HF pressure of 500 torr and mixed with the Ar/N_2 or Ar/H_2 gas in a flowing system. Monel tubing was used to carry the HF to the mixing station and the mixture to the test section. A short length (50 cm) of polyethylene tubing was used just prior to the test section. The test cell filling rate was approximately 100 torr/minute. Exit gases were passed through a liquid nitrogen cooled trap (T_1), and later transferred to trap T_2 for disposal at the conclusion of an experiment.

Electric Circuitry

A block diagram of the electrical system built for the five tube plasma diode and the electrical discharge cell is shown in Figure 21. The electron gun was driven by a 4 stage Marx bank which was initiated with no delay by the gate output of an oscilloscope. The effective capacitance of the Marx bank was 0.1 μf at a voltage of about 130 kV. The same oscilloscope gate output fired both the electrical discharge bank (100 μf capacitor) and the electrical discharge dump through variable time delays.

2.4.2. Measurements of Electron Attachment to HF

The effect of electron attachment to HF was determined experimentally by measuring the electrical discharge current in the test cell as a function of HF concentration. This was carried out initially in the 10-cm x 10-cm thermionic cathode electron gun facility. The basic gas mixture used was 20% hydrogen, 80% argon at a pressure of 190 torr.

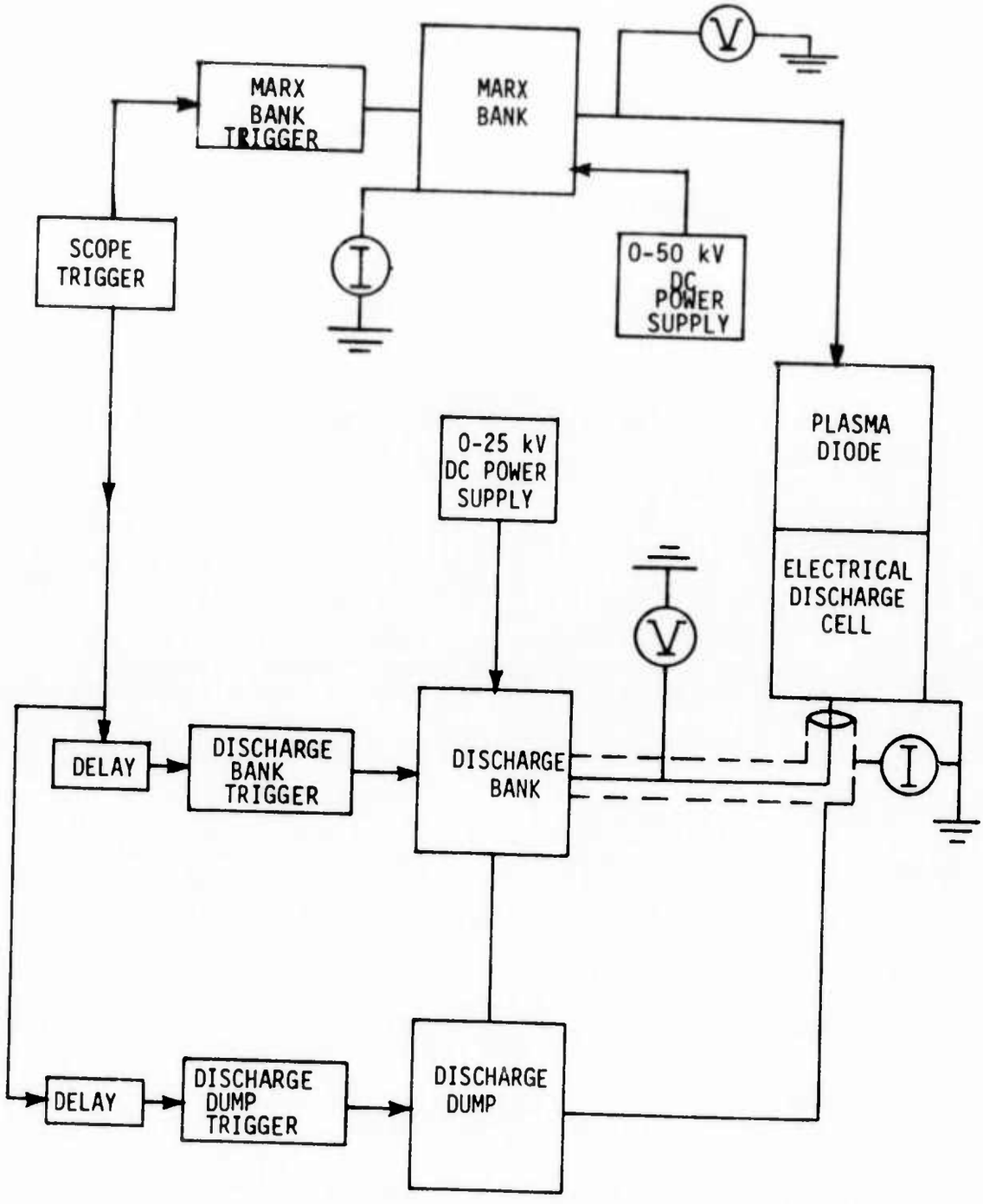

Figure 21. Block Diagram of the Electric Circuitry Used with the Plasma Diode Electron-Gun and Electrical Discharge Cell

A voltage corresponding to a value of E/N of 2 x 10^{-16}V-cm^2 was applied to the test chamber. The electron beam was operated at a voltage of 125 kV and an average current density in the gas of 2 mamps/cm^2. The initial data obtained in this facility indicated an electron attachment rate coefficient for HF of 1.5 x 10^{-12}cm^3/sec, as described in more detail in the First Semi-Annual Report (Ref. 7).

Subsequently, more careful measurements of the HF concentrations and the e-beam current density were made in the higher current ceramic and five-tube plasma diode devices and yielded considerably higher values of the attachment rate; a value of 10^{-10}cm^3/sec was obtained in Ar/H_2/HF (89/10/0.2) mixtures at values of E/N ranging from 0.5 to 1 x 10^{-16}V-cm^2. This rate is based on a calculation which uses the measured discharge current density without HF present to equate the e-beam production rate ($j_e \Sigma g_i N_i$) to the dissociative recombination rate ($\alpha N_{e_o}^2$). N_{e_o} is the value of the electron density without HF, and is derived from the discharge current, J_o, where $J_o = N_{e_o} \bar{v}_D q_e$. The electron density with HF present, N_e, is found in an identical fashion from the discharge current, $J_{HF} = N_e \bar{v}_D q_e$. By balancing the electron production and loss rates at a known HF concentration, the following equation was solved for the HF attachment rate, β,

$$\alpha N_{e_o}^2 = \alpha N_e^2 + \beta N_e N_{HF} \qquad (12)$$

Values of 3 x 10^6 cm/sec and 1.1 x 10^{-7} cm^3/sec were used for $\bar{v}_D$ and α, respectively. The results are summarized in Table V.

Table V

Electron Attachment Rate Coefficients Obtained From Discharge Current Measurements in HF Gas Mixtures at 200 Torr

GAS MIXTURE	DISCHARGE CURRENT (A/cm^2)	E/N ($V\text{-}cm^2$) x 10^{16}	β (cm^3/sec)
Ar/H_2, 90/10	12.3	0.4	
$Ar/H_2/HF$, 89.65/10/0.35	9.3	0.6	0.7×10^{-10}
Ar/N_2, 90/10	11.9	0.5	
$Ar/N_2/HF$, 89.7/10/0.3	11.2	0.5	2×10^{-11}
Ar/H_2, 90/10	8.8	0.4	
$Ar/H_2/HF$, 89.85/10/0.15	6.1	0.5	1.5×10^{-10}
Ar/H_2, 90/10	11.2	0.8	
$Ar/H_2/HF$, 89.85/10/0.15	9.2	0.9	1.04×10^{-10}

It is surprising to find that the HF attachment rate coefficient in $Ar/H_2/HF$ mixtures is so large (about $10^{-10}cm^3/sec$). However, the threshold energy for the attachment process ($e^- + HF \rightarrow H + F^-$) is 2.4 eV and the characteristic electron energy at an E/N of approximately 0.7×10^{-16} $V\text{-}cm^2$ is 2.0 eV for a 90/10 Ar/H_2 mixture (Section 2.2). Therefore, a significant portion of the electrons will have energies in the range necessary for dissociative attachment of HF. Nitrogen can effectively reduce the electron distribution function at energies above 2 eV for a 90/10 Ar/N_2 mixture, and, as seen in Table V, the attachment rate measured at moderate values of E/N ($0.5 \times 10^{-16} V\text{-}cm^2$) in $Ar/N_2/HF$ (89.7/10/0.3) mixtures is smaller by a factor of about 5 than in $Ar/H_2/HF$ mixtures.

The attachment rate for HF(v = 1) can be higher than for HF (v = 0), since approximately 0.5 eV of the 2.4 eV threshold energy is available in the vibrational energy mode of the molecule. Electron attachment for vibrationally excited HF could have a high probability due to the crossing (Ref. 30) of the calculated HF and HF^- potential curves. Since the HF^- potential energy curve is repulsive, dissociative attachment will result. This mechanism would lead to an increasing attachment rate as the HF vibrational excitation increases. However, the decrease in the discharge current with added HF is uniform throughout the current pulse, rather than steadily changing; thus the effect of HF vibrational excitation on the attachment rate is not noticeable in the present experiments.

It is concluded from these measurements that a high electron beam current density is required to provide a high electron density in the presence of high HF concentrations. However, the attachment problem

with HF is considerably less severe than it is for HCl, which exhibits a rate coefficient of 10^{-10} cm^3/sec in an Ar/N_2/HCl (89/10/0.3) mixture (Ref. 31).

2.4.3. Time Resolved Spectral Measurements of Laser Emission in HF and DF Mixtures

Laser emission from HF was not observed in the initial experiments that were carried out in the thermionic cathode electron gun facility. This was due to the short optical path (14 cm) and to the low e-beam current density in the gas (5 to 10 ma/cm^2) which resulted in a low discharge current. To overcome these limitations the 5 tube plasma diode electron gun facility was constructed which provided a total optical path of 50 cm and an average e-beam current density of 25 to 50 ma/cm^2. The laser cavity experiments were conducted using the arrangement described in Section 2.4.1.

Laser cavity oscillation was verified by observing a change in intensity of more than 3 orders of magnitude when the cavity mirror furthest from the detector was blocked. A means for optimizing the laser cavity mirror alignment, at the HF laser wavelengths, was found using chemical laser emission from a mixture of Ar/H_2/SF_6. This mixture will lase for a time duration of about 50 μsec using the electron beam alone to dissociate SF_6 and produce vibrationally excited HF by chemical reaction. Following the mirror alignment procedure laser emission was observed in Ar/H_2/HF mixtures by V-V pumping using an e-beam sustained electric discharge to vibrationally excite H_2. Laser emission from HF was also produced in Ar/N_2/HF, N_2/HF and Ar/HF mixtures, and from DF in Ar/D_2/DF and Ar/DF mixtures. In the following paragraphs the dependence of HF and DF laser emission on gas mixtures

and discharge parameters is discussed along with the laser wavelengths observed and possible mechanisms responsible for these observations.

$Ar/H_2/SF_6$ and $Ar/D_2/SF_6$ Chemical Laser Emission

Dissociative electron attachment of low energy electrons in SF_6 is an effective way of producing F atoms for the chemical laser reaction $F + H_2 \rightarrow HF^{\dagger} + H$. Hence we found that the 5-tube plasma diode electron beam source was sufficient to produce HF laser emission in $Ar/H_2/SF_6$ mixtures, without the use of an applied electric field. The application of an electric discharge voltage caused no change in laser emission and drew no measurable discharge current because of the high electron attachment rate constant for SF_6. An $Ar/D_2/SF_6$ mixture readily produced DF laser action as well.

A typical oscilloscope trace is shown in Figure 22, indicating long pulse laser emission at high pressure (200 torr), which would provide a useful probe laser. A single plasma diode tube having an effective excitation path length of only 8 cm was also used to produce HF laser emission. The chemical laser output lasted about 50 μsec, corresponding to the duration of significant electron beam current through the foil.

Detailed spectral measurement of the emitted laser lines were made using an 87/10/3 $Ar/H_2/SF_6$ gas mixture at 200 torr. The observed lines, using the entire plasma diode, are given in Table VI. Although the lines observed here are not the same as those observed in the HF electric discharge laser (see below and Table VII), it is very likely that a cavity with a grating could be used to select the desired lines. This approach would provide a useful probe laser, since it can be operated at the same

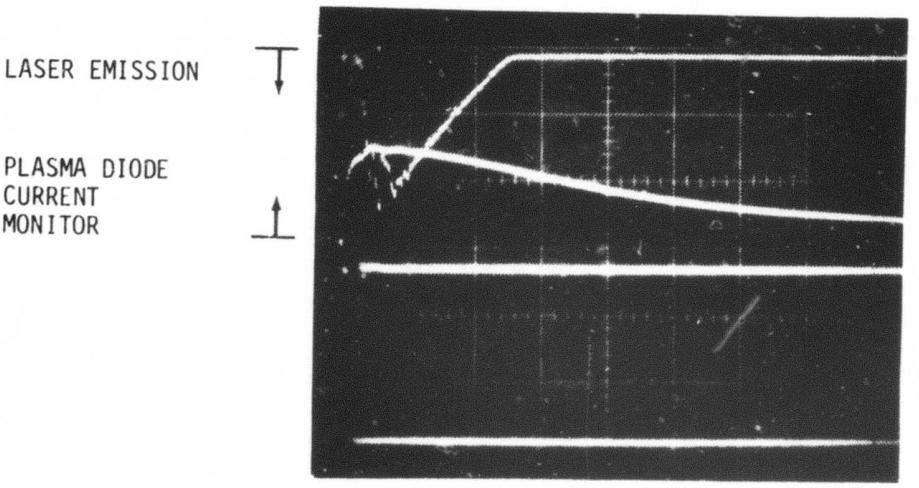

Figure 22. HF Laser Emission on All Lines from $Ar/H_2/SF_6$ Gas Mixtures at 200 Torr Pumped Directly by External Electron Beam Excitation Alone (Time Scale - 20 μsec/div)

pressure and with the same diluent gas as used in the electric discharge laser, thereby providing the same line shift. In addition the long duration of this chemical probe laser would permit optical gain or absorption to be measured throughout the electric discharge pulse.

Table VI

Spectroscopic Measurements of Chemical Laser Emission in $Ar/H_2/SF_6$ Mixtures

(Gas Pressure 200 Torr)

Transition V	Transition P(J)	Wavelength, μm	Time Duration* (μsec)
2-1	5	2.795	6-16
	6	2.832	13-42
3-2	5	2.926	7-23

*Relative to start of electron beam pulse.

Ar/H_2/HF and Ar/HF Electric Discharge Laser Emission

In accord with the theoretical predictions on which this experimental work was based, HF laser emission at 2.8 to 3.1 μm was produced by electric discharge excitation of gas mixtures containing predominantly argon, about 10 percent H_2, and less than 1 percent HF. The first observations of HF laser emission were made using the 5-tube plasma diode electron gun facility. The total gas pressure ranged from 50 to 760 torr, and the initial gas temperature was 295 to 300 °K. A slow gas flow was maintained to clear out the discharge chamber between pulses.

The added HF (0.2 to 0.5 percent) had a measurable effect on the electric discharge current, indicating that dissociative attachment to HF was comparable with dissociative recombination of molecular ions under these conditions. This was discussed in more detail in Section 2.4.2. The applied electric field (E/N) ranged from values of 0.3×10^{-16} to 0.7×10^{-16} V-cm^2 and resulted in maximum average electrical discharge

currents of 8 to 10 A/cm^2. The electrode spacing was 3 cm and the anode was 5 cm wide by 48 cm long.

The laser lines observed in various gas mixtures are shown in Table VII. Only P-branch lines were seen. The times given in Table VII are referred to the start of the electrical discharge pulse in the laser gas and represent the time of onset and the time of termination of laser emission for a single set of operating conditions in each gas mixture.

In Table VII it is seen that laser emission often occurs simultaneously on more than one rotational line of a particular vibration band. This indicates a partial lack of rotational equilibration, although the continuing shift from lower to higher J values throughout the pulse duration indicates that the rotational distribution follows the rising gas temperature. This effect is similar to that observed in pulsed HF chemical lasers by Suchard (Ref. 32). It is also seen in Table VII that there is considerable correlation between laser emission on $P_v(J)$ and emission on $P_{v-1}(J+1)$, indicating significant cascade coupling.

Laser emission from HF was also produced by electric discharges in mixtures containing only Ar and HF, demonstrating that direct electron impact excitation of vibration of HF is effective in producing a partial inversion in the low vibrational levels of HF at room temperature. For this mixture the optimum E/N was only 0.1 x 10^{-16} V-cm^2 and the electrical discharge current density was about 4 A/cm^2. Higher values of E/N could not be used in Ar/HF mixtures due to early formation of an unstable electrical discharge. It was found that HF concentrations greater than 0.5 percent led to little or no laser emission because of the rapid V-R,T decay rate of HF. The observed spectral lines for Ar/HF mixtures are summarized in Table VII.

Table VII

Time Resolved Spectroscopic Measurements of the Vibration Rotation Lines Observed in HF and DF Electric Discharge Lasers (Gas Pressure, 200 torr; time in μsec is given in parentheses)

Transition		Wavelength, μm	Gas Mixture				Wavelength, μm	Gas Mixture	
V	P(J)	HF	$Ar/H_2/HF$	Ar/HF	$Ar/N_2/HF$	N_2/HF	DF	Ar/DF	$Ar/D_2/DF$
1-0	9	2.823			(25-57)		-		
2-1	7	2.870		(10-32)	(6-44)	(12-28)	-		
	8	2.911	(8-22)	(12-40)	(8-66)		-		
	9	2.954	(11-32)				3.837	(17-43)	
	10	2.999	(22-38)				3.876	(17-42)	
	13	-					3.999		(27-36)
3-2	6	2.964		(9-13)	(6- 9)		-		
	7	3.005	(10-18)	(10-28)	(7-45)		-		
	8	3.048	(10-27)		(32-48)		3.927	(15-24)	
	9	3.094	(24-32)				3.965	(15-46)	
	11	-					4.046		(15-30)
	12	-					4.089		(20-36)
	13	-					4.134		(32-38)
4-3	10	-					4.141		(15-25)
	11	-					4.184		(19-34)

The laser cavity intensity (on all lines) is shown as a function of time in Figure 23 for $Ar/H_2/HF$ and Ar/HF mixtures. Also shown are the e-beam current monitor, which is the internal plasma diode current (the current through the foil shows a much faster fall off after 30 μsec), the applied discharge voltage, and the resulting discharge current density. The laser cavity intensities are relative, and not the same for the two gas mixtures. The laser intensity for Ar/HF mixtures was 1 to 2 orders of magnitude lower than that for $Ar/H_2/HF$ mixtures.

It is evident that both the discharge voltage and current are much higher for the $Ar/H_2/HF$ mixture than for the Ar/HF mixture. It is also seen that the onset time and laser output pulse duration are about the same for the two gas mixtures. The termination of laser emission for Ar/HF mixtures is apparently related to the collapse of the glow discharge, as indicated by the voltage dropoff after about 35 μsec. The termination of laser emission for $Ar/H_2/HF$ mixtures occurs prior to the termination of the glow discharge and is apparently related to the gas heating that has occurred through the direct electric discharge excitation of H_2 rotation, the V-R,T decay of HF and H_2, and the drop off in electric discharge current.

Very weak laser emission from HF was also observed in $Ar/D_2/HF$ mixtures. It was verified that the emission with D_2 was an order of magnitude smaller than that with H_2, indicating the importance of near-resonant V-V transfer from H_2 to HF.

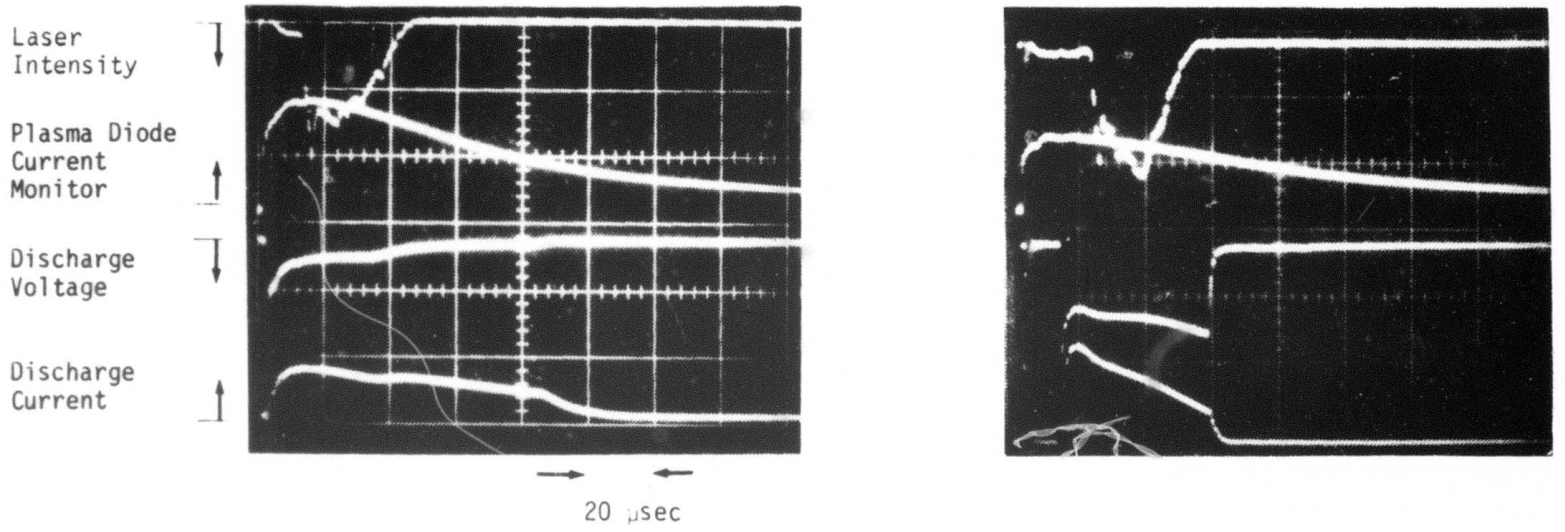

Figure 23. Electric Discharge Excitation of HF Laser Emission in Mixtures of (a) 0.99 Ar and 0.004 HF, and (b) 0.89 Ar, 0.10 H_2, and 0.004 HF. The Discharge Voltage Sensitivity is 700 V/Div and the Discharge Current Sensitivity is 1380 A/Div

$Ar/N_2/HF$ and N_2/HF Electric Discharge Laser Emission

While searching for multiple pulse fluorescence of the first and second positive systems of N_2 observed in $Ar/N_2/HF$ mixtures (see Section 3.3), HF infrared laser emission was obtained at 2.8 to 3.1 μm. The lines observed are summarized in Table VII. Quite surprisingly, a 1-0 line was observed, which indicates a high vibrational temperature among the lowest vibrational states of HF. In Figure 24 the inversion necessary to achieve gain on 1-0 P(9) rather than P(8) or P(10) is shown at various gas temperatures. Assuming only slight heating by the discharge, N_1/N_0 must be approximately 0.2 to 0.25 for the gain to exceed cavity losses.

Gas mixtures were typically 90/10 Ar/N_2 with 0.2 to 0.5 percent HF producing optimum output at an E/N of 0.5×10^{-16} V-cm^2 and discharge currents of 10 A/cm^2. In the absence of Ar, laser output was observed, but at considerably lower intensity; typical values of E/N were 0.5×10^{-16} to 0.9×10^{-16} V-cm^2 and discharge currents ranged from 4 to 6 A/cm^2.

The pumping mechanism operating in the N_2 gas mixtures may be either (1) direct electron impact excitation of HF, with the N_2 serving to create a favorable electron energy distribution function in the discharge, or (2) a two-quantum V-V transfer process from $N_2(v = 2)$ to excite $HF(v = 1)$. The latter has been ruled out through probe laser measurements which showed that the decay of $HF(v = 1)$ following termination of the electric discharge excitation pulse was very rapid and agreed with the decay rate of HF due to collisions with HF and N_2 (see Section 2.5.2). If $N_2(v = 2)$ were a significant source of vibrational energy for HF, the decay of HF vibration would have been much longer.

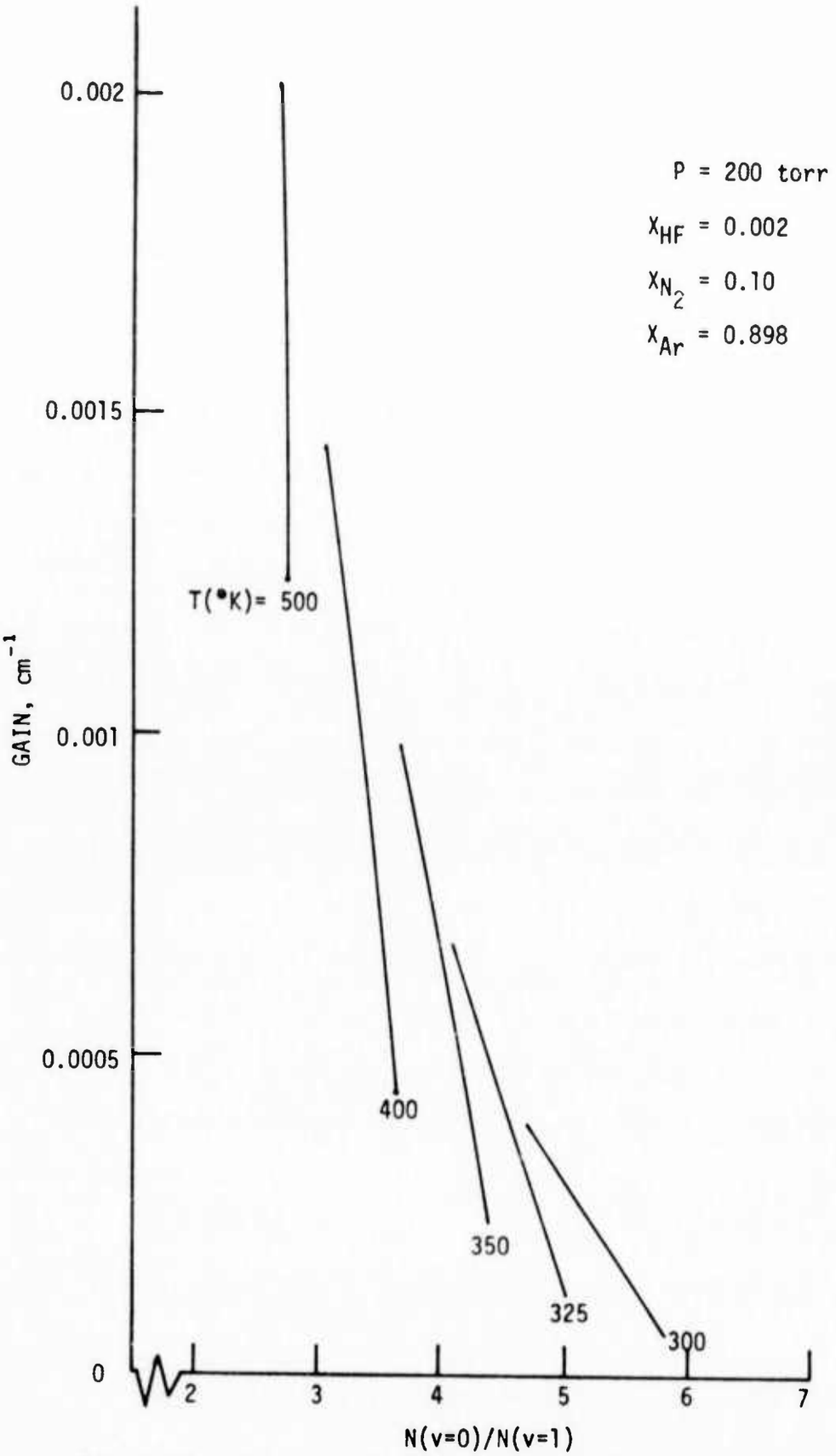

Figure 24. Range of Population Ratios for v = 1 → 0 Gain to be at a Maximum on P(9)

Time resolved measurements of laser cavity intensity for $Ar/N_2/HF$ mixtures are shown in Figures 25(a) and 25(c). It is seen here and in Table VII that the laser pulse duration is longer for $Ar/N_2/HF$ mixtures than for $Ar/H_2/HF$ or Ar/HF mixtures, and that it is apparently terminated by cutting off the electric discharge.

Rotational Equilibration in HF Gas Mixtures

The effect of helium on the total HF laser intensity in a high-Q cavity is shown in Figures 25 and 26. As seen by comparing Figure 25(a) with 25(b), the addition of helium increased the laser cavity intensity by about a factor of 4 in $Ar/He/N_2/HF$ mixtures compared to $Ar/N_2/HF$ for nearly equal values of E/N and discharge current. The e-beam current was adjusted in order to produce equivalent discharge currents at fixed E/N for this comparison, since the added helium reduces the discharge current for a fixed e-beam current. When the e-beam current was not attenuated by running the plasma diode at low voltages and pressures, about the same cavity intensity was observed in $Ar/He/N_2/HF$ and $Ar/N_2/HF$ (compare Figures 25(b) and 25(c)). However it is seen that the $Ar/N_2/HF$ mixture required higher discharge current to achieve the same laser cavity intensity. This is illustrated quantitatively in Figure 26.

The increase in cavity intensity in mixtures containing helium is attributed to rotational relaxation of the HF by helium. Rotational heating of HF by V-R,T decay processes has been observed previously in measurements of vibrational decay of HF (Ref. 33). In those experiments, heavy dilution by argon was required to provide sufficiently rapid rotational relaxation during vibrational decay of HF. In our HF electric

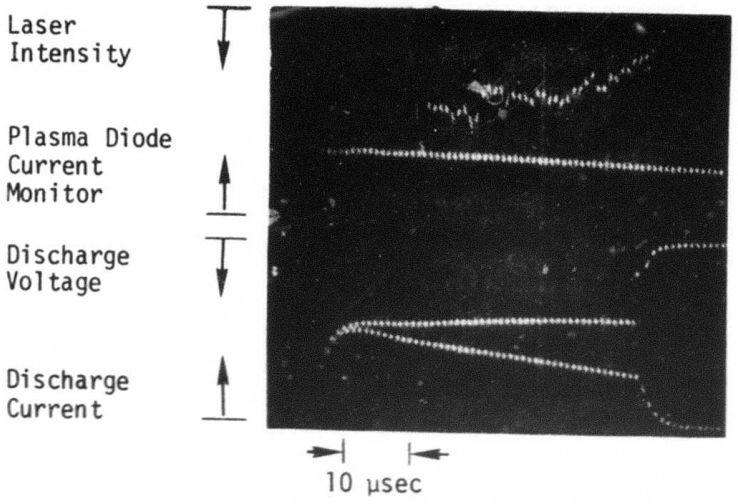

(a)

90/10 Ar/N_2

AT LOW DISCHARGE CURRENT

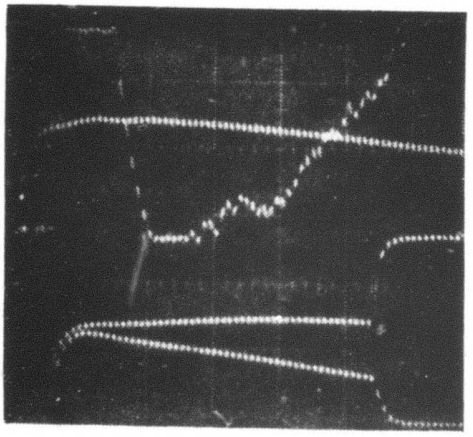

(b)

45/45/10 $Ar/He/N_2$

AT LOW DISCHARGE CURRENT

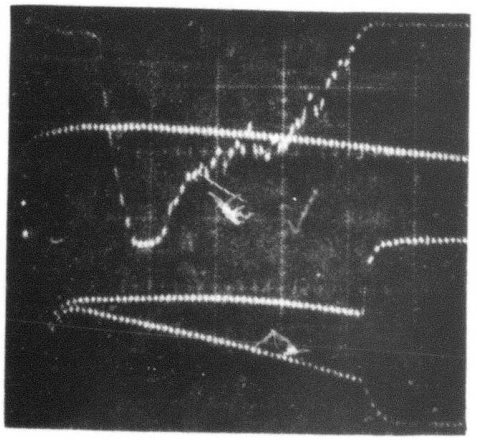

(c)

90/10 Ar/N_2

AT HIGH DISCHARGE CURRENT

Figure 25. HF Laser Cavity Intensity in Ar/N_2 and $Ar/He/N_2$ Mixtures at 200 Torr, Using 0.4 Percent HF

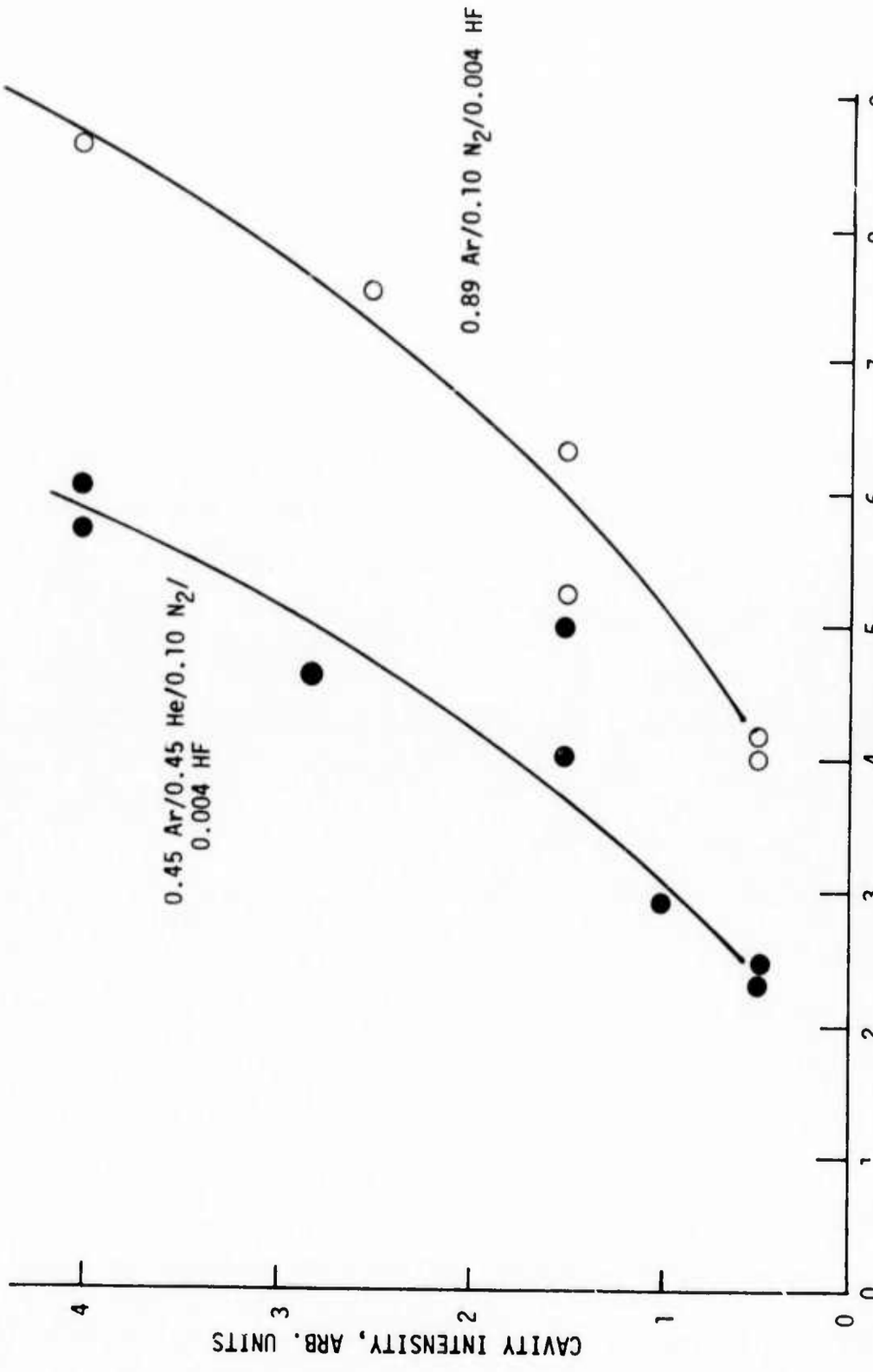

Figure 26. Effect of Helium Diluent on HF Laser Emission at 200 Torr and E/N = 0.7 to 1.0 x 10^{-16} V-cm²

discharge laser strong rotational excitation of HF occurs through V-R,T decay and also by direct electron impact excitation of HF rotation. Thus the addition of helium can reduce the HF rotational temperature by increasing the rate of R-T relaxation. This in turn could increase the partial population inversion responsible for laser emission.

$Ar/D_2/DF$ and Ar/DF Electric Discharge Laser Emission

Using the 5-tube plasma diode electron gun facility, laser emission was also observed in $Ar/D_2/DF$ and Ar/DF mixtures at wavelengths from 3.8 to 4.2 μm. The total gas pressure used was 200 torr, and the DF mole fraction was approximately 0.4 percent. As with the Ar/HF laser, the value of E/N for Ar/DF mixtures was only 0.1 to 0.2 x 10^{-16} V-cm^2 and the discharge current density was about 4 A/cm^2. The optimum E/N for the 92/7/0.4 $Ar/D_2/DF$ mixture was 0.4 x 10^{-16} V-cm^2 and a maximum average discharge current of 12 A/cm^2 was used. The observed wavelengths and onset and termination times are given in Table VII.

Typical oscilloscope traces of DF(3 → 2) laser emission on several rotational lines are shown in Figure 27. It is apparent that maximum laser emission occurs sequentially at increasing J-values throughout the pulse. This indicates significant gas heating and partial equilibration of rotational populations by collisional processes. By contrast, the observed time sequence in $Ar/N_2/HF$ mixtures shows strong laser emission simultaneously on adjacent rotational lines indicating considerably less collisional equilibration of HF rotation in $Ar/N_2/HF$ mixtures.

Addition of only 3 percent O_2 to an Ar/DF laser mixture completely quenched DF laser emission. When an 89/10/0.3 mixture of $Ar/N_2/DF$ was

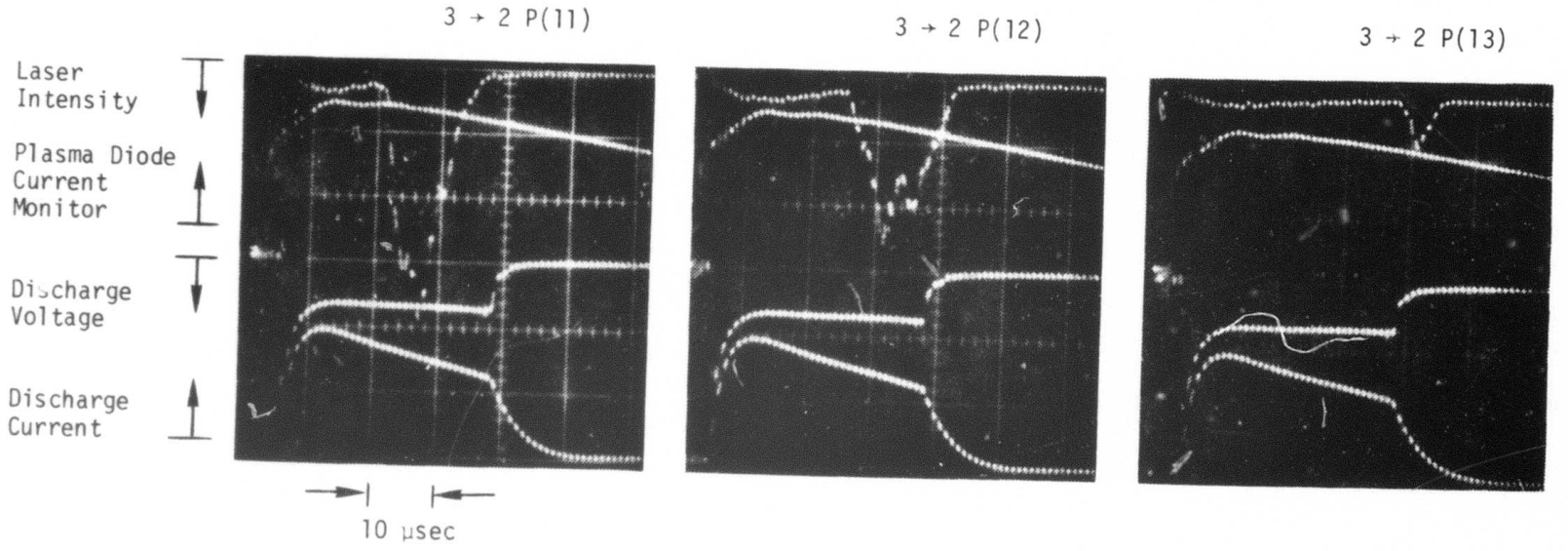

Figure 27. Time Sequence of Laser Emission from $Ar/D_2/DF$ Mixtures at 200 Torr. The Discharge Voltage Sensitivity is 700 V/Div and the Discharge Current Sensitivity is 1380 A/Div.

used, the HF isotopic impurity in the DF supply (about 10 percent) produced laser emission at 2.9 μm, but no laser emission from DF was observed. This confirms the detrimental role of O_2 and N_2 on the DF laser (due to rapid vibrational quenching of DF by O_2 and N_2), and illustrates the importance of careful gas preparation and purification.

The DF laser emission observed in these experiments was achieved by eliminating the use of pre-mixed Ar/D_2 gas stored in conventional mild steel gas bottles. Flowmeters connected directly to the pre-purified argon and deuterium gas tanks by polyethylene tubing permitted mixing of the gases as they were flowing into the discharge chamber. This apparently yielded better gas purity than was achieved with the procedures used previously for pre-mixing Ar/D_2 samples.

HF Laser Emission Using the Ceramic Plasma Diode Electron Gun

HF laser emission observed in the new ceramic plasma diode electron beam apparatus is presented in Table VIII. One new line is observed (2-1 P(11)) and two lines (3-2 P(9), 3-2 P(7)) are missing for an $Ar/H_2/HF$ (89.9/10/0.2) mixture compared to the HF emission from the same mixture in the five-tube plasma diode device (Table VII). The discharge current density for the five-tube device was approximately 10 percent higher than in the ceramic plasma diode. In addition, the value of E/N needed to produce approximately 9 A/cm^2 in the ceramic device was nearly twice as large (approximately 1×10^{-16} $V\text{-}cm^2$) as used in the five-tube device. This indicates a greater degree of dissociation of H_2 for the discharge conditions under which the data of Table VIII were taken.

Table VIII

Time Resolved Spectroscopic Measurements of the Vibration Rotation Lines Observed in HF Electric Discharges in the New Ceramic Plasma Diode Electron Gun

Gas Mixture: $Ar/H_2/HF$ (89.8/10/0.2)
Gas Pressure: 200 torr

Transition Band	J	Wavelength	Time of Laser Emission* (μsec)
2-1	8	2.911	6-13
2-1	9	2.954	7-18
2-1	10	2.999	12-20
2-1	11	3.046	17-19
3-2	8	3.048	8-13

*Relative to the start of discharge pulse.

2.4.4. Laser Output Energy Measurements in HF Gas Mixtures

An optical output coupler was added to the high-Q laser cavity used in the HF laser experiments by introducing a CaF_2 flat between one CaF_2 Brewster angle window and one total reflector. The normal to the CaF_2 output coupler was rotated at various angles in a plane containing the optical axis and the normal to the Brewster window. Thus, the round trip output coupling for both surfaces ranges from near zero at the Brewster angle to a maximum of 12.8 percent at near normal incidence (3.2 percent per surface per pass). With the output coupler at 45 degrees to the

optical axis, the output coupling is 2.3 percent, and with the normal at 30 degrees to the optical axis, it is 7.8 percent. In later experiments a 5-inch focal length CaF_2 lens (2 inches diameter) was used to collect the entire output energy and focus it down into the energy meter.

Output energy measurements were made for $Ar/N_2/HF$ and $Ar/He/N_2/HF$ mixtures using a "rat's-nest" energy meter (sensitivity 0.6 J/mV) having a collecting aperture of 2 cm diameter. For 7.8 percent output coupling, 11 millijoules output was measured for (89/10/0.3) $Ar/N_2/HF$ at 200 torr. This corresponds to about 0.06 percent of the input discharge energy and an output energy density of about 0.3 J/ℓ-atm. An $Ar/He/N_2/HF$ (78/14/7/0.3) mixture under nearly identical e-beam current, discharge voltage, and output coupling gave approximately 65 percent of the output measured without helium. Hence, any effect helium may have on the rotational equilibration of HF (as noted in the previous section) is apparently offset by the reduced discharge current produced by the presence of large helium fractions and/or by an increase in the V-R,T decay of HF caused by the helium.

Laser output measurements were also made for $Ar/H_2/HF$ mixtures (94/5/0.2). Using the same output coupling(7.8 percent) and energy meter described above, 4 millijoules of laser output energy was obtained, which is only about 30 percent of the maximum energy measured for $Ar/N_2/HF$ mixtures. This reduced output energy may be due in part to the nonuniform electric discharge, which produces regions of absorption as well as regions of gain for $Ar/H_2/HF$ mixtures. To overcome the effects of nonuniformity, a uniform, 50-cm long, plasma diode electron beam was constructed (Appendix A).

The e-beam current density supplied by the uniform, ceramic plasma diode was a factor of about 2 less than that delivered by an individual diode section of the five separate tube device. In addition, the maximum operating voltage of the multi-tube plasma diode array was 6 to 8 kV higher than the continuous 50 cm device, which resulted in less scattering of the electron beam in the 5-tube device. As a result, it was necessary to use a higher E/N in the discharge chamber of the uniform, ceramic plasma diode facility in order to achieve comparable electric discharge power input as in the 5-tube facility.

Figure 28 shows that for the same power input into a 94.85/5/0.15 $Ar/H_2/HF$ mixture, the output power obtained in the 5-tube facility was approximately a factor of two higher than that for the ceramic plasma diode facility. In order to make this comparison it was necessary to assume that the active area for the five tube plasma diode discharge was 35 cm long by 5 cm wide (175 cm^2), based on previous measurements of the electron beam current density profile (Appendix A). In order to obtain comparable discharge current densities in the two devices, a higher value of E/N must be used in the ceramic device (by a factor of about 1.5) which causes increased molecular dissociation and is detrimental to laser performance.

Figure 29 shows the laser performance for an 89.8/10/0.15 $Ar/H_2/HF$ mixture in the ceramic plasma diode apparatus. Mixtures containing 5 percent H_2 (Figure 28) show slightly better output power versus input power compared to 10 percent H_2 mixtures (Figure 29). Laser power output for $Ar/N_2/HF$ mixtures, shown in Figure 30 for the 5-tube facility, was a factor of about 1.5 times higher than that obtained from $Ar/H_2/HF$ mixtures. Higher

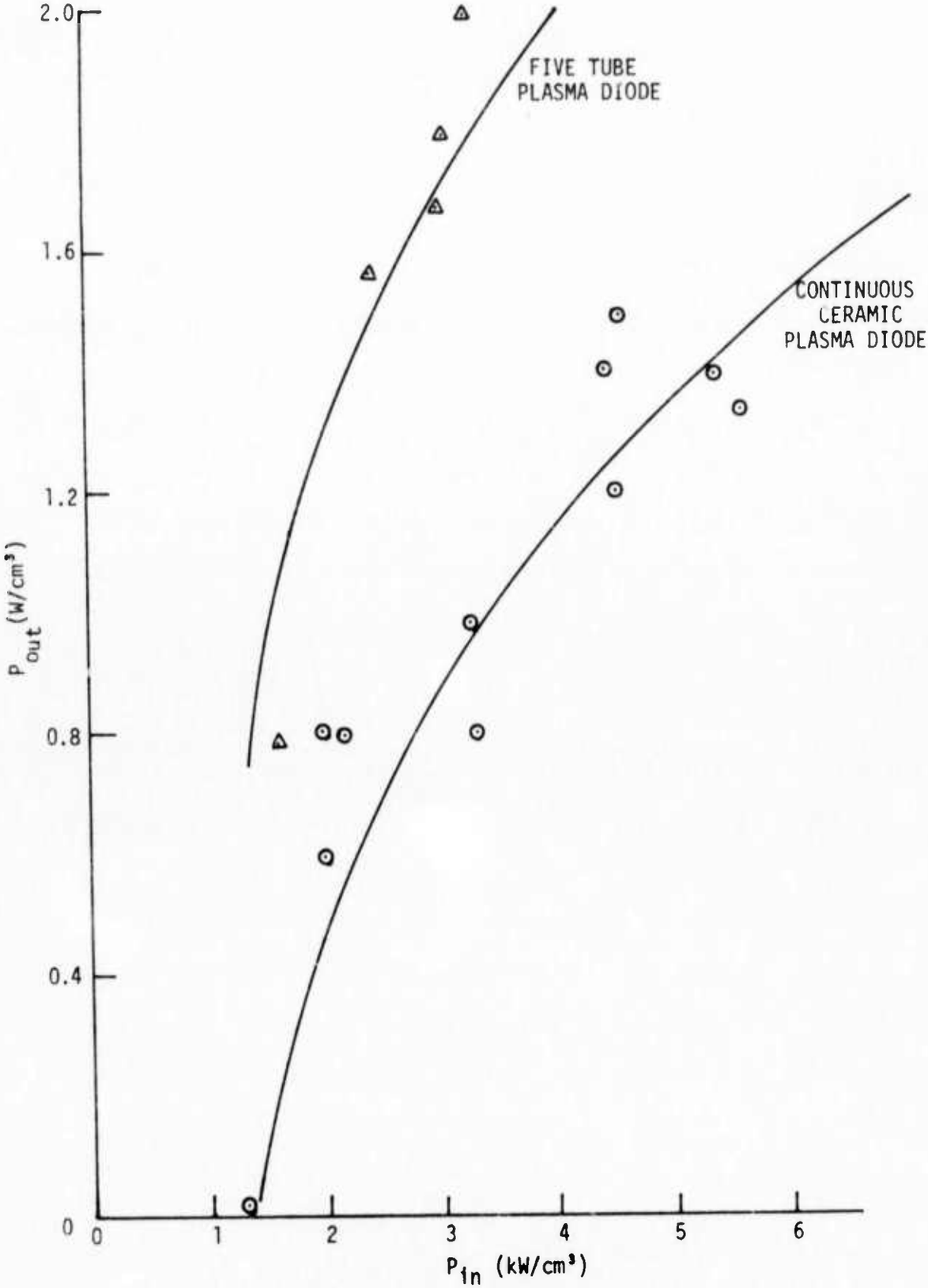

Figure 28. Output Power Measured in the Five-Tube and Ceramic Plasma Diode Devices for $Ar/H_2/HF$ (94.8/5/0.15) Mixtures at 200 Torr Pressure

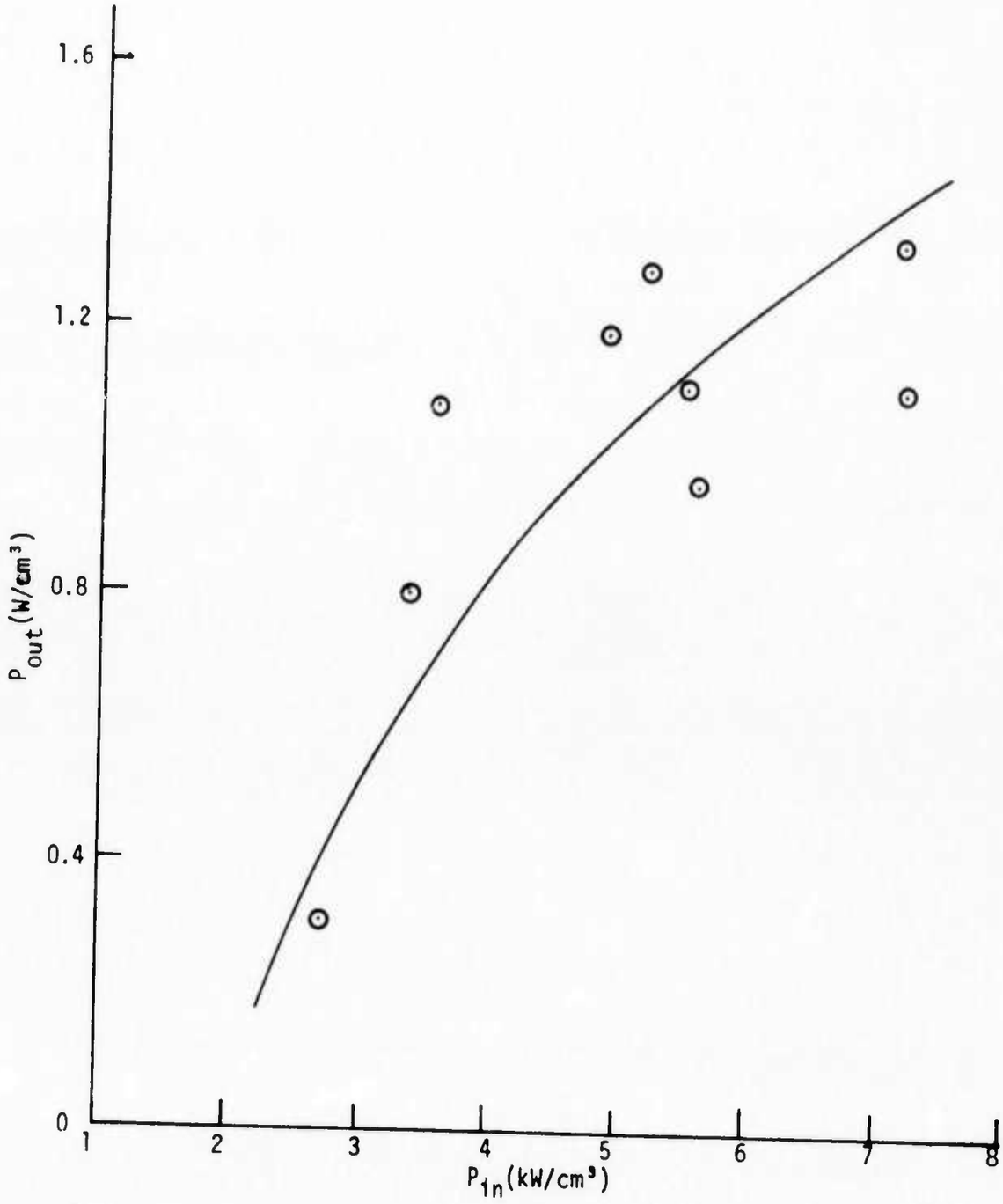

Figure 29. Output Power Measured for an Ar/H_2/HF (89.8/10/0.15) Mixture in the Continuous, Ceramic Plasma Diode Apparatus

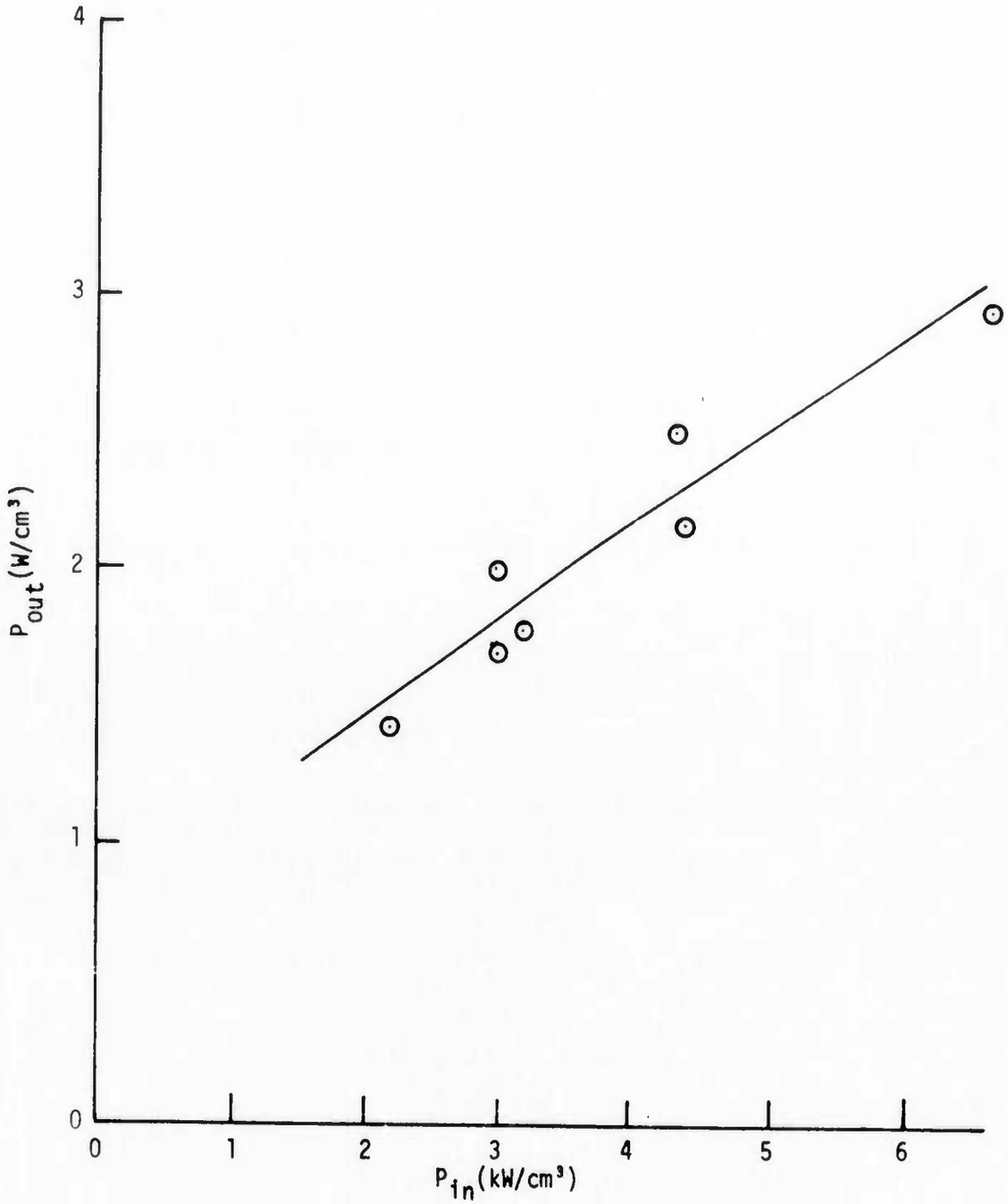

Figure 30. Output Power Measured for $Ar/N_2/HF$ (89.8/10/0.2) Mixtures in the Five-Tube Plasma Diode Apparatus

discharge current densities (13 to 20 A/cm^2) could be obtained in Ar/N_2/HF mixtures than was possible for Ar/H_2/HF mixtures (6 to 11 A/cm^2). In addition the applied E/N for the N_2 mixtures was about 30 percent lower than the optimum value for the H_2 mixtures.

2.5. HF Probe Laser Absorption and Gain Measurements

Time resolved probe laser measurements of HF gain and absorption were made to obtain information on the population of HF vibrational/rotational levels. This information was needed to verify the V-V pumping mechanism in H_2/HF mixtures, to determine the pumping mechanism in N_2/HF mixtures, and to obtain more quantitative information on the V-V and V-R,T rate constants in these mixtures by comparing the results with those obtained from the computer model. The following section describes the experimental measurement of gain and absorption, and summarizes the results that have been obtained. The comparisons with computer calculations are presented and discussed in Section 2.6.

2.5.1. HF Probe Laser Absorption Measurement Technique

A resistor loaded pin laser (Ref.33) was used as a probe for the gain and absorption measurements. The pin discharge initiates the HF chemical laser by dissociation of SF_6 which leads to reaction of F atoms with either H_2 or CH_4. Figure 31 shows the optical arrangement used for the initial measurements that were carried out in the 5-tube plasma diode electron gun facility. The teflon scatterer in front of the monochromator slit was used to eliminate probe laser beam deflection caused

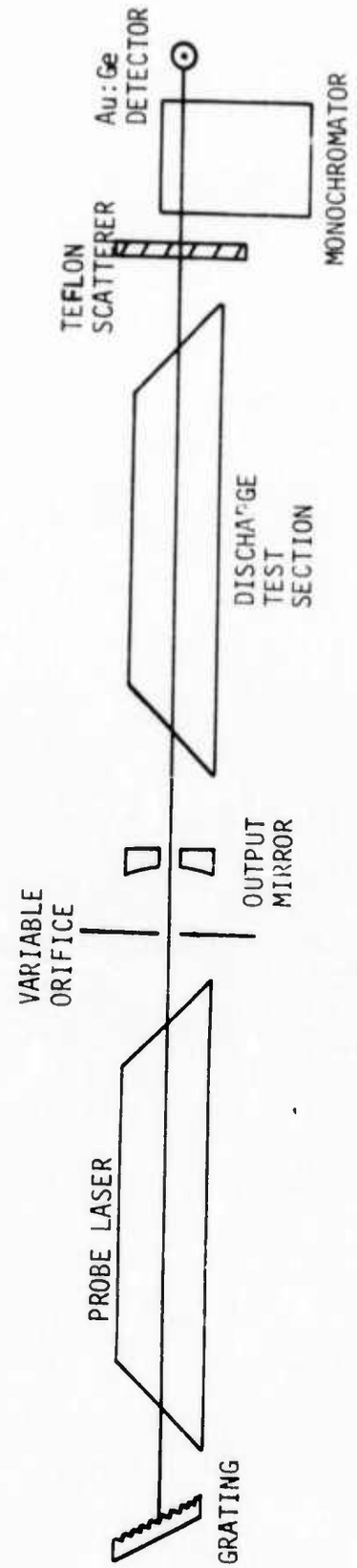

Figure 31. Optical Arrangement Used for HF Probe Laser Absorption and Gain Measurements

by the heated gases in the e-beam discharge chamber. The effect of this deflection was especially evident for $Ar/H_2/HF$ mixtures, where rotational heating was significant and led to a time dependent index of refraction change in the gas, causing severe deflection of the probe laser beam. The teflon scatterer eliminated signal changes at the detector caused by refractive index changes in the gas, as verified by experiments in Ar/H_2 gas mixtures.

Since the probe laser pulse lasted only about 1 μsec, a series of experiments at one operating condition was required to obtain the time history of the gain or absorption in the long pulse electric discharge laser. The accuracy of the measurement depended principally on the reproducibility of the peak intensity of the probe laser pulse. With a variable orifice aperture in the probe laser cavity to improve shot-to-shot reproducibility, the accuracy realized in these initial measurements was 10 to 20 percent. In subsequent measurements taken in the ceramic plasma diode electron gun facility, considerable improvement in the accuracy of absorption data was obtained using the dual detector arrangement shown in Figure 32, which corrected for the shot-to-shot variations in the HF pin laser pulse. The accuracy obtained was then ± 5 percent.

For line selection, a Bausch and Lomb 3.0 μm blazed grating (blaze angle 26 degrees, 45 minutes) was used in the probe laser cavity and a 1/4-meter Jarrel-Ash monochromator was used just prior to the detector. The cavity grating alone was sufficient to isolate individual HF P-branch transitions on the 1-0, 2-1, and 3-2 bands. For convenience, the

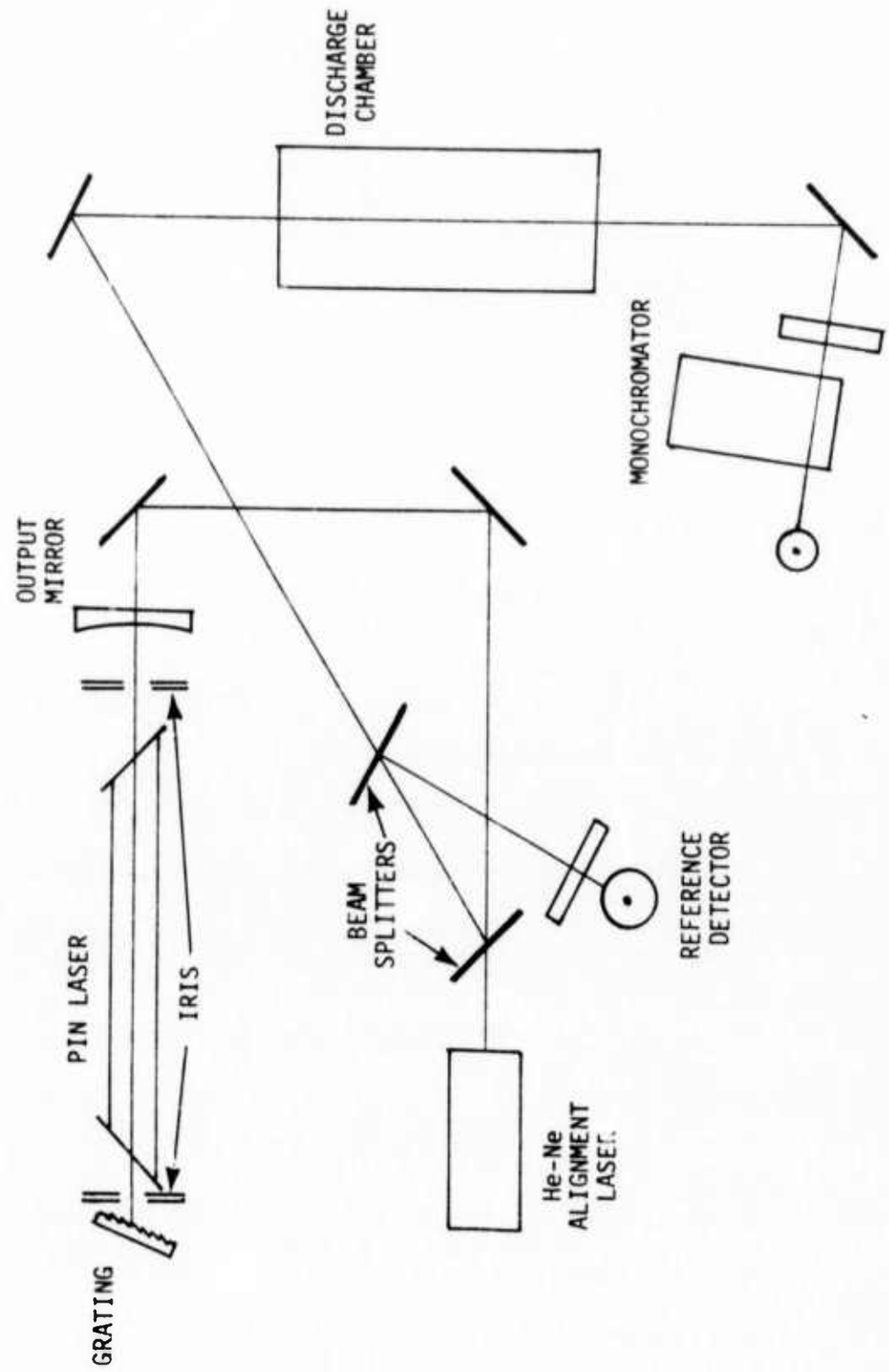

Figure 32. Optical Arrangement Used for the Gain and Absorption Measurements Made with the Continuous, Ceramic Plasma Diode Electron Beam. Two Infrared Detectors Provide a Reference and Signal Channel which Eliminates Problems Encountered in Single Channel Experiments Due to Fluctuations in the Pin Laser Output.

monochromator was left in the optical path for checking the wavelength calibration of the cavity grating.

HF concentrations in the test gas mixtures were measured using the 1-0 P(7) absorption line. This measurement permitted reasonably accurate HF concentration determination even at values as low as 0.1 percent. In subsequent experiments that were carried out in the ceramic plasma diode electron gun facility, the measurement of HF concentrations was improved by using a small, calibrated volume attached to the HF inlet flow system to determine the HF flow rate. This permitted the direct measurement of HF concentration to be compared with the concentration derived from the pin laser absorption measurement, which was used to verify the HF line shift in an argon gas mixture relative to the center of the HF probe laser.

The probe laser could be fired at any desired time during or after the e-beam sustained discharge by a delay circuit. Typically five probe laser pulses were measured prior to a test; reproducibility of these traces was typically 15 percent. The buildup of gain or absorption was mapped by firing the 1 μsec long probe laser once for each discharge pulse in the test gas, which required several oscillograms to be taken for an adequate time history.

2.5.2. Probe Laser Absorption Measurements of HF Vibrational Decay in Ar/HF, Ar/N_2/HF, and Ar/H_2/HF Mixtures

Initially, gain and absorption measurements were made following the discharge pulse in HF test gas mixtures. The decay rate following the

pulse was used to evaluate the qualitative aspects of V-V and V-T processes. The measurements were made using the HF probe laser on 2-1 and 3-2 transitions at various time intervals following the crow-bar of the electric discharge. The electric discharge pulse duration was about 30 μsec at current and voltage conditions comparable to those used to produce laser output as given in Section 2.4. Decay rates of the v=1 and 2 levels of HF were then calculated from the e-folding time of the absorption decay as the vibrational energy of the gas mixture decayed.

Ar/HF Mixtures

The HF vibrational decay measurements obtained in a 99.8/0.2 Ar/HF mixture at 200 torr showed a short decay time (38 μsec) for HF(v=1), in agreement with the calculated decay time for this mixture using the rate constants given in Section 2.3. Hence laser action observed for Ar/HF mixtures is due to electron impact pumping of HF, combined with VV ladder climbing of the HF as found in CO lasers. In contrast to CO systems, HF self-V-R,T deactivation is extremely rapid, and electron attachment to HF is much larger than to CO. For these reasons large HF concentrations probably cannot be used for an efficient, e-beam-stabilized, electrically excited HF laser system.

Ar/H_2/HF Mixtures

In experiments performed with 89/10/0.3 Ar/H_2/HF mixtures at 200 torr, the HF vibrational decay times were all greater than 100 μsec. This verifies that the V-V transfer mechanism for H_2(v) to HF(v) is a dominant factor in the H_2/HF laser. Since the decay time is so long and

involves the decay of the combined H_2 + HF vibrational energy, no simple numerical comparisons can be made. The complete computer model, described previously in Section 2.3, is required for evaluation and interpretation of these data.

Ar/N_2/HF Mixtures

The decay time obtained for an 89/10/0.3 Ar/N_2/HF mixture at 200 torr for HF(v=1) was 21 μsec. This value agrees very well with the V-T decay time (20 μsec) calculated for this mixture using the data of Section 2.3. The rapid decay of HF observed here clearly demonstrates that there is no significant two-quantum N_2 V-V transfer mechanism to pump HF(v) from N_2(v) operating in the Ar/N_2/HF electric discharge laser. Therefore the principal pumping mechanism for Ar/N_2/HF mixtures is direct electron impact vibrational excitation of HF.

2.5.3. Time Resolved Probe Laser Absorption Measurements in Ar/H_2/HF Mixtures

Initial Measurements in 5-Tube Plasma Diode Electron Gun Facility

Measurements of gain or absorption on the 2 → 1 P(5), P(6) and P(7) and the 3 → 2 P(5) transitions were made in 89/10/0.3 Ar/H_2/HF mixtures at 200 torr using a 30 μsec duration excitation pulse at a power input rate of 1.6 kW/cm^3. The experimental results are shown in Figure 33. Gain was not observed at any time on any of the lines studied. This result is consistent with the laser cavity tests made in the same mixture under the same conditions (Section 2.4), which showed no laser emission on the lines monitored in this set of tests.

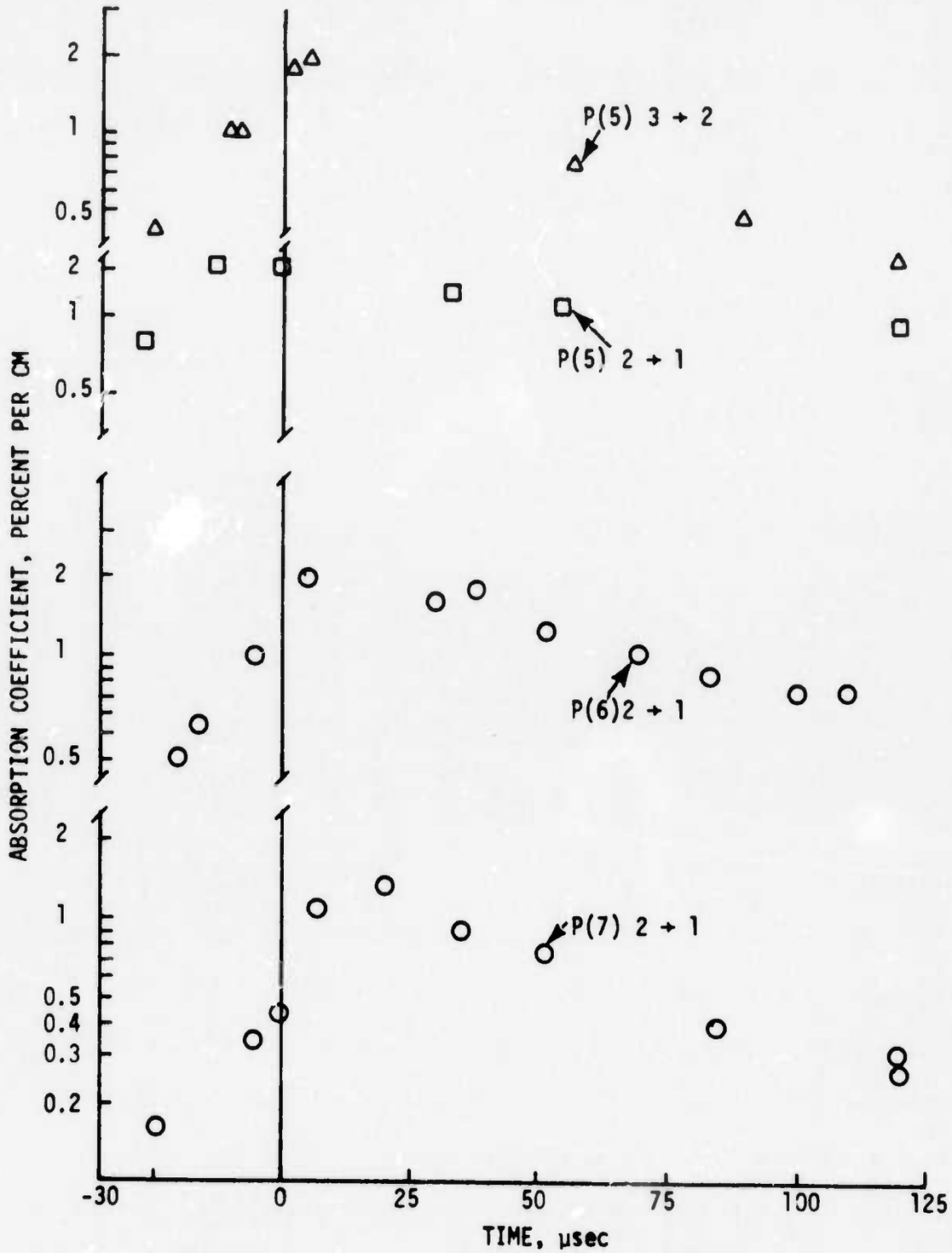

Figure 33. Probe Laser Measurements of HF Absorption in the 5 Tube Plasma Diode Facility for 89/10/0.3 Ar/H_2/HF Mixtures at 200 Torr, using a Power Input of 1.6 kW/cm^3 for 30 μsec at an E/N of 0.43 x 10^{-16} V-cm^2.

The MSNW H_2/HF kinetics model was applied to the conditions of these experiments in order to evaluate the model. This comparison is discussed in Section 2.6. The results of the comparison indicated considerable discrepancy between theory and experiment during the excitation portion of the electric discharge pulse. To be sure this discrepancy was not caused by the nonuniform excitation associated with the spatially nonuniform e-beam current of the 5-tube plasma diode, a second set of absorption and gain measurements was made using the uniform ceramic plasma diode.

Measurements in the Ceramic Plasma Diode E-Beam Facility

Using the uniform ceramic plasma diode electron gun, more accurate probe laser absorption measurements were made in Ar/H_2/HF (89.8/10/0.15) mixtures on the 2 → 1 P(5, 6, 7, and 9) lines. Considerable improvement in the accuracy of absorption data was obtained using the dual detector arrangement shown in Figure 32.

Figure 34 presents absorption data for the 2 → 1 P(6) line of HF made during the discharge pulse in an Ar/H_2/HF (89.8/10/0.15) mixture at 200 torr. The data shown in Figure 34(a) illustrate the good reproducibility (± 5%) and the small beam distortion caused by gas heating (refractive index change) in an Ar/H_2 (90/10) mixture containing no HF. The data shown in Figure 34(b) indicate that the measured absorption coefficient in HF is considerably larger than the data scatter, and that the value changes very little over the time period covered by the measurement. The time independent nature of the absorption coefficient of the 2 → 1

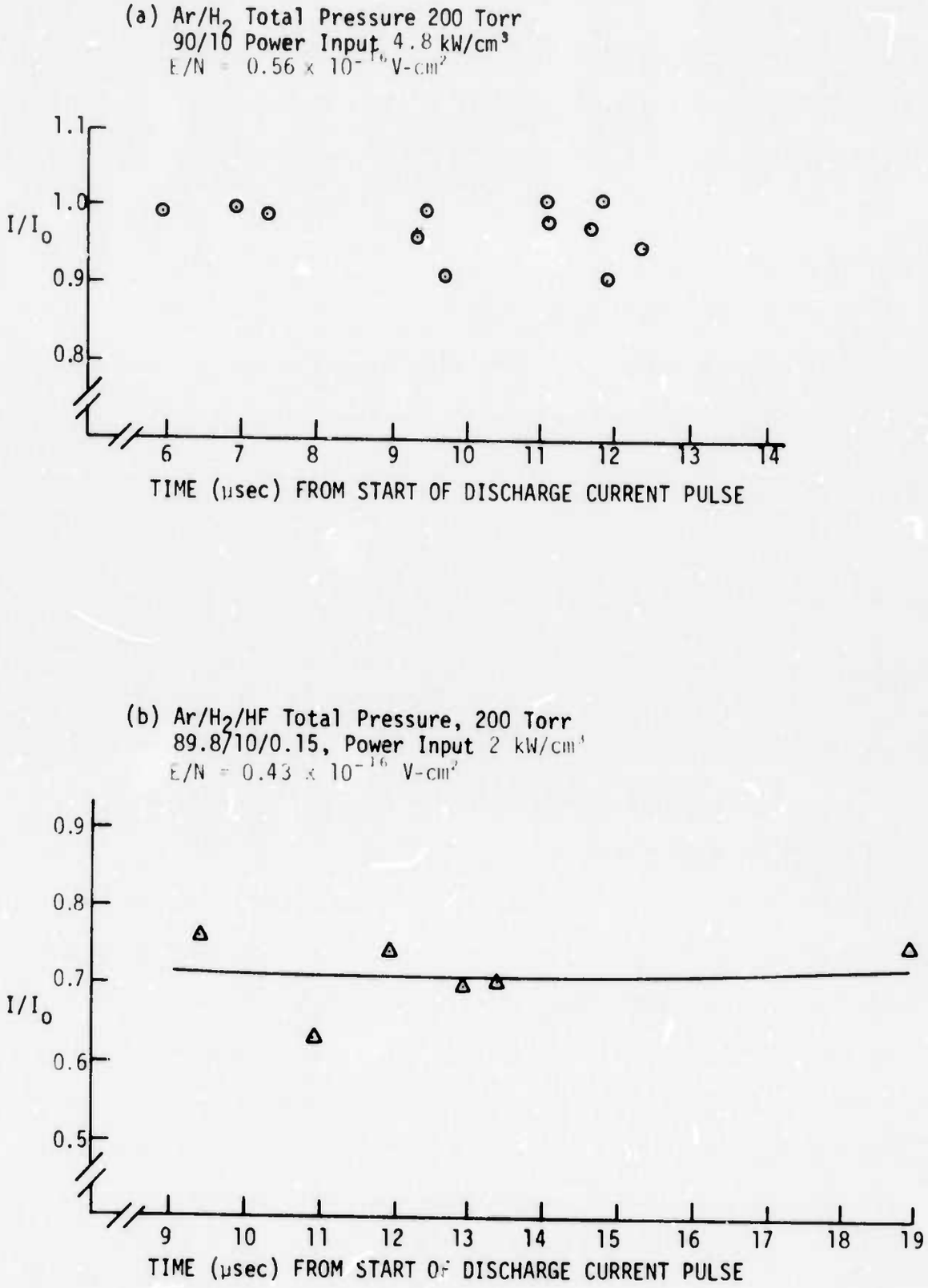

Figure 34. Comparison of Probe Laser Measurements on the 2 → 1 P(6) Line Through Gas Samples With and Without HF

P(6) line is also seen in Figure 35 where data for 2 → 1 P(5, 6, 7, 9) are plotted for a higher power input. The P(8) lines could not be studied because of interference with the nearby 1 → 0 P(11) line. The absorption curves generally show a gradual increase in absorption during the course of a discharge pulse, without any noticeable oscillation characteristics of the type predicted by the analysis described in Section 2.3.

A very pronounced increase in the absorption of all the lines studied occurred immediately following the discharge crowbar. This large perturbation in the absorption was not produced in Ar/H_2 mixtures which did not contain HF. Hence the dramatic change in absorption was probably not due to gas heating effects.

Following the discharge crowbar, absorption measurements made in Ar/H_2 (90/10) mixtures containing no HF showed significant distortion of the sample beam at approximately 30 μsec following a 10 to 15 μsec excitation pulse. Additional diffusers used in the sample beam optical path could correct for this, but this reduced the signal levels below the noise level and therefore was not done. For this reason, quantitative measurements were carried out only during the short (10 to 15 μsec) excitation pulse since gas heating and gas density changes are at a minimum during this time.

Less specific gain measurements were made for the ceramic device using a variable insertion loss and observing the total laser emission. Insertion of two CaF_2 flats at near normal incidence to the laser cavity

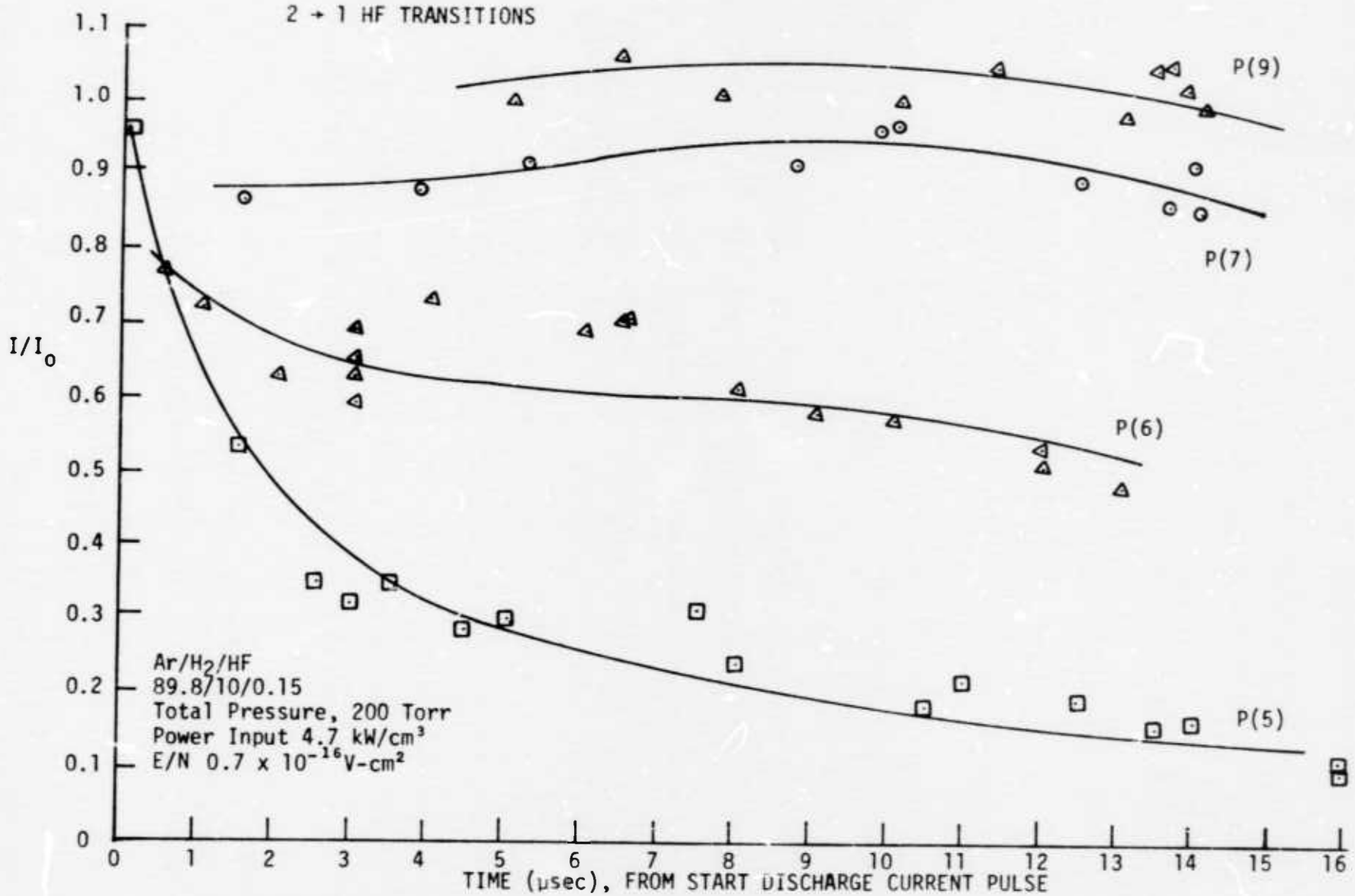

Figure 35. Probe Laser Measurements of HF Absorption in the Ceramic Plasma Diode Facility

produces a 25 percent round trip loss in the cavity. Laser action occurred with this loss, although a time of 10 μsec was required for the laser to reach threshold. Therefore, the single pass low signal gain was about 12 percent, which was within the probe laser measurement sensitivity. Since the probe laser measurements for 2-1 P(9) could not detect significant gain, even though this line did lase (Table VII), it is very likely that a different line, such as 2-1 P(8), 2-1 P(10), or 3-2 P(8), has highest gain. It is also possible that the effect of probe laser beam spread due to gas heating plays a role in the probe laser measurements, and introduces a small apparent absorption contribution.

The probe laser measurements described here are compared with the results of the computer model in the next section.

2.6. Comparison of Computer Model with HF Laser Measurements

Interpretation of the vibrational decay observations in $Ar/N_2/HF$ and Ar/HF mixtures (Section 2.5.2) is relatively simple and does not require extensive computer modeling. However, interpretation of measurements of the HF vibrational level populations during the excitation pulse and the more complex decay in $Ar/H_2/HF$ mixtures can only be done with the aid of computer modeling. The major elements of the computer model were described in Sections 2.2 and 2.3, where the specific rate constants and other assumptions used in the model were presented. Comparisons are made here with the results of absorption measurements described in Section 2.5 and the laser emission measurements described in Section 2.4.

2.6.1. Time Resolved Probe Laser Absorption and Gain

$Ar/N_2/HF$ Excitation Processes

The vibrational decay measurements described in Section 2.5.2 indicated that the vibrational coupling between $N_2(v)$ and $HF(v)$ is very weak. Thus the electric discharge excitation process occurs primarily through electron impact with $HF(v = 0)$ to produce $v = 1$ and possibly higher v levels. By carrying out probe laser absorption measurements on several $v = 2 \rightarrow 1$ and $3 \rightarrow 2$ transitions, the $v = 1$ and $v = 2$ populations were determined as a function of time (assuming the rotational temperature remains at 300 °K).

Experimental data are shown in Figure 36 for a 50 μsec electric discharge pulse duration. It is interesting to note that the value of the observed minimum in the $1 \rightarrow 0$ P(7) absorption at 13 μsec is equal to the value computed on the basis that virtually all of the HF in the 50-cm long electric discharge region is removed by excitation, leaving only a 30-cm long residual absorption path.

Experimental data, using a 30 μsec pulse duration, have been reduced to provide populations of the $v = 1$ and $v = 2$ levels, as shown in Figure 37. It is seen that the $v = 1$ and $v = 2$ populations rise together during the pulse, maintaining a ratio of about 3.7. From the initial slope of the $v = 1$ population an averaged cross-section for direct electron impact excitation of HF ($v = 0$) to HF ($v = 1$) can be estimated. The electron density is estimated to be $1 \times 10^{13} cm^{-3}$ on the basis of the measured electric discharge current density (8 amp/cm^2) and an estimated

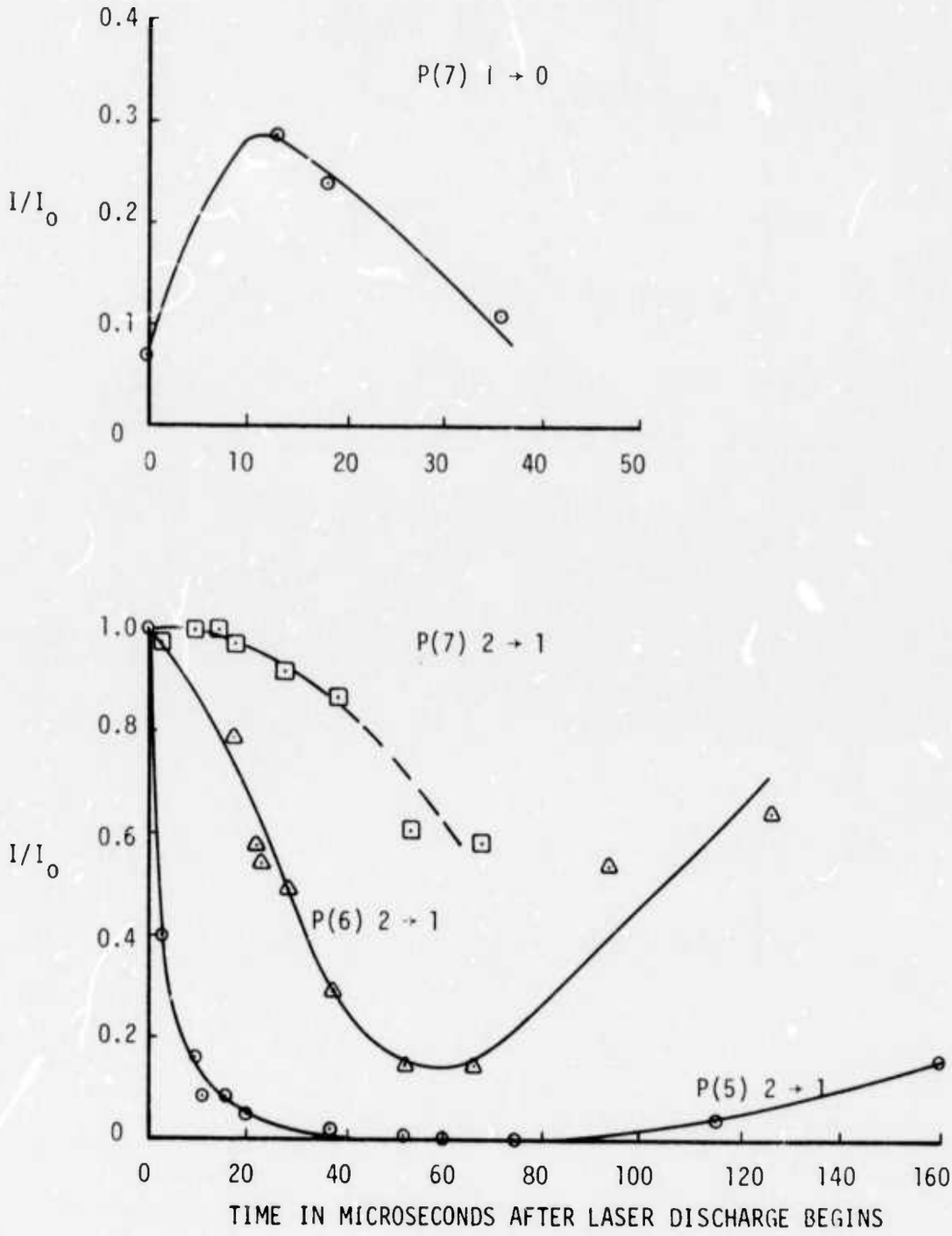

Figure 36. Probe Laser Measurements for a 50 μsec Discharge Pulse in 89/10/0.4 Ar/N_2/HF Mixtures at 200 Torr and a Power Input of 2 kW/cm^3 and an E/N of 0.36 x 10^{-16} V-cm^2.

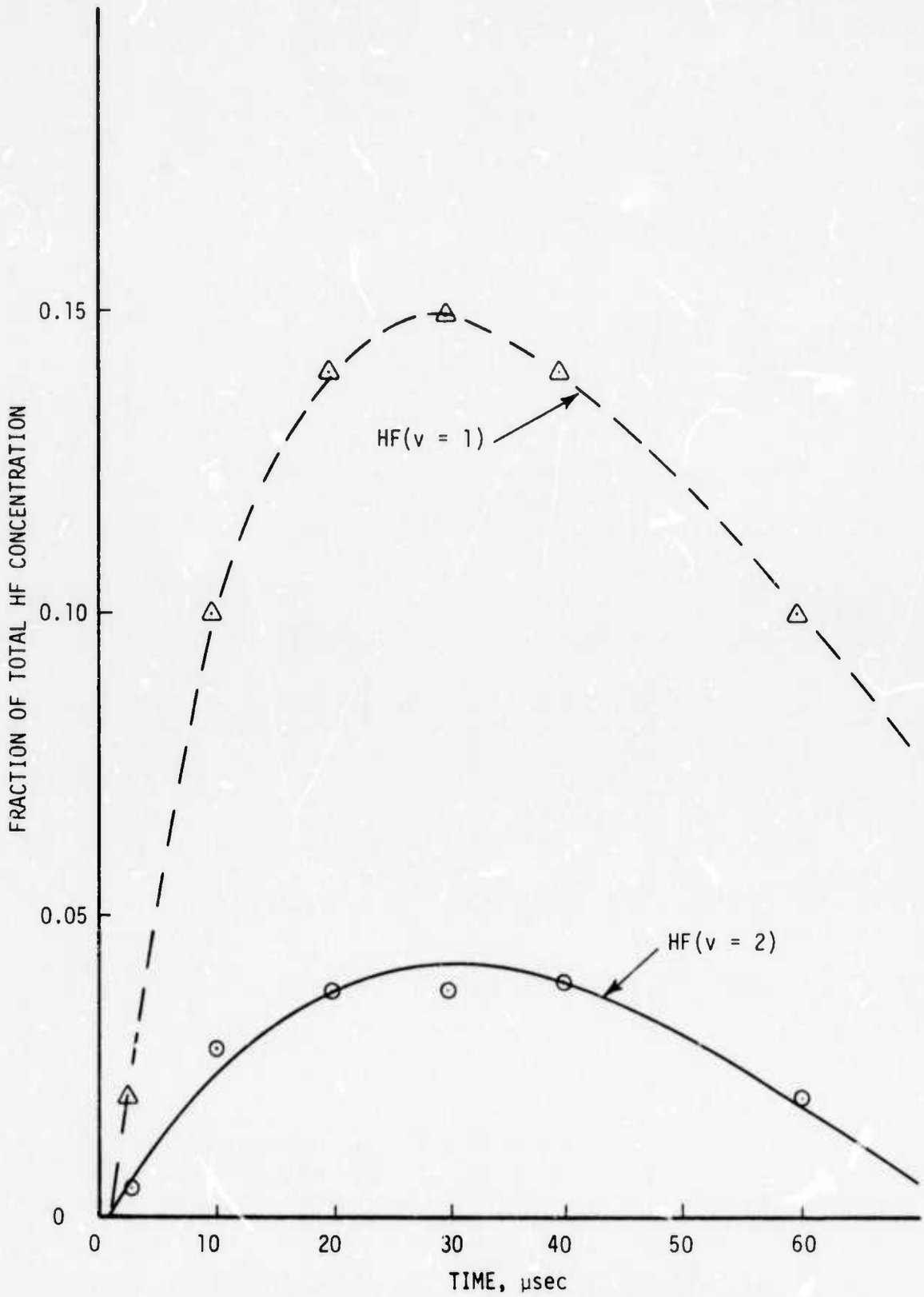

Figure 37. Measured HF Fraction in v = 1 and v = 2 in 89/10/0.4 $Ar/N_2/HF$ Mixtures at 200 Torr for a Power Input of 2 kW/cm^3, a Pulse Duration of 30 μsec, and an E/N of 0.36 x 10^{-16} $V\text{-}cm^2$.

drift velocity of 5×10^6 cm/sec. An excitation cross-section of about $3 \times 10^{-17} cm^2$ is computed, assuming that the mean electron temperature is 1 eV and that the average is taken over the range of 0 to 2 eV. This value is comparable with the cross-section for electron impact vibrational excitation of H_2 and may therefore play a significant role in the kinetics of $Ar/H_2/HF$ mixtures.

Attempts to fit the results of Figures 36 and 37 using the present MSNW computer model for HF kinetics and the limited kinetic data available (Section 2.3) have not yet yielded satisfactory agreement. However, the initial computations indicate some important trends. A simple model was assumed for the partitioning of electron pumping energy between HF and N_2, with N_2 absorbing 96 percent and HF the remaining 4 percent. This 4 percent was partitioned on a trial basis between direct excitation of $v = 1$ and $v = 2$ of HF. Vibrational energy transfer from N_2 to HF was assumed insignificant. Otherwise, the rate data given in Section 2.3 were used.

The computed gain or absorption of the $2 \rightarrow 1$ P(7) transition is shown in Figure 38 for 2 specific cases. Referring back to Figure 36, we note that the measured gain or absorption on this transition was quite small throughout the first 20 μsec of the pulse. This measured value differs from the computer model results that assume electron impact pumping only into the $v = 1$ level, which show strong absorption at early times. By assuming that HF ($v = 2$) is pumped at approximately the same power fraction as HF ($v = 1$), the initial absorption is removed. However, strong optical gain is predicted at later times during

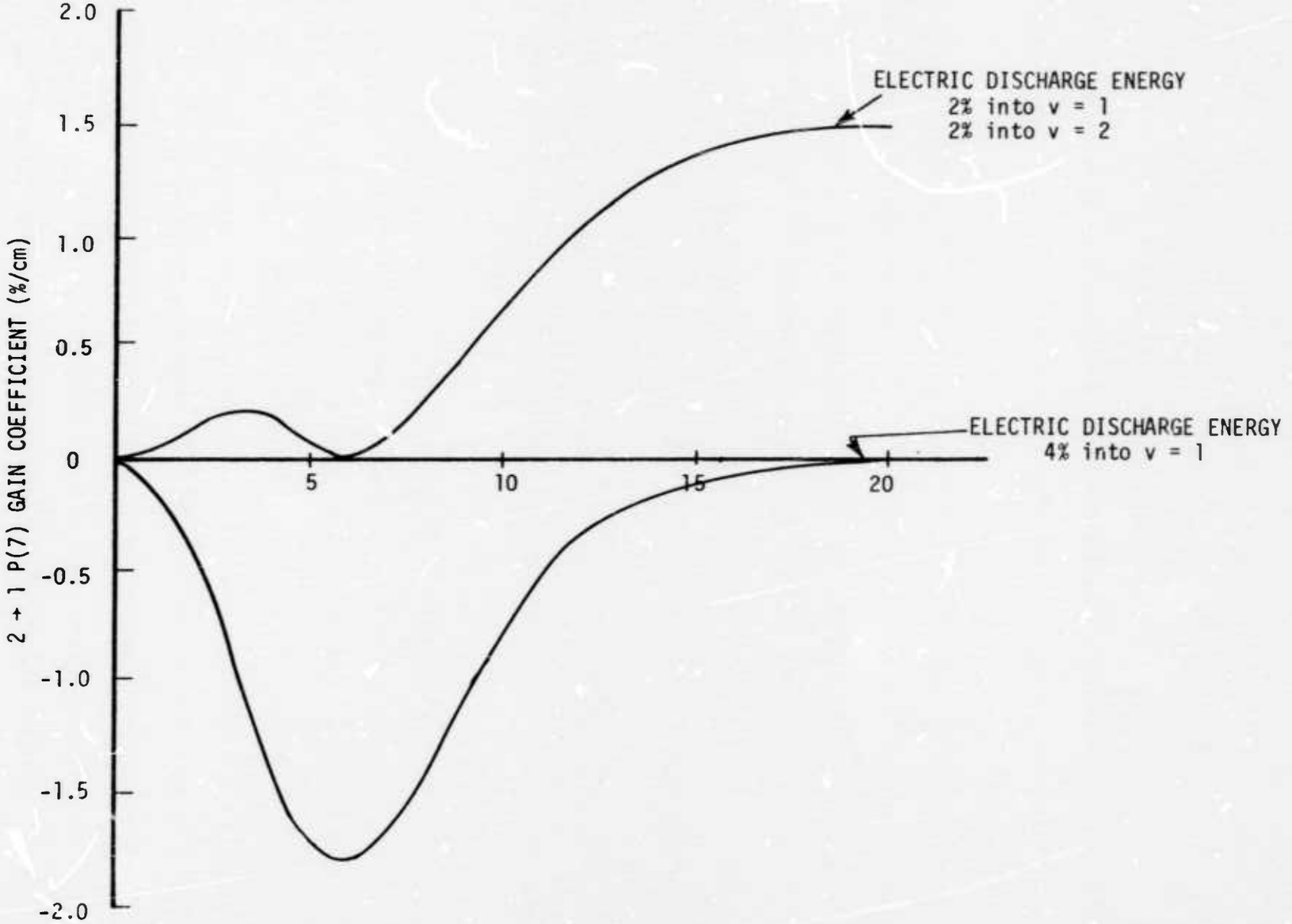

Figure 38. Computer Model Calculations of Optical Gain or Absorption on the 2 → 1 P(7) Transition of HF in 89/10/0.4 Mixtures of $Ar/N_2/HF$ at 200 Torr for a Power Input of 3 kW/cm^3.

the pulse, but is not observed experimentally. This latter discrepancy may be due to the fact that superelastic collisions were omitted, or that the kinetic model of V-V and V-R,T processes is seriously in error. At a minimum, it can be concluded from this comparison that direct electron impact pumping of various vibrational levels of HF is significant.

Ar/H_2/HF Vibrational Decay

The experimental measurements of HF absorption in Ar/H_2/HF mixtures obtained in the 5 tube plasma diode electron gun facility (Section 2.5.3) have been compared with the MSNW computer model using the rate data given in Sections 2.2 and 2.3. There was no single set of the adjustable parameters that provided a good fit to all of the data. One of the best fits obtained is shown as the solid curves in Figure 39. For this computation, the partitioning of electric discharge energy was the following:

$H_2(v = 1)$ excitation = 0.63

H_2(rot) excitation = 0.27

HF(v = 1) excitation = 0.02

HF(v = 2) excitation = 0.01

Direct heating(elastic) = 0.07

In addition, the effects of the following changes in parameters in the model were investigated:

(1) The vibrational dependence of the V-R,T decay rate of HF due to HF collisions was varied.

(2) The temperature dependence of the V-R,T decay rate of HF was included with a T^n law where n was varied between 0 and -2;

(3) The V-V rate of H_2 (v) + H_2(v) was varied both in magnitude and in the v denendence;

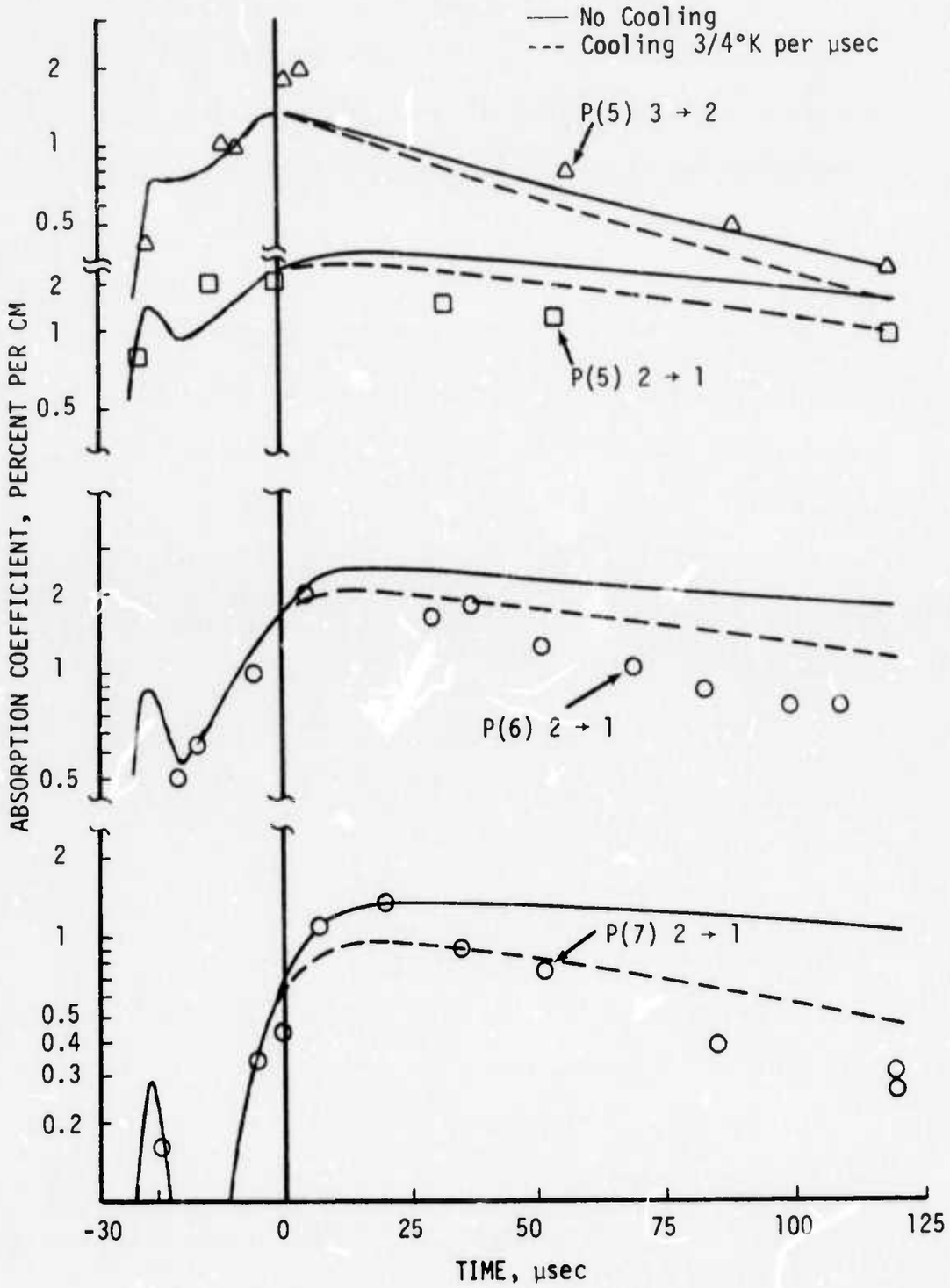

Figure 39. Comparison of Probe Laser Absorption Measurements with Computer Model Results in 89/10/0.3 Ar/H_2/HF Mixtures at 200 Torr and a Power Input of 1.6 kW/cm^3 for 30 µsec at an E/N of 0.43 x 10^{-16}V-cm^2.

(4) The V-V transfer rate from $H_2(v)$ to HF was varied both in magnitude and in the v dependence;

(5) The direct electric discharge excitation rate of HF to produce v = 1 and v = 2 was varied;

(6) The uppermost v levels (v = 6) of H_2 and HF were assumed to be excited rapidly to higher levels.

None of the variations listed above improved the agreement between theory and experiment shown in Figure 39.

It is seen in Figure 39 that there is general agreement between the computer model and the magnitude of the measured absorption coefficients; however, important details differ significantly. One of the principal differences is the discrepancy in rotational temperature during the excitation pulse. The 2 → 1 P(7) line is predicted to go into optical gain midway in the excitation pulse, but this is not seen in the absorption measurements nor in the laser cavity measurements. The second principal discrepancy is in the decay following the discharge pulse. The results for 2 → 1 P(5) and 3 → 2 P(5) indicate that the computed decay rate is in fair agreement with experiment. However, the P(6) and P(7) lines of 2 → 1 indicate a much faster decay than that predicted by the computer model. This suggests a faster cooling mechanism for the gas temperature or the rotational temperature than has been incorporated in the model. The addition of an artificial gas cooling rate (to model expansion cooling) at the rate of 0.75 °K per μsec reduces the discrepancies somewhat as shown by the dashed curves of Figure 13. However, it is concluded that the computer model is not yet satisfactory, particularly in describing the rotational populations of HF. It appears likely that the

rotational populations do not fit a Boltzmann distribution and that the transfer of rotational energy to translation is not as fast as assumed in the present model. This possibility is supported by the measured effect on laser output caused by replacing Ar with He, as discussed in Section 2.4.

Ar/H_2/HF Excitation Processes

The time resolved absorption and gain measurements on the P(5), P(6), P(7), and P(9) lines of the HF ($v = 2 \rightarrow v = 1$) transition (Section 2.5.3) were compared to the computer model predictions during the excitation pulse in a 0.15 percent HF, 10 percent H_2 and 89.8 percent argon mixture with 4.7 kW/cm^3 power input. The theoretical values of the absorption (or gain) coefficient were adjusted for the shift of the line center wave number (due to argon) relative to the line center of the probe laser gas.

The results of this comparison are shown in Figure 40. It is seen that the overall trends in I/I_0 with rotational level and with time are in rough agreement. However, specific details differ. In particular the experimental values of I/I_0 do not exhibit the pronounced minimum seen in the theoretical curves after about 3 μsec of pumping. Also the theoretical curves indicate positive gain from 6 to 11 μsec for the P(7) line whereas the experimental data for the P(7) line remains in absorption throughout the discharge pulse duration. Experimentally, only the P(9) line shows positive gain; however, the peak gain predicted theoretically for this line is a factor of about 3 larger than the measured value.

It is concluded from these comparisons that the gross features of the kinetics of Ar/H_2/HF mixtures are satisfactorily modeled by the computer program. However, there is apparently a kinetic process present

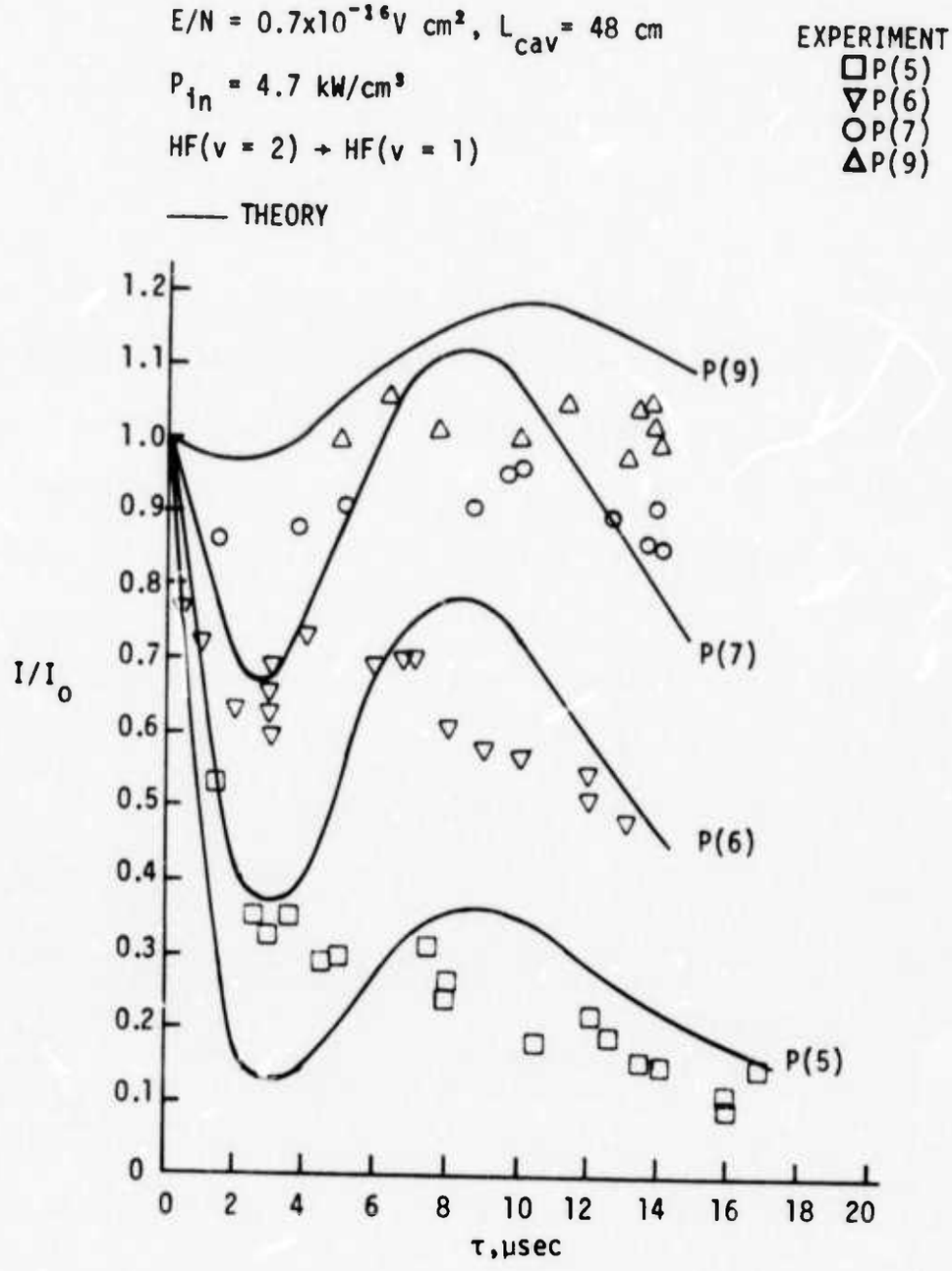

Figure 40. Comparison of Probe Laser Absorption Measurements in the Ceramic Electron Gun Facility with the Computer Model in an 89.85/10/0.15 Ar/H_2/HF Mixture at 200 Torr

that smooths out the absorption and gain curves. It appears that neither high absorption nor high gain is produced during the pulse on those lines that are near an inversion (e.g., P(7) and P(9)). This may indicate that the V-V transfer rates are dependent on the rotational levels, or that the effects of rotational non-equilibrium are more complex than the description used in the present computer model. An alternative interpretation of the observed trend in the data is that electron impact directly with the upper levels of H_2 and/or HF (including superelastic collisions) tends to drive the population ratios of various pairs of adjacent vibrational states toward equilibrium with the electron distribution function. This competes with the V-V processes that tend to drive the upper vibrational and rotational states toward an inversion. Further study, both theoretical and experimental, is required to reach a full understanding of these possibilities.

2.6.2. Laser Onset Time

Laser onset time for a 48-cm long electric discharge region and 120 cm between mirrors was experimentally determined using a variable insertion loss for a power input of 4.6 kW/cm^3 into a 0.15 percent HF, 10 percent H_2, and 89.85 percent Ar gas mixture. A plot of the gain coefficient at threshold versus the laser onset time for three output couplings (2.3 percent, 12.8 percent, and 25.6 percent) is shown in Figure 41.

The small signal gain coefficient for P(8) of the HF ($v = 2 \rightarrow v = 1$) transition is also shown for comparison. This line was chosen since it was the first line to turn on in previous measurements of the

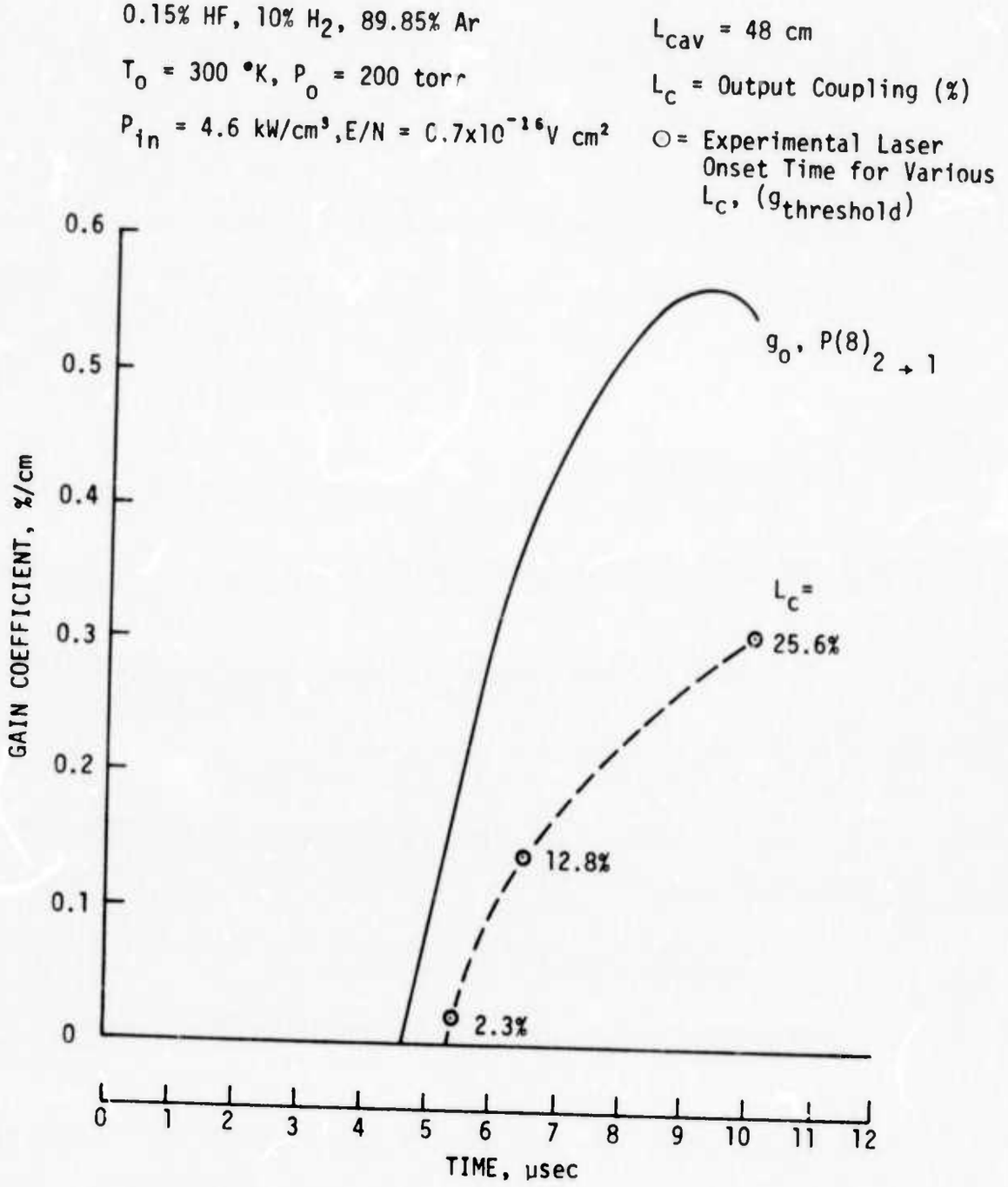

Figure 41. Experimentally Observed Laser Onset Time as a Function of Output Coupling, Compared with Computed Low Signal Gain Versus Time

laser output wavelength versus time. It is seen that the two curves agree quite well at low output coupling, but differ increasingly as the output coupling increases. Theoretical laser turn on time would be approximately 0.6 usec after threshold is reached for gain thresholds up to about 0.4 percent per cm. This time is considerably less than the discrepancy between theory and experiment and is therefore not included as a correction factor. The long delay in the appearance of lasing of the 25.6 percent output coupling case relative to the 12.8 percent output coupling case indicates that the maximum small signal gain coefficient is only slightly higher than 0.3 percent per cm (the gain threshold for the 25.6 percent output coupling case).

The comparison discussed here indicates that the gross features of the kinetics are modeled satisfactorily. However, the smaller value of the experimentally determined maximum low signal gain indicates that a kinetic process has been omitted that reduces the population inversion that can be achieved.

2.6.3. Laser Power Output

The peak power output per unit volume of a 48-cm long cavity with 10 percent output coupling was determined experimentally and theoretically for various power input levels. Experimental measurements were made in a 0.15 percent HF, 5 percent H_2, 94.85 percent Ar gas mixture for both the five tube and the ceramic plasma diode electron gun facilities. Laser power output varied from 0.7 to 2 W/cm^3 for electric discharge power input levels of 2 to 6 kW/cm^3. As seen in Figure 42, the experimental power output was a factor of 30 to 60 times smaller than the theoretically predicted value.

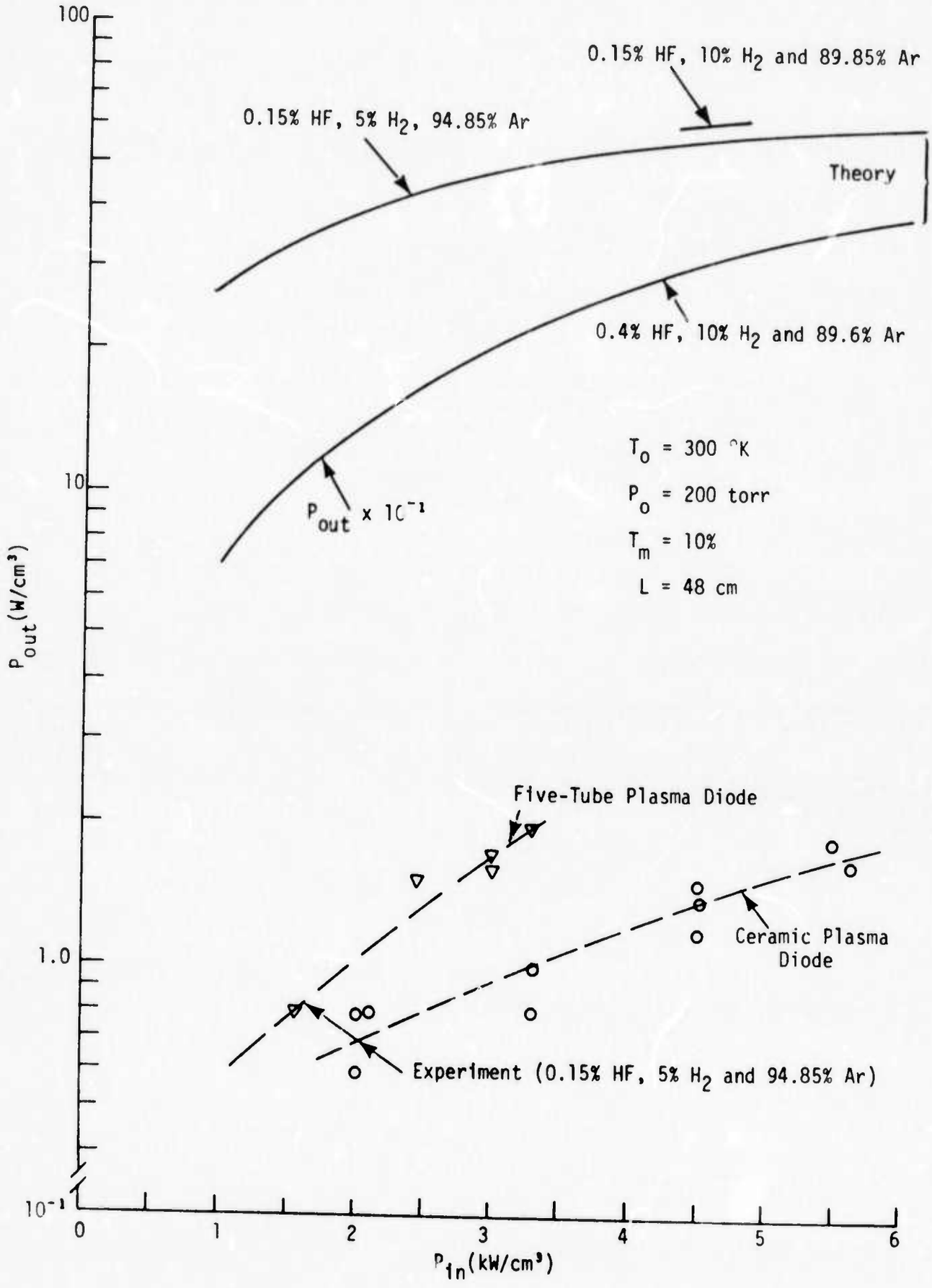

Figure 42. Comparison of Theoretical and Experimental Dependence of Maximum Laser Power Output on Power Input

For comparison, the theoretical power output of a 0.4 percent HF, 10 percent H_2, 89.6 percent Ar gas mixture is also shown in Figure 42, although no experimental data are shown for this mixture. It is seen that the predicted power output for the higher HF concentration is a factor of 3 to 6 times greater than for the 0.15 percent HF mixture. This increased power output with increasing HF concentration was not realized experimentally; it was found that at higher HF concentration (up to 0.3 percent) the laser output power was roughly the same as it was at 0.15 percent HF. Further increase in HF concentration led to lower power output.

These results suggest that a kinetic mechanism is present that causes a far greater reduction in the population inversion than is presently predicted theoretically. We think that rotational non-equilibrium, superelastic collisions of electrons with HF and/or H_2, and major errors in the V-V rates are the most likely causes for this discrepancy.

SECTION III

ELECTRONIC STATES LASER TECHNOLOGY

3.1. Summary

A unique laser concept has been established at MSNW which offers excellent prospects for developing high efficiency, high energy density, visible gas lasers. This approach borrows three principles that have been well established in high power infrared laser development and applies these to visible electronic state lasers.

The first principle is the use of electron-beam-stabilized electric discharge excitation which has proved very efficient in IR lasers. The second principle is the use of preferential collisional processes to provide a two-temperature system, in this case a high temperature among electronic states and a low vibrational temperature within each electronic state. The third principle is to recycle the laser molecule many times during the laser pulse, thereby using the gas to its full (thermal) limit; electron impact pumping of the upper laser level and rapid VV and/or VT collisional quenching of the (vibrationally excited) lower laser level accomplish the recycling process.

Three key elements must be combined in order to make this concept a reality. First, a stable pulsed discharge is required which can provide a high rate of electronic excitation, a low rate of vibrational excitation, and sufficient time duration without arc formation. Second, molecular laser systems must be found which exhibit an allowed visible transition between electronic states for which the potential curve minima

are displaced, yielding a high Franck-Condon factor for transitions from the low vibrational levels of the upper state to high vibrational levels of the lower state. This is shown schematically in Figure 43. Third, for candidate laser molecules, collisional processes must be found that provide more rapid quenching of the vibrational levels of the lower state than either the radiative decay or the collisional decay of the upper state.

In searching for candidate laser molecules, attention has been directed initially to molecules which have already produced visible laser output in short pulse electric discharges, such as $N_2(C^3\pi_u \rightarrow B^3\pi_g)$ and $CO(B^1\Sigma^+ \rightarrow A^1\pi)$. However, these molecules do not completely fulfill the prescription outlined above; the minima in the potential curves are not markedly shifted, the electronic states involved in laser emission are not among the lowest electronic states of these molecules, and both N_2 and CO have large cross sections for vibrational excitation by electron impact. Nevertheless, if preferential collisional quenching of the vibrational energy within each electronic state can be achieved in these molecules, this will provide the initial foundation for long pulse visible electronic state electric discharge lasers.

Initial experiments at MSNW were directed toward the study of N_2 and CO visible electronic state emission in electric discharges stabilized by a moderate current density (~ 50 ma/cm^2) electron beam. Qualitative studies of kinetic mechanisms and discharge stability were carried out. The principal results are summarized here very briefly.

PRINCIPAL REQUIREMENTS:

1. $T_{el}/T_{vib} > E_{el}/E_{vib}$

2. $\sum_i k_{vib,i} N_i \gg \sum_i k_{el,i} N_i + A_{el}$

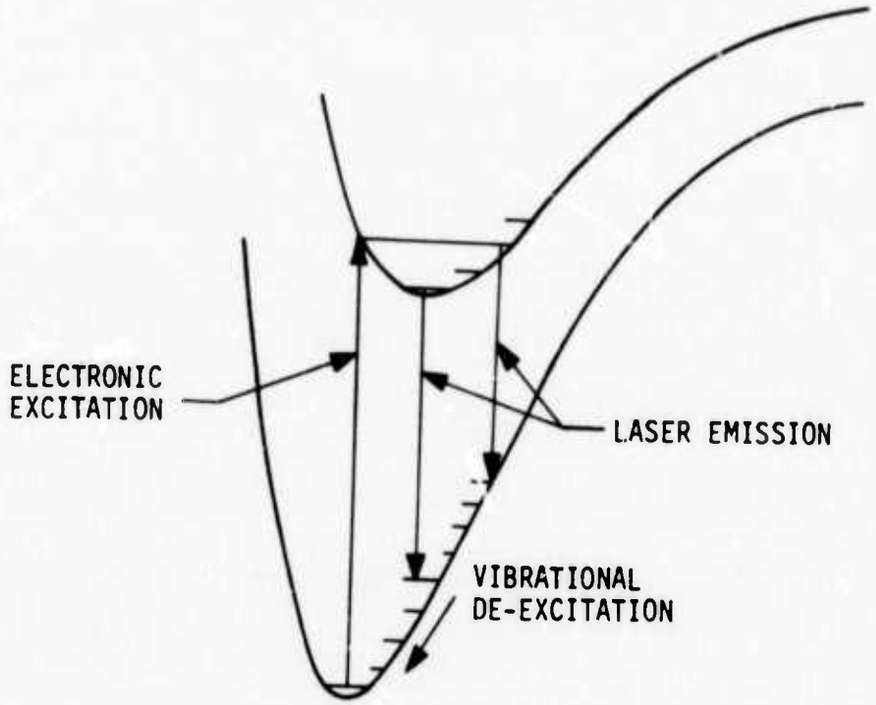

Figure 43. Collision Dominated Visible Electronic State Laser Concept

1. Fluorescence from electric discharges in N_2/Ar mixtures showed evidence of the production of $N_2(C)$ and $N_2(B)$ states by transfer from excited Ar atoms, and by the energy pooling reaction, $N_2(A) + N_2(A) \rightarrow$ products. Measurements in N_2/He mixtures showed direct electron impact excitation of $N_2(C)$ and $N_2(B)$ in addition to energy pooling. The addition of SF_6 to either mixture permitted higher voltage, lower current operation and led to a higher ratio of the $N_2(C)$ and $N_2(B)$ state population by a factor of about 10. However, the maximum $N_2(C)$ population could not be increased above a certain level because of arc formation.

2. It was determined from the experimental observations that arc formation is intimately related to the population of the excited electronic state responsible for laser emission.

3. Laser output has not yet been observed in these discharges.

3.2. Electronic State Kinetic Processes

In developing a more quantitative understanding of the general principles on which visible collisional electronic state lasers will be based, some of the kinetic requirements and restrictions are noted here. To achieve a significant low signal optical gain (0.1 cm^{-1}) in the visible (about 5000 Å), using a diatomic molecule such as N_2, the upper laser level electronic state population must exceed the lower level

population by about 10^{13} cm^{-3}, assuming Doppler broadening and a 10^{-7} sec radiative lifetime for the lasing transition. The dependence of the required population on lifetime is shown as the lower curve in Figure 44. An upper limit to this curve is shown, above which the collisional self-destruction loss process exceeds spontaneous emission as a decay mechanism for the upper laser level (assuming a rate constant of 10^{-9} cm^3/sec). Thus, to avoid self-quenching losses, the radiative lifetime of the laser transition must be less than about 3 μsec. Assuming a 6 eV excitation energy, the population of the radiating state can be provided by a volume pumping rate of 1 kilowatt/cm^3 at 10 percent efficiency (assuming no collisional decay of the upper electronic state). An excitation rate of this magnitude is quite readily achieved in e-beam stabilized electric discharges.

The population inversion mechanism being considered here involves the simultaneous production of a high molecular electronic temperature and a low vibrational temperature. In addition, a displacement of the minimum in the electronic potential curves is advantageous since it yields a high probability of spontaneous emission from the low vibrational levels of an upper electronic state to the upper vibrational levels of a lower electronic state (see Figure 43). An inversion can be produced if the ratio of the electronic temperature of the two electronic states to the vibrational temperature of the lower electronic state exceeds the ratio of the electronic energy level difference to the energy of excitation of the vibrational level of the lower electronic state. This requirement is expressed by:

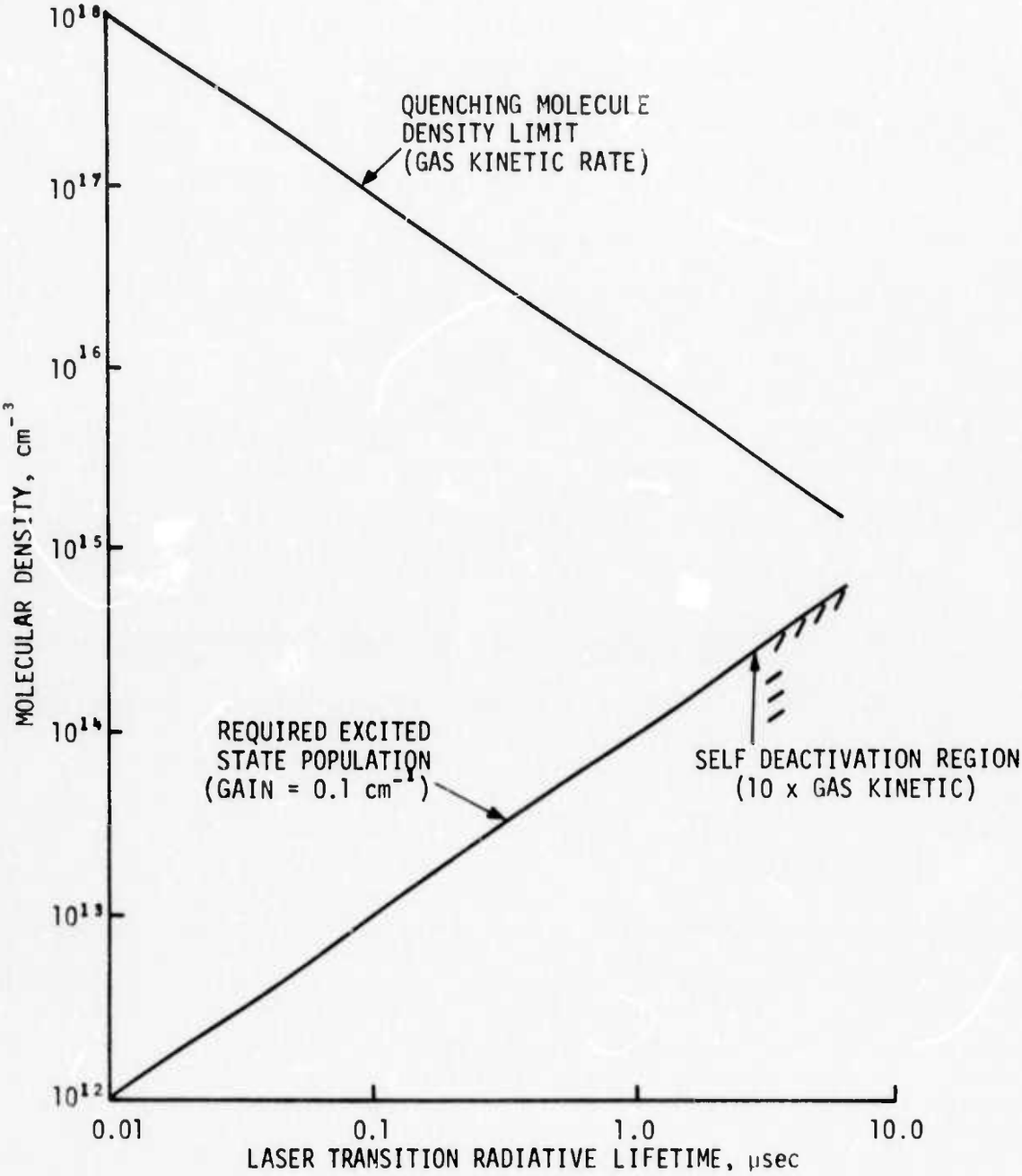

Figure 44. Competing Rate Processes for Collision Dominated Visible Electronic State Molecular Lasers

$$\frac{T_{el}}{T_v} > \frac{\Delta E_{el}}{\Delta E_v} \tag{12}$$

To achieve high specific laser power from the gas being used, it is necessary to recycle the excited laser molecules many times; this requires that the collisional quenching of the vibrational excitation of the lower electronic state must occur at a rate, k_v, that exceeds the sum of the collisional quenching rate, k_{el}, plus the (spontaneous) radiative decay rate, A_{el}, of the upper electronic state. This requirement is expressed by:

$$\sum_i N_i k_{vib,i} > \sum_i N_i k_{el,i} + A_{el} \tag{13}$$

In order to achieve a collisional decay time of the lower laser level that is shorter than the radiative decay time of the upper laser level, the required minimum product of the collision probability times the density of the quenching molecule is shown as the upper curve of Figure 44. Note that the actual required density is inversely proportional to the quenching probability.

The upper curve of Figure 44 also represents a maximum density-probability product for a gas component that causes collisional quenching of the upper electronic state. It should be noted, however, that the upper laser level may have a shorter total radiative lifetime than that due only to spontaneous emission corresponding to the laser transition. In this case the upper state quenching limit is increased by the ratio of the two radiative lifetimes.

It is seen from Figure 44 that the useful range of molecular electronic state radiative lifetimes lies between 0.01 and 10 μsec. It is also seen that the gas density requirements for collisional quenching

are reasonable, provided favorable lower level vibrational quenching cross-sections, ranging from 10^{-2} to 1 times gas kinetic, can be found.

A review of the presently available kinetic data on excited states of N_2 and CO was carried out in a search for favorable collisional quenching rates among the laser levels of these molecules. The results of this survey are summarized in Table IX. It is seen that favorable possibilities exist for N_2 ($B^3\pi_g$, v = 3) quenching by N_2 and for CO($A^1\pi$, v = 1) quenching by He. It appears that the use of Ar with CO would yield poor results because of the high collisional quenching rate of the $B^1\Sigma^+$ state of CO by Ar. On the other hand, Ar is a good diluent for N_2, since it causes very little quenching of either the upper or the lower state. An additional candidate molecule for quenching the $N_2(B^3\pi_g)$ state is C_2H_6 which has been observed to cause rapid vibrational quenching of the $N_2(A^3\Sigma_u^+)$ state (Ref. 34). This effect, together with the potential curve coincidence between the $A^3\Sigma_u^+$ state and the v = 3 level of the $B^3\pi_g$ state of N_2 may lead to a rapid collisional quenching rate of the v = 3 level of the $B^3\pi_g$ state of N_2. However, the collisional quenching rate of the $C^3\pi_u$ state of N_2 by C_2H_6 is not yet known, and it may be quite large. The effect of adding C_2H_6 to N_2 in e-beam stabilized electric discharge experiments is discussed in Section 3.3.2.

Table IX

Summary of Collisional Quenching Data (cm^3/sec) for N_2 and CO Electronic States by Various Molecules

	Transition	λ(Å)	A_λ^{-1}(μsec)	K_Q(upper level)	k_Q(lower level)	References
N_2^*/He	$C^3\pi_u \rightarrow B^3\pi_g$	4058(0,3)	0.8	?	8×10^{-13}†	35
N_2^*/Ar	same	same	same	?	1.6×10^{-12}†	35
N_2^*/N_2	same	same	same	1×10^{-11}	2.5×10^{-11}	36, 37
CO^*/He	$B^1\Sigma^+ \rightarrow A^1\pi$	4835(0,1)	0.4	3.1×10^{-12}	1.5×10^{-11}	38, 39
CO^*/Ar	same	same	same	1.4×10^{-10}	1.6×10^{-10}	38, 39
CO^*/CO	same	same	same			

†unspecified v level.

3.3. Electronic State Fluorescence Measurements

3.3.1. Multiple Pulse Fluorescence from N_2 and H_2 Electronic States

A series of fluorescent emission spikes was observed unexpectedly in the 1 to 2 micron region during the HF fluorescence observations on HF-H_2-Ar mixtures excited by e-beam stabilized electric discharges using the thermionic electron gun (Appendix A). Furthermore, when the gas mixture was changed to HF-N_2-Ar, emission spikes were also seen, but the specific wavelengths were quite different and extended from 1.5 microns in the infrared down to 3371 Å in the ultraviolet. Subsequent spectroscopic studies showed that the emission in HF-N_2-Ar mixtures was from N_2 electronically excited states. It is believed that the emission from HF-H_2-Ar mixtures is from H_2 electronic states although definite identification has not yet been made. In both gas mixtures it was established that HF was required in small concentration in order to obtain these emission pulses. These observations were reported in Applied Physics Letters (Ref. 8); a more extensive discussion of the possible interpretations of the results is given here.

Experimental Observations

A large-area thermionic cathode electron beam (Appendix A), operated at 125 kV, was used in these experiments to provide a stable high-pressure pulsed electric discharge for a time duration of 20 - 40 μsec. The electron beam provided a current density of up to 4 mA/cm^2 through a 0.04-mm-thick high-strength aluminum foil. The electric discharge pulse was terminated by controlling the voltage on the grid of the electron

gun to terminate the external source of ionization. A cylindrical Teflon discharge chamber was used with calcium fluoride windows mounted opposite each other, 21 cm apart. A 4 x 15-cm aluminum screen with about 50 percent porosity was used as the discharge cathode. A 50-Ω copper sulfate resistor was used in series with a spark-gap triggered capacitor (0.4 μF) to supply current at 5 - 10 kV across a 7-cm gap in the chamber. An operating pressure of 200 torr was generally used. A Jarrell-Ash 0.25-m Ebert spectrometer, equipped with both 6000-Å and 2.1-μ blazed gratings, was used for spectral measurements, together with a liquid-nitrogen-cooled Ge:Au detector for the near IR and a 1P28 photomultiplier for the UV-visible portion of the spectrum. The rise time of each detector was less than 1 μsec.

Argon (Airco, 99.995%), hydrogen (Airco, 99.999%), and nitrogen (Airco, 99.99%) gases were used without further purification. HF supplied by Matheson was purified by distillation at liquid-nitrogen and chloroform slush temperatures and held in a monel cylinder. Vacuum lines were constructed of monel and passivated at 1 atm of chlorine trifluoride. A short length of polyethylene tubing connected the monel vacuum system to the Teflon test section. The HF was used from the monel storage vessel at an HF pressure of 500 torr and mixed with the Ar/N_2 or Ar/H_2 gas in a flowing system. The test-cell filling rate was approximately 350 torr/min. Exit gases were passed through a liquid-nitrogen-cooled trap. The gas temperature and pressure in the test section were maintained at 20 °C and 200 torr, respectively.

Figure 45 illustrates the repetitive superfluorescent pulses observed at 3370 Å in N_2. The behavior is very similar to that seen for H_2

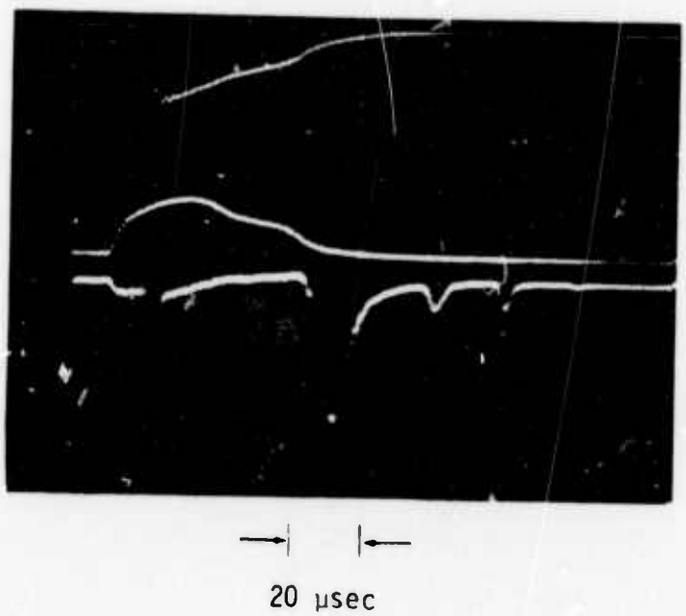

Figure 45. Superfluorescent Pulses at 3370 Å in a Mixture of 10% N_2, 89% Ar, and 1% HF at 200 Torr Pressure. The Initial Capacitor Voltage is 11 kV. The Upper trace is the total discharge current through a 57.5-cm^2 area (100 A/div), the middle trace monitors the relative electron-beam current, and the lower trace (signal increasing downward)is the relative fluorescent emission at 3370 Å with a 5-A spectral slit width.

and N_2 in the near IR. By scanning 30 Å to either side of the 3370-Å emission, no pulsed output was observed. Table X lists the other wavelengths at which maximum superfluorescent emission was observed. The emission is characterized by a sharp initial pulse at the onset of the electrical discharge, during a period of high E/p and low current, followed by a series of long-duration pulses during the decay of the discharge when the electron-beam current is terminated. The intensity and frequency of the long-duration pulses increase (roughly linearly) as the HF concentration is increased from 0.75% to 3%.

In Figure 46 the near-IR emission from the nitrogen first-positive system is shown with the use of a semiconfocal resonator with internal gold-coated mirrors and a 1-mm diameter output coupling hole. An active discharge length of 15 cm was used between the mirrors. It was found that the mirrors enhanced the intensity of the long-duration pulses by an order of magnitude over the background radiation, which suggests the possibility of optical gain at this wavelength.

The electron beam alone did not produce any detectable superfluorescent pulses. A threshold value of E/p was observed both for the initial pulse and the long-duration pulses. The superfluorescent pulse intensity increased with increasing E/p until arc formation prematurely terminated the electrical discharge. The arc formation occurred with less time delay as the HF concentration was increased at fixed discharge voltage. The discharge current during the superfluorescent pulse output ranged from 0.2 to 1.0 A/cm^2, and the values of E/p ranged from 3 to 5 kV/cm atm.

Table X

Locations of Peak Superfluorescence in N_2 and H_2

$N_2(B^3\pi_g \rightarrow A^3\Sigma_u^+)$ First-Positive System		$N_2(C^3\pi_u \rightarrow B^3\pi_g)$ Second-Positive System		$H_2(E,F^1\Sigma_g^+$ or $C^1\pi_u \rightarrow B^1\Sigma_u^+)$	
Wavelength[a]	Assignment (v', v")	Wavelength[b]	Assignment (v', v")	Wavelength[a]	Assignment (v', v")
1.04 μ	0,0	3370 Å	0,0	1.50 μ	0,2 P(4)[c]
1.23 μ	0,1	3576 Å	0,1	1.63 μ	0,3 P(6)[c]
1.48 μ	0,2	3804 Å	0,2		
		4058 Å	0,3		

[a] 0.02 μ spectral slit width.

[b] 5 Å spectral slit width.

[c] Tentative assignment.

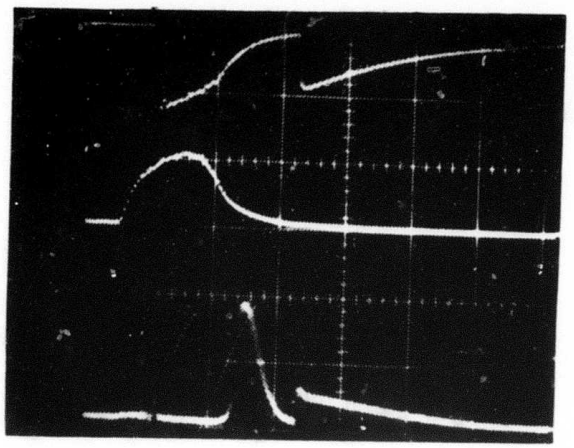

Figure 46. Optical-Cavity Emission in the IR from a 10% N_2, 89% Ar, 1% HF Mixture at 200 Torr Pressure. The sweep speed is 20 μsec/div. The initial capacitor voltage is 12 kV. The upper trace is the total discharge current through a 37.5-cm^2 area (100 A/div), the middle trace monitors the relative electron-beam current, and the lower trace is the total IR emission observed through a 1-mm output coupling hole using a Ge:Au detector. A small initial-emission spike is seen at the onset of the discharge current. A 10-μsec duration emission pulse is seen as the discharge current decays following termination of the electron-beam current. This is followed by an arc in the discharge region. Both emission pulses were identified as belonging to the first-positive band of N_2.

The effect of the HF concentration on the time interval and the amplitude of the N_2 first positive emission pulses is shown in Figure 47. The interval is roughly inversely proportional to the HF concentration and the amplitude increases roughly in proportion to the HF concentration. At the highest amplitude the detector circuit approaches saturation.

In an attempt to suppress the emission spikes, the internal reflectivity of the test cell was reduced by using Nextel flat black paint. It was found that the emission spikes were increased rather than suppressed and that they appeared with no HF in the flow. This indicates that volatile hydrocarbons may have an effect similar to that of HF in causing these repetitive emission pulses.

In subsequent experiments using the 5-tube plasma diode facility (Appendix A), an effort was made to reproduce the superfluorescent emission pulses previously observed in the Teflon discharge chamber. We searched for laser emission from $Ar/N_2/HF$ mixtures at both 1 μ and 3371 Å when the discharge chamber was placed in a high-Q cavity formed by gold-coated spherical mirrors. Even though an E/N of 1.5×10^{-16} V - cm^2 (3.7 kV/cm-atm) was reached for 89% Ar/10% N_2/1% HF mixtures at 200 torr, no superfluorescent pulses were observed.

At present we have no definite explanation for the absence in our present apparatus of the superfluorescent pulses which had been obtained in the old apparatus. One difference between the two experiments is that the plasma diode e-beam is not crowbarred. Another factor which

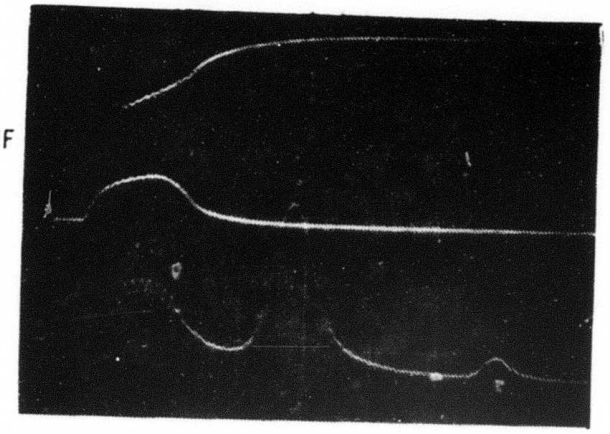

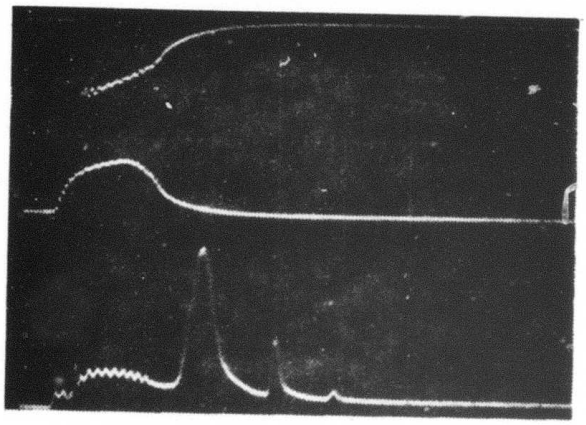

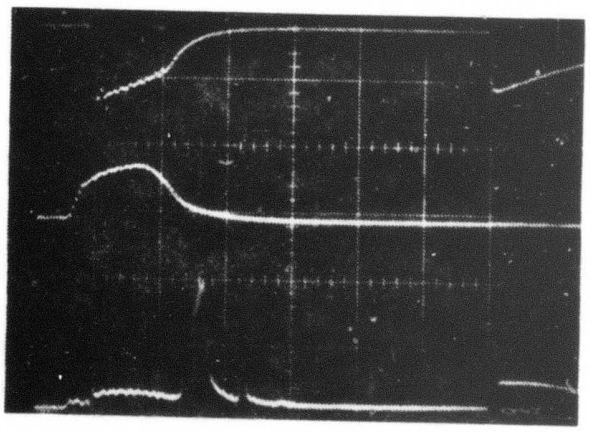

Figure 47. Fluorescence in 10% N_2, 90% Argon with Trace HF
P = 200 Torr E/P = 3 kv/cm - atm 20 μsec/cm
1 to 11 Microns 57.5 cm^2 Cathode Area

could be responsible for the differing results is the dimensions of the discharge volume. In the Teflon apparatus the anode was 15 cm x 10 cm with a 7 cm electrode gap; in the plasma diode discharge chamber the anode is 5 cm x 50 cm with only 2.5 cm between electrodes.

Interpretation of Results

The effects described here are quite new and unexpected. At present there is no accepted theoretical explanation or quantitative model with which these results can be compared. The data indicate that electron impact excitation is very important and that collisional processes involving HF are important.

The N_2 fluorescence spikes, when seen, occur on transitions which are well known to produce laser oscillation, but at considerably different conditions and over a much different time scale. The N_2 laser pulse duration is much shorter than the pulses seen here and is produced by an electric discharge at considerably higher voltage than used here. The discharge excites the upper electronic states of N_2 by electron impact faster than the lower electronic states. As stimulated emission rises, the rate of populating the lower states rises until the inversion is finally lost by the filling of the lower electronic states.

This process could be stretched in time if the HF molecule were significant in removing the lower electronic states. In the case of the N_2 first positive band the lower laser level is the lowest metastable state, $A^3\Sigma_u^+$. One possibility is the electronic transfer from $N_2(A^3\Sigma_u^+)$

to a repulsive electronic state of HF which leads to dissociation. However the $N_2(A^3\Sigma_u^+)$ electronic energy is only slightly greater than the dissociation energy of HF, whereas the only known vacuum uv absorption continuum of HF is at 1400 Å. Thus collisional quenching of the $N_2(A^3\Sigma_u^+)$ state by HF is not a very likely explanation of the observed pulses.

A second possibility is the efficient vibrational quenching property of HF. A mechanism may be found which involves two temperatures, a high electron temperature that is maintained by the electric field, and a low vibrational temperature that is maintained close to the translational temperature by VT relaxation in collisions with HF or another molecule that serves as a vibrational decay catalyst. This may occur on the second positive band system by the two steps

$$\text{electronic transfer:} \quad N_2(B^3\pi_g) + N_2 \rightarrow N_2(A^3\Sigma_u^+)^{VIB} + N_2$$

$$\text{vibrational quenching:} \quad N_2(A^3\Sigma_u^+)^{VIB} + HF \rightarrow N_2(A^3\Sigma_u^+) + HF$$

However, in order to compete with the $N_2(C^3\pi_u)$ spontaneous decay lifetime under the experimental conditions used here, the HF vibrational quenching probability must be close to 1. Furthermore, the emission spikes are observed on the (0,0) transitions of both the first and second positive bands of N_2, indicating that vibrational quenching is not a likely explanation.

A third, and most likely, explanation of these observations is the possible occurrence of striations in the gas similar to those observed in

the positive column of low pressure glow discharges (Ref. 40). An instability in the current-voltage characteristic of high pressure, e-beam stabilized discharges in $He/N_2/CO_2$ mixtures has been observed by Douglas-Hamilton (Ref. 41) and is believed to be connected with dissociative attachment of CO_2. Since HF has a similar energy dependence for dissociative attachment, and probably has a larger cross-section, the same effect may occur in mixtures containing small amounts of HF. The observations of Douglas-Hamilton showed that the instability appears as oscillations in the current and voltage carried by the gas. In the present experiments with HF, there is no apparent modulation of the current or the voltage. However, if the instability develops in the HF mixtures studied here, it may produce local regions of high E/N, which would produce correspondingly high electronic state emission.

3.3.2. Time Resolved Fluorescence from $N_2(C^3\pi_u)$ and $N_2(B^3\pi_g)$

The laser modeling studies described in Section 3.2 suggest the following mechanisms for achieving a long pulse nitrogen laser: 1) pumping of the $N_2(C)$ and (B) states by direct electron impact or Ar^* energy transfer; 2) pumping of the $N_2(C)$ state and removal of the $N_2(A)$ state using the energy pooling reaction, $N_2(A) + N_2(A) \rightarrow N_2(C) + N_2(X)$; 3) selective collisional removal of the $N_2(B)$ state (e.g., by C_2H_6) to eliminate the self-terminating nature of the $C \rightarrow B$ laser; and 4) use of small concentrations of electronegative molecules such as SF_6 to increase the effective E/N by attaching low energy electrons and thus more effectively

pump the N_2 electronic states. These ideas have been examined experimentally during this program, and the results are discussed in the following text.

The experimental set-up is identical to the 5-tube plasma diode facility used in the HF/DF experiments (Section 2.4.1 and Appendix A), with the exception of the mirror coatings and the ultraviolet detector. Gold mirrors were employed for the N_2 first positive cavity tests, and two pairs of dielectric coated mirrors having maximum reflectivities of 99.9% at 3370 Å and 3650 Å, respectively, were used for the N_2 second positive studies. Wavelength selection was obtained with a Jarrel-Ash 0.25 m Ebert Monochromator equipped with both 6000 Å and 2.1 μ blazed gratings. The infrared emission was monitored with an Au:Ge detector while the ultraviolet emission was detected with an RCA 1P28 photomultiplier tube.

It was found in the early experiments that the onset of arcing prevented the achievement of the high E/N required for efficient pumping of the N_2 electronic states. In an effort to alleviate the arcing, a new anode with a Rogowski profile at the edges was installed. In addition, the modular design of the e-beam apparatus results in non-uniformities in the discharge, as discussed in Appendix A. These non-uniformities will result in some variation in the excited state population densities and could represent a serious loss due to absorption of the laser emission. An attempt to correct this problem was made by lowering the discharge screen 4 cm below the e-beam foil. Spreading of the electron beam due to scattering tends to make its profile more uniform at greater distances from the foil; however, the e-beam current

density also decreases with distance from the foil, which results in lower discharge current densities. The results of this study indicated no improvement in emission characteristics, and the electrodes were returned to their original positions with the discharge screen adjacent to the e-beam foil.

Fluorescence Decay Studies

Time resolved observations of the nitrogen C → B and B → A fluorescence indicate that the C and B states are formed by 1) direct electron impact and/or Ar^* excitation transfer, 2) metastable $N_2(A)$ state self-collisions (energy pooling), and 3) electron impact on metastable $N_2(A)$. Experiments with no applied discharge voltage show that the $N_2(C)$ and (B) states are formed either directly by the e-beam itself, or by energy transfer from Ar^* produced by e-beam excitation. Figure 48 (a) shows the time dependence of the nitrogen C → B and B → A fluorescence produced by the e-beam only, while Figure 48(b) shows the effect on these emissions of applying a discharge voltage to the gas. Note that the B → A sensitivity has been reduced by a factor of 20 in Figure 48(b), whereas the C → B sensitivity has been increased by a factor of 2. The nonlinear increase in both the 3371 Å and 1 μ emission indicates that the C and B states are formed by some multi-step process, possibly by electron collisions with $N_2(A)$, by collisions between two A state molecules, or by electron impact with excited vibrational levels of ground state N_2.

Another important point to be noticed in Figure 48(b) is that the 3371 Å emission decays with a time constant two orders of magnitude longer than the C state radiative lifetime (~ 40 nsec). This observation

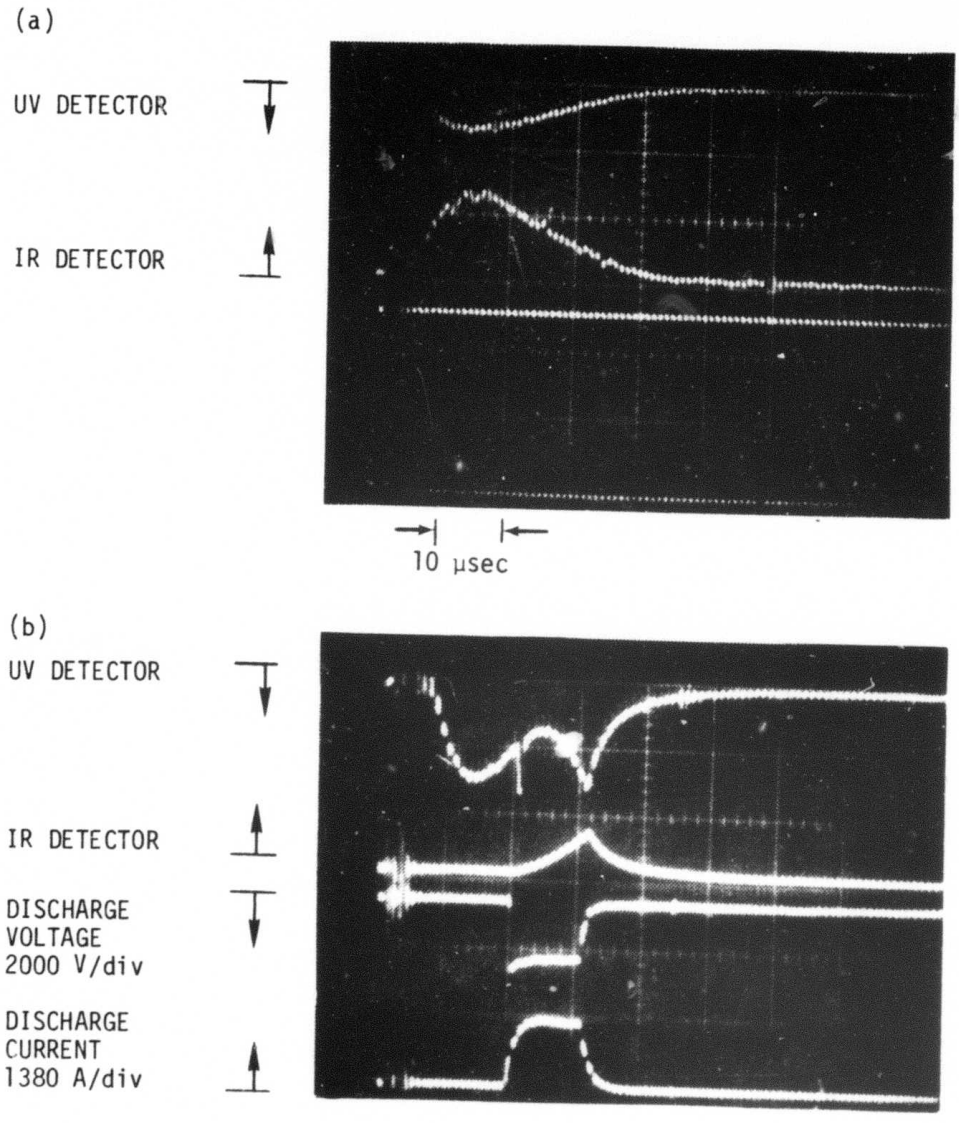

Figure 48. Time History of the Nitrogen C → B (3370 Å) and B → A (1.04 μm) Fluorescence Produced a) by the E-Beam and b) by the E-Beam Stabilized Electric Discharge in an 85/15 Ar/N_2 Mixture at 200 Torr Total Pressure.

suggests that the $N_2(C)$ state is being produced from some long-lived excited species. The most likely candidates are excitation transfer from metastable Ar states or energy pooling by collisions of two metastable $N_2(A)$ molecules. Transfer from metastable Ar atoms can be ruled out on the basis of the measured deactivation rate of Ar^* by N_2. The rate coefficient is $3 \times 10^{-11} cm^3/sec$ (Reference 42) which, for 20 torr of N_2, implies a transfer time of 50 nsec and an Ar^* decay time of 500 nsec. This is an order of magnitude shorter than the observed decay time.

Whether or not $N_2(A)$ energy pooling is indeed responsible for the formation of $N_2(C)$ should be apparent from the form of the second positive emission decay curve. Loss of the $N_2(A)$ state is controlled by the energy pooling reaction until its population decays sufficiently that quenching predominates. Thus, if the energy pooling reaction, which depends quadratically on the A state concentration, is the source of the C state, the 3371 Å emission will exhibit a nonexponential decay. In Figure 49, the intensity of the 3371 Å and 1 μ emission is shown as a function of time after the discharge crowbar. At early times (< 10 μsec) the decay is clearly nonexponential; at later times it becomes more nearly exponential. The similarity between the B and C state decays indicates that there is a close relationship between their populations; the B state is either formed predominantly by radiative cascading from the C state, or it is also formed by A state self-collisions.

If the decay of the $N_2(A)$ state is controlled by self collisions, then it can be described by a differential equation of the form

$$\frac{dA}{dt} = - QA - k_p A^2 \qquad (14)$$

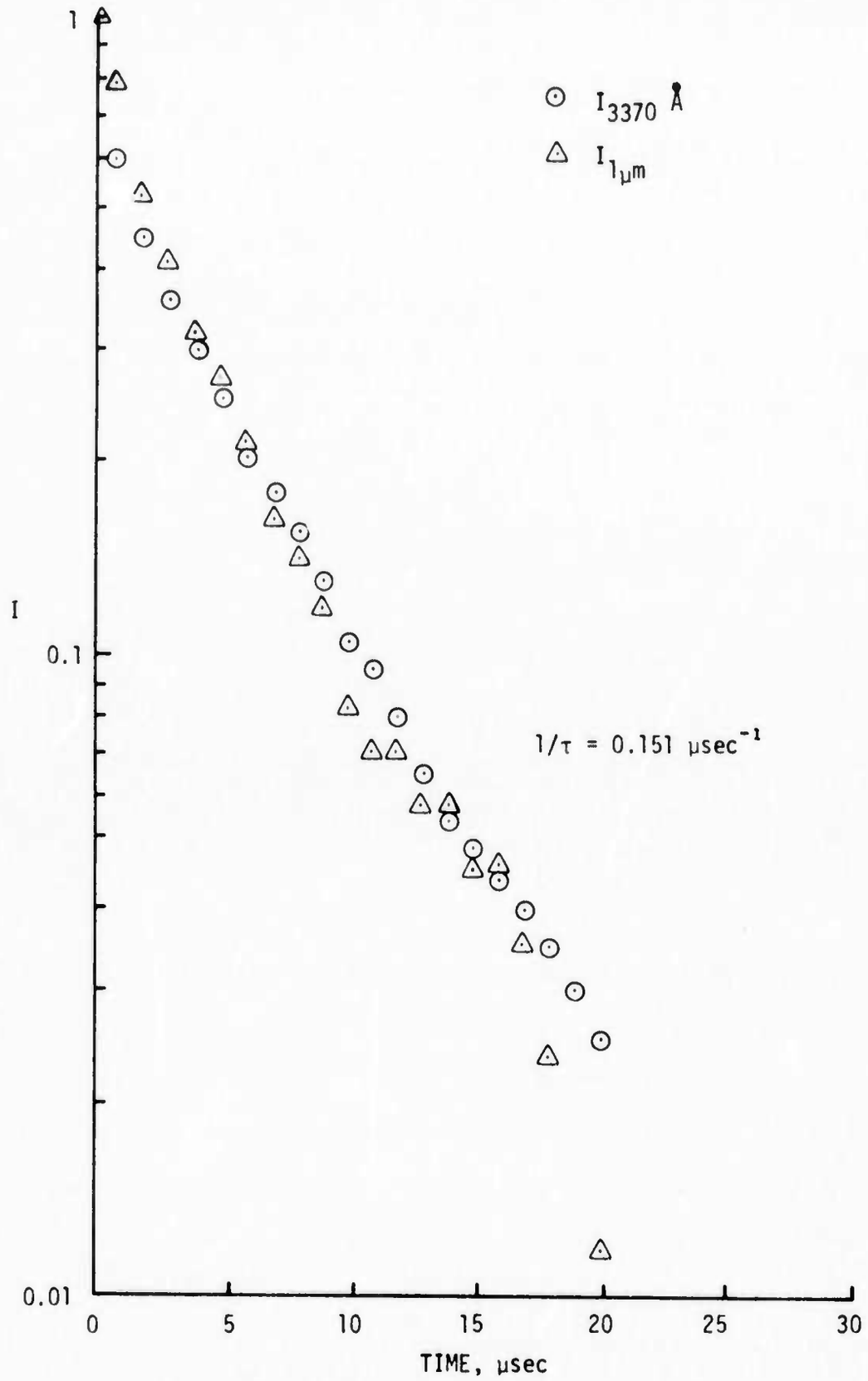

Figure 49. Time Decay of the 3370 Å and 1 μ Emission After the Discharge is Terminated for an 85% Ar/15% N_2 Mixture at 200 Torr Total Pressure

Here Q is an apparent A state quenching rate constant and k_p is the A state self-annihilation rate coefficient.

The general solution of this differential equation is

$$A = \exp(-Qt) \left[\left(\frac{1}{A_o} + \frac{k_p}{Q} \right) - \frac{k_p}{Q} \exp(-Qt) \right]^{-1} \qquad (15)$$

where A_o is the concentration of $N_2(A)$ at time t = 0. At early times ($Qt << 1$) this solution has the asymptotic form

$$A^{-1} \sim A_o^{-1} + k_p t \qquad (16)$$

and at late times ($Qt >> 1$)

$$A \sim \exp(-Qt) \left(\frac{k_p}{Q} + \frac{1}{A_o} \right)^{-1} \qquad (17)$$

Thus at short times, a plot of A^{-1} vs t should yield a straight line. If the C state is formed from the reaction

$$N_2(A) + N_2(A) \rightarrow N_2(C) + N_2(X) \ , \qquad (18)$$

then since the C state radiative lifetime is much shorter than its production time, the $N_2(C)$ population should be proportional to $[N_2(A)]^2$ and should have a decay rate equal to twice that of the A state. Hence at short times a plot of $C^{-\frac{1}{2}}$ vs t should also yield a straight line. Figure 50 shows the data of Figure 49 plotted as $I^{-\frac{1}{2}}$ vs t. The linear relationship exhibited by both the C and B state emission implies that the A state decay is indeed being controlled by the energy pooling reaction, and that the energy pooling reaction is the source of the C and B state populations.

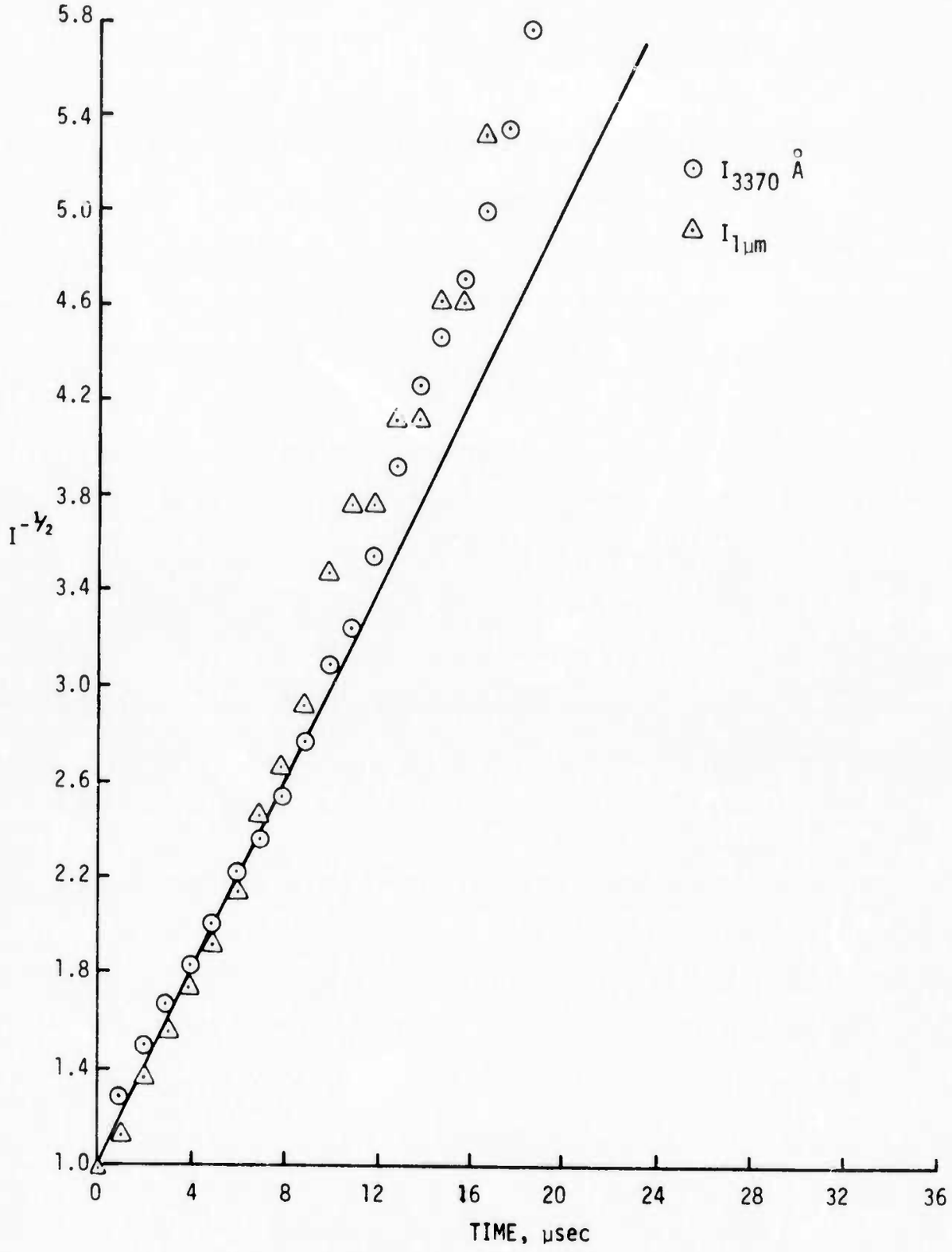

Figure 50. Plot of the Reciprocal of the Square Root of the N_2 First and Second Positive Intensities Versus Time After the Discharge Crowbar

At later times in the decay, the function $I^{-\frac{1}{2}}$ rises faster than the initial linear slope of Figure 50. This indicates the presence of an additional loss process for the $N_2(A)$ state such as collisional quenching by one of the gas constituents. However, the data in this region does not extend over a sufficient dynamic range to be certain that the subsequent decay of the C state and B state intensity is exponential. The effective rate constant for A state energy pooling may increase somewhat with time as the gas relaxes; the vibrational temperature of the $N_2(A)$ state may continue to change and may have an effect on the A state self-annihilation rate. The change in slope in Figure 50 corresponds to an increase in the rate constant by a factor of 1.5. Another possible effect is the decrease in gas density as the pressure rise produced by the electric discharge is relieved by expansion into the surrounding volume. For these reasons, the late time decay cannot be analyzed quantitatively with confidence.

Effect of Addition of SF_6

At high discharge current densities, the discharge was found to increase the $N_2(B)$ state emission (above that due only to the e-beam) by a much larger factor than the C state emission was increased (see Figure 48). However, the addition of small concentrations of SF_6 (~ 0.1%) to the gas mixture increases the ratio of the second positive emission to the first positive emission by an order of magnitude even though the discharge current decreases substantially. With no SF_6, the onset of arc formation limited the maximum obtainable E/N to a value of 1.3×10^{-16} V-cm^2 for an 85/15 Ar/N_2 gas mixture at 200 torr total pressure. However, the addition

of approximately 0.1% SF_6 to the gas mixture resulted in an E/N of 2.1×10^{-16} V-cm^2 before arc formation occurred.

The effect of SF_6 addition on the discharge voltage, discharge current, and 3370 Å emission is shown in Figure 51. This photograph should be compared with the oscilloscope traces of Figure 48, which were obtained without SF_6 added to the gas mixture. The discharge E/N in Figure 51 is approximately double that without SF_6 shown in Figure 48(b), while the discharge current is about an order of magnitude less in the SF_6 case. However, the ratio of the intensity of the 3370 Å emission produced by the discharge to that produced by the e-beam has increased substantially.

The abrupt increase of the C → B emission when the discharge voltage is turned on is due to direct electron impact excitation of the C state. The emission then increases non-linearly during the discharge most likely because of the increase in the A state density which populates the C state via the energy pooling reaction. When the discharge is terminated, the second positive emission drops abruptly due to the cessation of electron impact excitation. However, there is still a slowly decaying component to the C state emission after the discharge is turned off, which is probably produced by self collisions of the slowly decaying A state population.

Effect of Addition of C_2H_6

In Section 3.2 a collisional decay mechanism was suggested for the $N_2(B)$ state utilizing ethane (C_2H_6). This mechanism involves an intersystem potential curve crossing from the lower vibrational levels of the B state to the upper vibrational levels of the A state

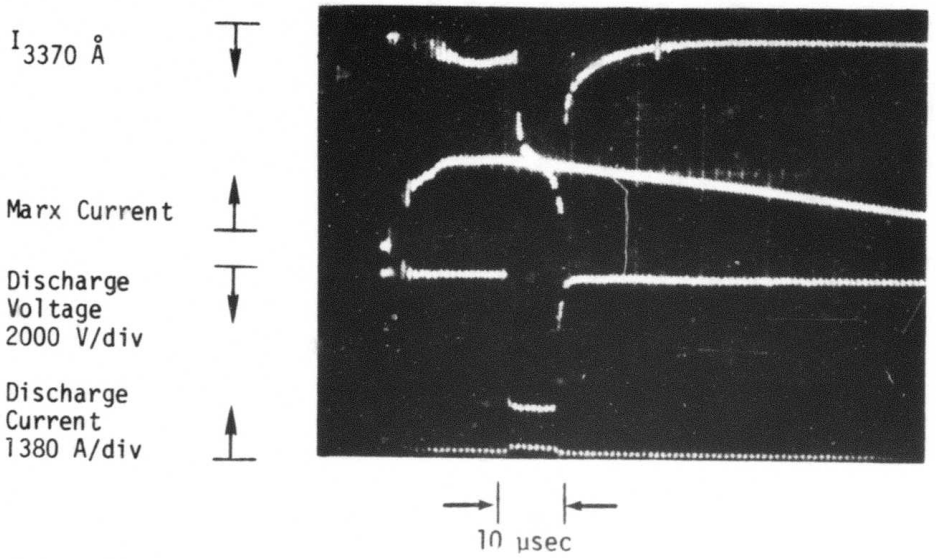

Figure 51. Effect of Approximately 0.1% SF_6 Addition on the Discharge Voltage, Discharge Current, and 3370 Å Emission for an 85/15 Ar/N_2 Mixture

$$N_2(B^3\pi_g)_{v=0} + N_2 \rightleftarrows N_2(A^3\Sigma_u^+)_{v=7} + N_2 + \Delta E \qquad (19)$$

The rate constant for the formation of $N_2(A)v = 7$ reported by Dreyer and Perner (Ref. 35) is $\sim 1 \times 10^{-11}$ cm^3/sec. The $N_2(A)v = 7$ then decays somewhat more slowly down its own vibrational ladder until a bottleneck at the $v = 3$ and 4 levels is reached. The addition of small concentrations of C_2H_6 increases the rate of decay down the A state vibrational ladder and removes the bottleneck at the $v = 3$ and 4 levels without having a significant effect on the A state population in lower vibrational levels (see Ref. 34).

These ideas were tested by observing the 3371 Å and 1 μ fluorescense with varying concentrations of C_2H_6 as a function of discharge E/N. However, the addition of C_2H_6 did not alter the ratio of second positive to first positive emission. The only observable effect due to the addition of C_2H_6 was the disappearance of the long time decay of both the 3371 Å and 1 μ emission. The apparent implication of this observation is that C_2H_6 removes the A state; however, for the C_2H_6 concentrations used here, this would be inconsistent with the rate constant for electronic quenching of $N_2(A)$ reported by Dreyer and Perner (Ref. 34). One explanation for this inconsistency is that the long time decay component of the first and second positive emission may be formed primarily by energy pooling of A state molecules in higher vibrational levels, which are quenched rapidly by C_2H_6. A second explanation is the formation of other species from C_2H_6 in the discharge, which have a high $N_2(A)$ state quenching rate. This question can be resolved by making direct measurements of the populations of the individual vibrational levels of the $N_2(A)$ state.

3.3.3. Time Resolved Fluorescence from Various Vibrational Levels of the $N_2(C^3\pi_u)$ and $N_2(B^3\pi_g)$ States

To gain further understanding of the kinetic processes occurring in high current discharges in Ar/N_2 and He/N_2 mixtures, we observed the time resolved fluorescence from individual vibrational levels of the nitrogen $C^3\pi_u$ and $B^3\pi_g$ states. The gas mixtures consisted of 15 to 20 percent N_2 in either He or Ar diluent at a total pressure of 200 torr. The fluorescence was produced in the e-beam stabilized electric discharge facility used for the results described in the previous section. The discharge voltage was applied near the peak of the e-beam current pulse and was terminated after 5 to 10 μsec. The electric discharge energy storage circuit was modified to reduce the inductance and provide a short (2 μsec) rise time of the current. The values of E/N were 1.2×10^{-16} V-cm^2 and 1.7×10^{-16} V-cm^2 while the discharge currents were 18 A/cm^2 and 6.6 A/cm^2 for the Ar/N_2 and He/N_2 mixtures, respectively. The applied voltage was slightly below the value that would cause an arc near the end of the discharge pulse.

Nitrogen $C^3\pi_u \rightarrow B^3\pi_g$ Fluorescence

Fluorescence emission from the v = 0 level of the $N_2(C^3\pi_u)$ state is shown in Figure 52. The upper trace shows the emission produced by the e-beam, while the lower trace shows the effects of the discharge on this emission. The C state emission due to the e-beam is probably produced by energy transfer from excited argon atoms which result from dissociative

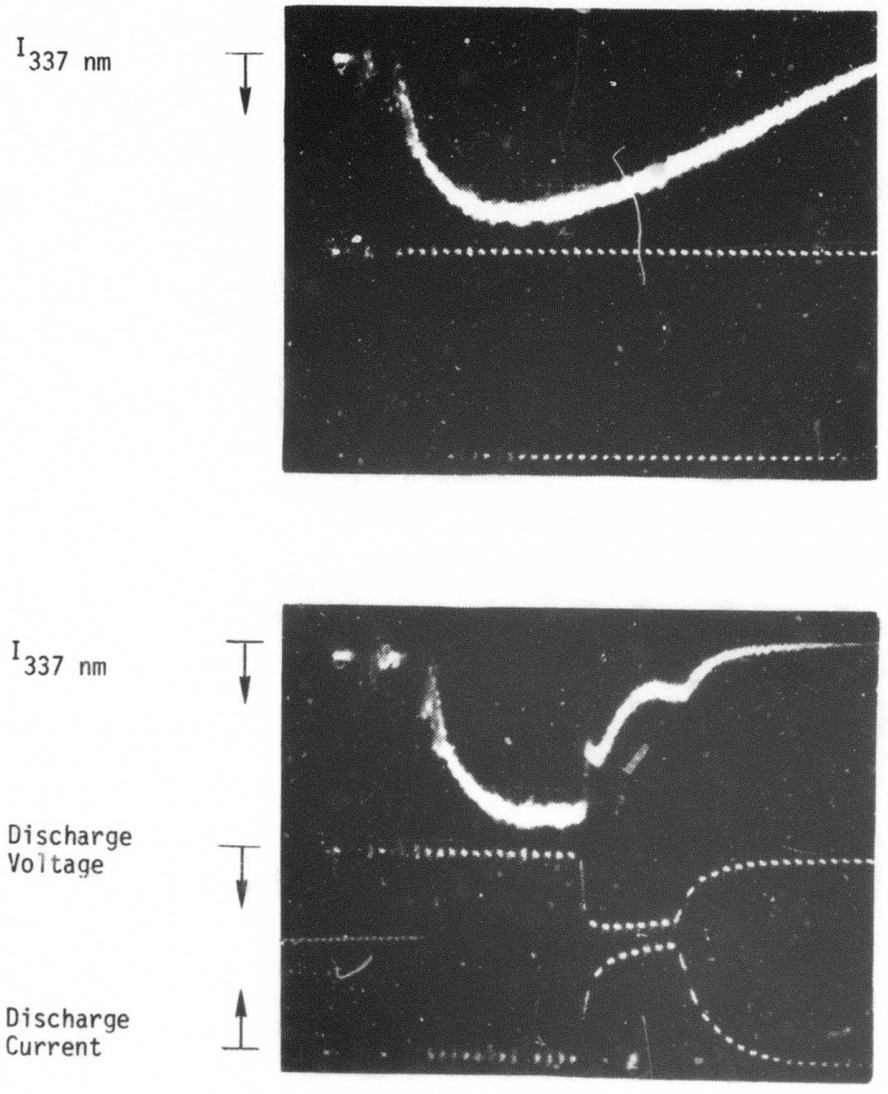

Figure 52. Fluorescence Emission from the v = 0 Level of the N_2 $C^3\pi_u$ State. The upper oscillogram shows the emission produced by the e-beam, while the lower oscillogram shows the effects of the discharge on this emission.

recombination of Ar_2^+ ions. From Figure 52, it is apparent that the v = 0 fluorescence of the nitrogen C state decreases abruptly when the discharge voltage is applied. As the discharge current increases, the C state emission increases slightly and then falls during the next 3 or 4 μsec. The emission then increases nonlinearly until the discharge is terminated, after which the fluorescence decays with a time constant much longer than the C state radiative lifetime.

The abrupt drop in the C state emission is most likely due to a decrease in the Ar^* population density caused by a decrease in the dissociative recombination rate when the electron temperature is increased by the application of the discharge voltage. The more gradual decrease in the C state emission during the early part of the discharge may be due to the production of some species which is an efficient deactivator of excited argon atoms or it may be due to a further reduction in the rate of producing excited argon atoms. This premise is supported by the observation that the C state emission due to the e-beam remains quenched even after the discharge has been terminated and the electrons have had a chance to cool. Further work would be necessary in order to identify the species and the process responsible for this interference in the nitrogen C state production channels.

In wavelength scanning experiments we have observed that the relative intensities of the emission from the v = 0 level of the nitrogen $C^3\pi_u$ state produced by the e-beam and by the electric discharge vary with wavelength within an emission band. This suggests that two distinct processes are responsible for this emission and that they result in different rotational distributions for the C state. Since individual

rotational lines were not resolved, no quantitative information about these distributions was obtained.

In Figure 53, fluorescence emission from the v = 0 and v = 1 levels of the nitrogen $C^3\pi_u$ state is compared. The difference is striking. Although the v = 1 emission produced by the e-beam drops abruptly when the discharge voltage is applied, it quickly recovers as the discharge current rises and then increases nonlinearly until the discharge is terminated. The electric discharge is evidentaly more effective than the high energy electron beam at producing the v = 1 level of the C state, although the e-beam produces the v = 0 level more strongly than the electric discharge does.

In the preceding section it was shown that the nonlinear increase and long time decay of the C state fluorescence were attributable to the energy pooling reaction

$$N_2(A^3\Sigma_u^+) + N_2(A^3\Sigma_u^+) \rightarrow N_2(C^3\pi_u) + N_2(X^1\Sigma_g^+) \qquad (20)$$

Since $N_2(A^3\Sigma_u^+)$ self-collisions produce the v = 1 and v = 0 levels of the $N_2(C)$ state with roughly equal probability (Ref. 43), excitation transfer from Ar^* must favor the v = 0 level of the C state. These observations are consistent with the results of Setser, Stedman, and Coxon (Ref. 44), who report that excitation transfer from $Ar(^3P_{0,2})$ to N_2 favors the production of $N_2(C^3\pi_g)$ v = 0 with a non-equilibrium rotational distribution.

When He/N_2 mixtures are excited, the behavior of the v = 0 and v = 1 levels is similar. Fluorescence arising from the same transitions

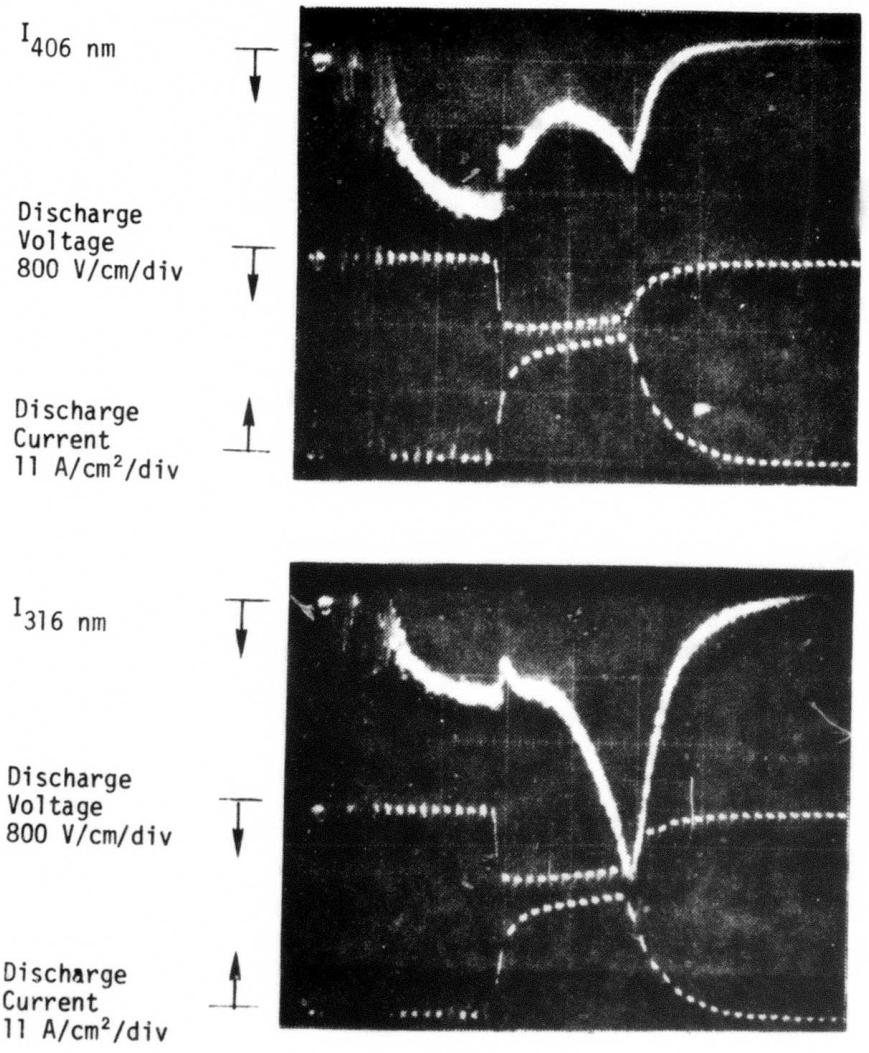

Figure 53. Comparison of Fluorescence Emission from the v = 0 and v = 1 Levels of the $N_2(C^3\pi_u)$ State in 5:1 Ar/N_2 Mixture at 200 Torr. The Upper Trace Shows the (0,3) Band, and the Lower Trace Shows the (1,0) Band of the Nitrogen Second Positive System.

shown in Figure 53 for Ar/N_2 mixtures is shown in Figure 54 for 5:1 He/N_2 mixtures. It is apparent that there is very little C state emission produced by the e-beam. During the discharge, the C state fluorescence increases nonlinearly until the discharge is terminated, after which the emission decays with a time constant much longer than the C state radiative lifetime. As in the case of Ar/N_2 mixtures, the electric discharge produces substantial excitation of the v = 1 level of the C state in He/N_2 mixtures.

In Figure 54, an abrupt drop in C state emission is seen at the time of termination of the discharge voltage. However, there was no abrupt rise in C state emission at the onset of the discharge voltage. This suggests that direct electron impact excitation of the C state increases during the pulse. This may be due to a shift in the electron distribution function to higher energies, as vibration of N_2 becomes excited, or it may be due to the buildup of the A state population, permitting electron impact with the A state to produce the C state. Both of these explanations illustrate how the energy deposition in the gas may have an important effect on the rate of excitation (and ionization) of the gas at low or moderate values of E/N. The volume rate of ionization in turn plays a major role in arc breakdown of these discharges.

Nitrogen $B^3\pi_g \rightarrow A^3\Sigma_u^+$ Fluorescence

We have observed fluorescence from the v = 0, 1, and 2 levels of the B state and find that it is essentially the same in both He/N_2 and Ar/N_2 mixtures. There is very little emission produced by the e-beam for any of these levels. During the discharge, the fluorescence from

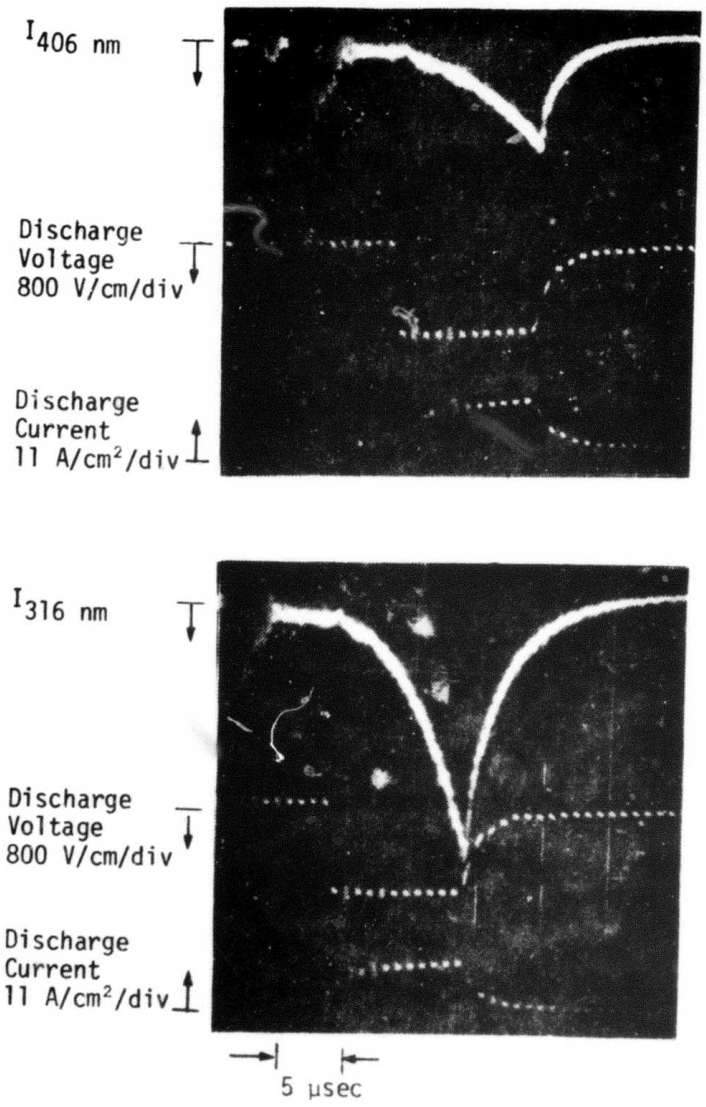

Figure 54. Comparison of Fluorescence Emission from the v = 0 and v = 1 Levels of the N_2 $C^3\pi_u$ State in a 5:1 He/N_2 Mixture at 200 Torr. The upper oscillogram shows the (0,3) band and the lower oscillogram shows the (1,0) band of the N_2 second positive system.

the v = 0, 1, and 2 levels increases linearly until the discharge is terminated, after which they decay. Oscilloscope traces showing the time history of the fluorescence from the v = 0 and v = 1 levels of the $N_2(B^3\pi_g)$ state are shown in Figure 55 for 5:1 Ar/N_2 mixtures. The B state emission shows no resemblance to the emission from the C state (Figure 53), nor to the integral of the C state, indicating that radiative cascade from C to B is not the only production mechanism for the B state. Evidently, the most important production process for the B state is direct excitation by electron impact with the ground state of N_2 or with the $N_2(A^3\Sigma_u^+)$ state.

Several important observations have resulted from this work which bear on the production of a long pulse laser based on the second positive system of N_2. From our observations of the fluorescence from various vibrational levels of the N_2(C and B) states, it is evident that the electric discharge excitation produces significantly more vibrational excitation than the high energy electron beam, at least for the conditions of the present investigation. Significant vibrational excitation is undesirable both from the standpoint of efficiency and because we are trying to achieve an inversion based on a high electronic temperature and a low vibrational temperature. Thus it appears that a high energy electron beam may be a more effective means of producing a large excited electronic state population without significant vibrational excitation. However, it should be pointed out that the vibrational fluorescence measurements were carried out with gas mixtures having a large fraction of N_2 (approximately 16 to 20 percent). The applied electric field was limited to a low value of arc breakdown for the pulse duration used, and led to a low electron temperature. By reducing the N_2 fraction,

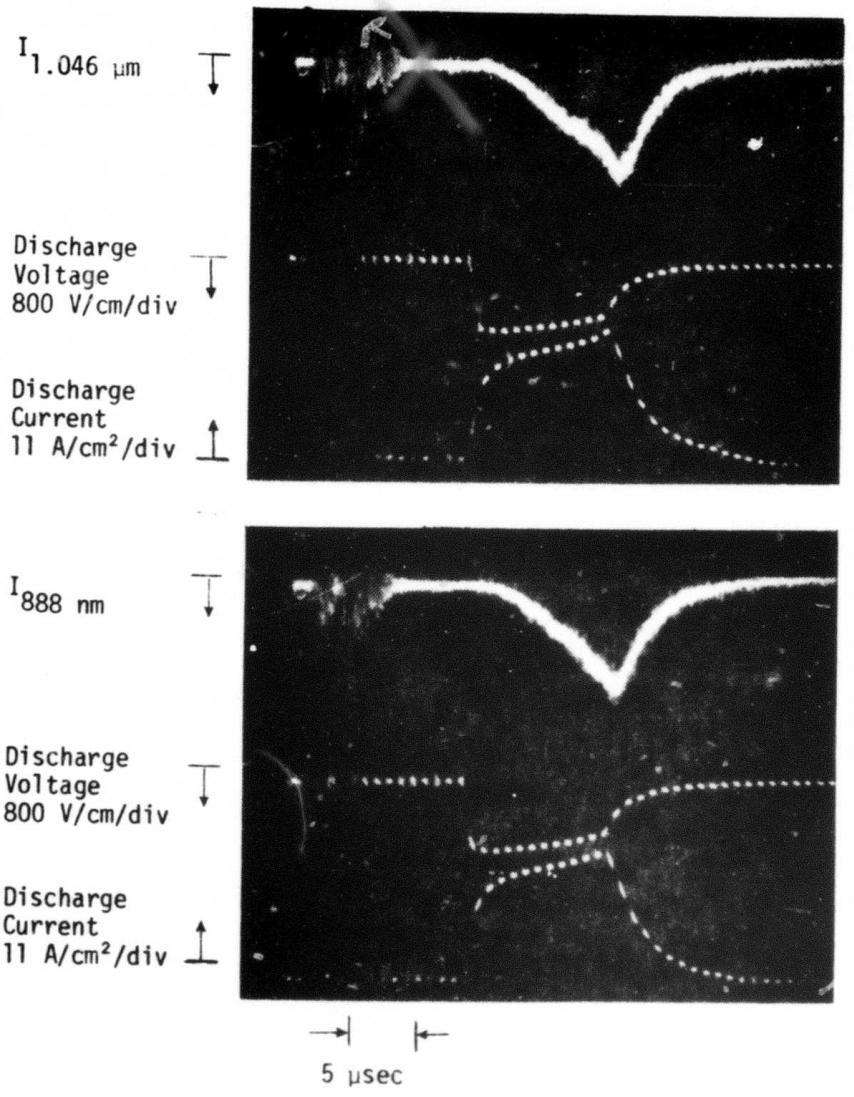

Figure 55. Fluorescence Emission from the v = 0 and v = 1 Levels of the $B^3\pi_g$ State in a 5:1 Ar/N_2 Mixture at 200 Torr. The upper oscillogram shows the (0,0) band and the lower oscillogram shows the (1,0) band of the N_2 first positive system.

decreasing the pulse duration, and raising the applied voltage, it should be possible to put a much larger fraction of the energy into electronic excitation in the electric discharge case.

In light of the large production rate of the $N_2(C^3\pi_u)$ v = 1 level observed in the case of electric discharge excitation, the (1,3) band of the nitrogen second positive system becomes an attractive candidate for a long pulse visible laser. In a 97:3 Ar/N_2 mixture at atmospheric pressure, the v = 3 level of the $N_2(B^3\pi_g)$ state would be collisionally deactivated much more rapidly than the (1, 3) and (0,3) radiative lifetimes for the C → B transition. In addition, the transition probability for the (1, 3) band of the second positive system is approximately 0.4 of the transition probability for the (0, 0) band and thus the population inversion density for the (1, 3) band only needs to be a factor of 2.5 greater than for the (0, 0) band in order to have the same gain. However, radiative trapping of the (0, 0) and (0, 1) bands of the second positive system may be needed to avoid serious radiative losses from the v = 0 level of the C state.

3.4. Laser Cavity Studies

A high-Q optical cavity was used with the 50-cm path, 5-tube plasma diode e-beam stabilized electric discharge facility (Appendix A) to investigate the possibility of long pulse laser emission from the nitrogen $C^3\pi_u \rightarrow B^3\pi_g$ transition. The optical cavity consisted of dielectric coated mirrors having a 2-meter radius of curvature and spaced 1 meter apart. The mirrors were mounted internally in order to reduce the transmission losses associated with Brewster angle windows. The mirror

coating has maximum reflectivity at 337 nm and provides a reflectivity greater than 99 percent over the range from 315 nm to 355 nm. This range includes the (0, 0) and (0, 1) bands of the nitrogen second positive system, which have wavelengths of 337.0 and 357.6 nm, respectively.

In addition to searching for lasing on the C → B (0, 0) and (0, 1) bands, we monitored the fluorescence from the (0,2) and (0,3) bands at 380.4 and 405.8 nm, respectively. Both 5:1 and 10:1 Ar/N_2 mixtures at 400 torr total pressure were investigated. Discharge currents of 22 A/cm^2 and values of E/N equal to 1.5 and 0.9 x 10^{-16} V-cm^2, respectively, were achieved for time durations of 2 to 3 μsec for the 5:1 and 10:1 Ar/N_2 mixtures. These values of E/N represent the maximum discharge voltage that could be applied to the gas without incurring an arc during the pumping phase. However, little or no contribution to the C state emission was produced by the discharge.

In order for the discharge to contribute to the nitrogen C state fluorescence it was necessary to either reduce the N_2 concentration or add small amounts of SF_6. When the N_2 concentration was reduced to approximately 3 percent, the nitrogen second positive emission produced by the discharge became more intense than that produced by the e-beam. This effect was observed at 400 torr total pressure with a discharge current density of 22 A/cm^2 and an E/N = 0.6 x 10^{-16} V-cm^2. The addition of approximately 0.1 percent SF_6 to the 5:1 Ar/N_2 mixture permitted a higher value of E/N, 2 x 10^{-16} V-cm^2, to be applied, which appreciably enhanced the C state emission produced by the discharge, even though the discharge current decreased by an order of magnitude. The enhancement of the nitrogen second positive emission when small concentrations of SF_6 are added to

the gas mixture was discussed in Section 3.3 for long duration pulses (10 μsec). The fluorescence emission pulse shape observed under these conditions (2 μsec discharge pulse length and low N_2 concentration or addition of small concentrations of SF_6) followed the discharge current quite closely with no apparent contribution from the $N_2(A)$ state pooling reaction and is most likely produced by direct electron impact with ground state N_2 or by excitation transfer from excited Ar. This behavior is in contrast to that previously observed with longer discharge pulses and higher N_2 concentrations; under these conditions, self-collisions of metastable $N_2(A)$ to produce $N_2(C)$ contributed significantly to the observed emission (as noted previously in Section 3.3).

Cavity tests were also conducted at a total pressure of 700 torr for both Ar/N_2 and $Ar/N_2/SF_6$ mixtures. At this pressure, the $N_2(B)$ state is collisionally deactivated by Ar in a time that is less than the $N_2(C)$ state radiative lifetime (Ref. 35), thus satisfying one of the conditions for a long pulse laser. However, the time history of the fluorescence emission was similar to that observed at 400 torr total pressure and no laser emission was observed.

Cavity measurements were also conducted with dielectric coated mirrors covering the range from 3500 Å - 3800 Å. This range includes the $C \rightarrow B(0, 1)$, (0, 2), and (1, 3) bands. Mixtures containing $He/N_2/SF_6$ and $Ar/N_2/SF_6$ at a total pressure of 200 torr were employed, using a discharge current density of about 1 amp/cm^2 and a pulse duration of 4 μsec. The composition of the mixtures tried and the maximum E/N achieved without arcing are listed below:

Composition	Maximum E/N($\times 10^{16}$ V-cm^2)
69.9% He/30% N_2/0.1% SF_6	3.0
89.9% He/10% N_2/0.1% SF_6	1.7
89.9% Ar/10% N_2/0.1% SF_6	1.7
94.9% Ar/5% N_2/0.1% SF_6	1.4

No laser emission was detected for any of these mixtures.

SECTION IV

CONCLUSIONS AND RECOMMENDATIONS

4.1. HF and DF Electric Discharge Lasers

The experimental studies carried out under this contract have demonstrated that laser emission can be produced from HF and DF by means of the partial inversion generated in a high current electron-beam-stabilized electric discharge. The usefulness of vibrational transfer from H_2 to HF and D_2 to DF was demonstrated, and the addition of N_2 to HF mixtures was seen to be beneficial. The laser output efficiency from HF and DF mixtures was unexpectedly low, less than 0.1 percent; the electron attachment loss to HF and DF was significant. This, combined with the current density limit of the electron beam equipment, prevented the simultaneous use of a high concentration of HF or DF and high electric discharge power input.

The computer model for electric discharge power partitioning in Ar/H_2 mixtures indicated that up to 65 percent of the power can be put into H_2 vibration, with the balance going into heat and rotation of H_2. The vibrational kinetics model of H_2/HF mixtures, based on presently available V-V and V-T rates, predicts a potential laser output efficiency of the order of 10 percent. The large discrepancy between the experimental and theoretical values of efficiency indicates that the molecular kinetics model is not yet correct. Portions of the

model that may require revision are the V-V rate matrix, the treatment of HF and H_2 rotation, the inclusion of direct electron impact excitation of the various vibrational levels of HF, and the determination of the effects of superelastic electron impact collisions.

To achieve high output from HF and DF electric discharge lasers, it is clear that a very high electron beam current density is needed. As yet the molecular kinetics are not sufficiently well understood, particularly for D_2/DF gas mixtures. Further experimental study, especially on the DF system, is recommended to evaluate and improve the kinetic model and to determine the laser performance at high e-beam current.

4.2. Molecular Electronic State Lasers

A feasible collisional mechanism has been formulated as a basis for efficient, long pulse visible lasers operating on excited electronic states of diatomic molecules. Experimental studies of electron-beam-stabilized electric discharge excitation of N_2 showed two major difficulties; considerable vibrational excitation attendant with electronic excitation, and arc breakdown restrictions on the E/N that could be sustained. It is concluded that visible lasers to be operated on high electronic states may be more amenable to excitation from above (e.g., by electron-ion recombination during e-beam ionization) rather than from below by electron impact excitation. In order to develop efficient collisional lasers on molecular electronic states excited by e-beam stabilized electric discharges, it will be necessary to utilize

molecules with suitable low-lying electronic states. Since much of the basic kinetic data required to evaluate possible molecular systems is not currently available, it is recommended that further experimental studies be instrumented to provide direct measurements of the absolute populations of the individual vibrational levels of upper and lower electronic states.

APPENDIX A

E-BEAM STABILIZED ELECTRIC DISCHARGE FACILITIES

A.1. Thermionic Cathode Electron Gun

The thermionic cathode electron gun is the first of three electron gun facilities used during this contract for the study of HF and DF electric discharge lasers. The electron gun and electrical equipment was furnished by Physics International, and is described in detail in Reference 7. This grid pulsed device was operated at 130 to 150 kV and an e-beam current density of 1 to 5 ma/cm^2 through a 0.025 mm aluminum foil for a pulse duration of 10 to 30 μsec. The electron beam covers an area of only 10 cm by 10 cm.

The electric discharge and optical arrangement used with this electron gun are shown in Figure A-1. This configuration was used for exploratory studies of HF emission and was the device in which repetitive pulses were observed during electric discharge excitation of N_2 and H_2 containing small amounts of HF.

A.2. Five-Tube Plasma Diode Electron Gun

This facility was developed initially at MSNW because of the need for a higher electron beam current density than the thermionic gun could produce, and a longer optical path length to achieve laser threshold conditions in electrically excited HF and DF gas mixtures. The device is described in more detail in References 45 and 46.

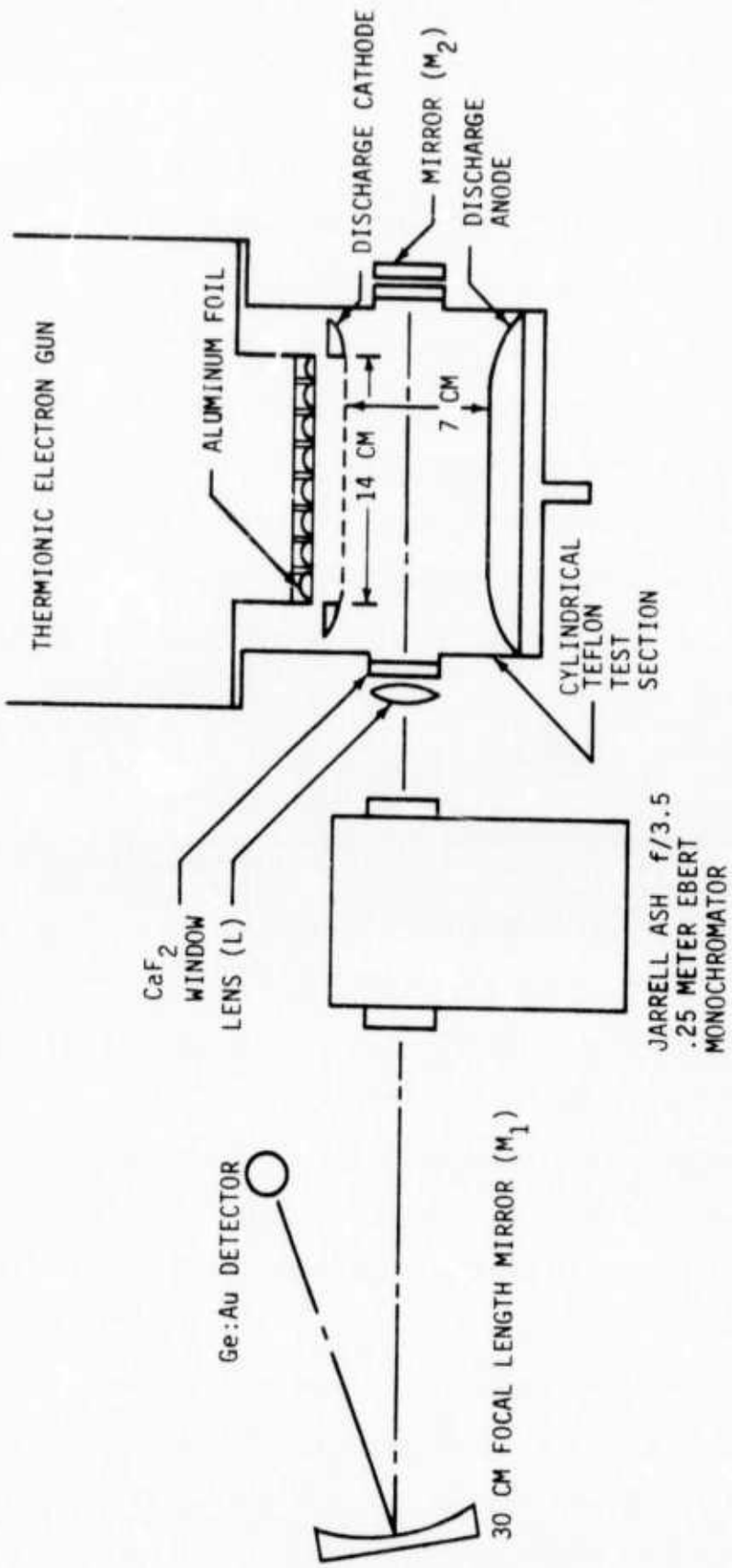

Figure A-1. Thermionic Cathode Electron Gun and 0.7 Liter Teflon Discharge Chamber Used for Initial Fluorescence Studies in HF and N_2 and H_2

The electron gun used for this purpose is a plasma diode; a low pressure, high voltage glow discharge of the type that has been described recently by O'Brien (Ref. 47). The configuration used here is shown schematically in Figure A-2. Each 7.6-cm inside diameter glass envelope was fitted with a solid, polished aluminum cathode and a 60 percent transmitting anode screen. A 1.25-cm radius of curvature edge on the cathode was used to reduce field concentrations and minimize glow-to-arc transition at high voltage. After evacuating and outgassing the diode, helium at pressures of 50 to 100 microns was admitted. A stable, high voltage glow discharge was produced in the tube which provided an internal electron beam current density of up to 0.5 amps/cm^2 at a voltage up to 125 kV.

It was found that a conditioning process was required to eliminate glow to arc transition in the plasma diode tube during pulsed operation at high voltage. Starting at low pressure (less than 50 μ of helium), the voltage and pressure were gradually raised until a glow discharge could be obtained reliably without arcing. Several hundred pulses were required to eliminate glow to arc transition at high voltage. Once conditioned, the plasma diode ran in the glow discharge mode with excellent repeatability in its operating characteristics.

Typical performance of a single plasma diode tube is shown in Figures A-3 and A-4. The maximum diode voltage was 125 kV without

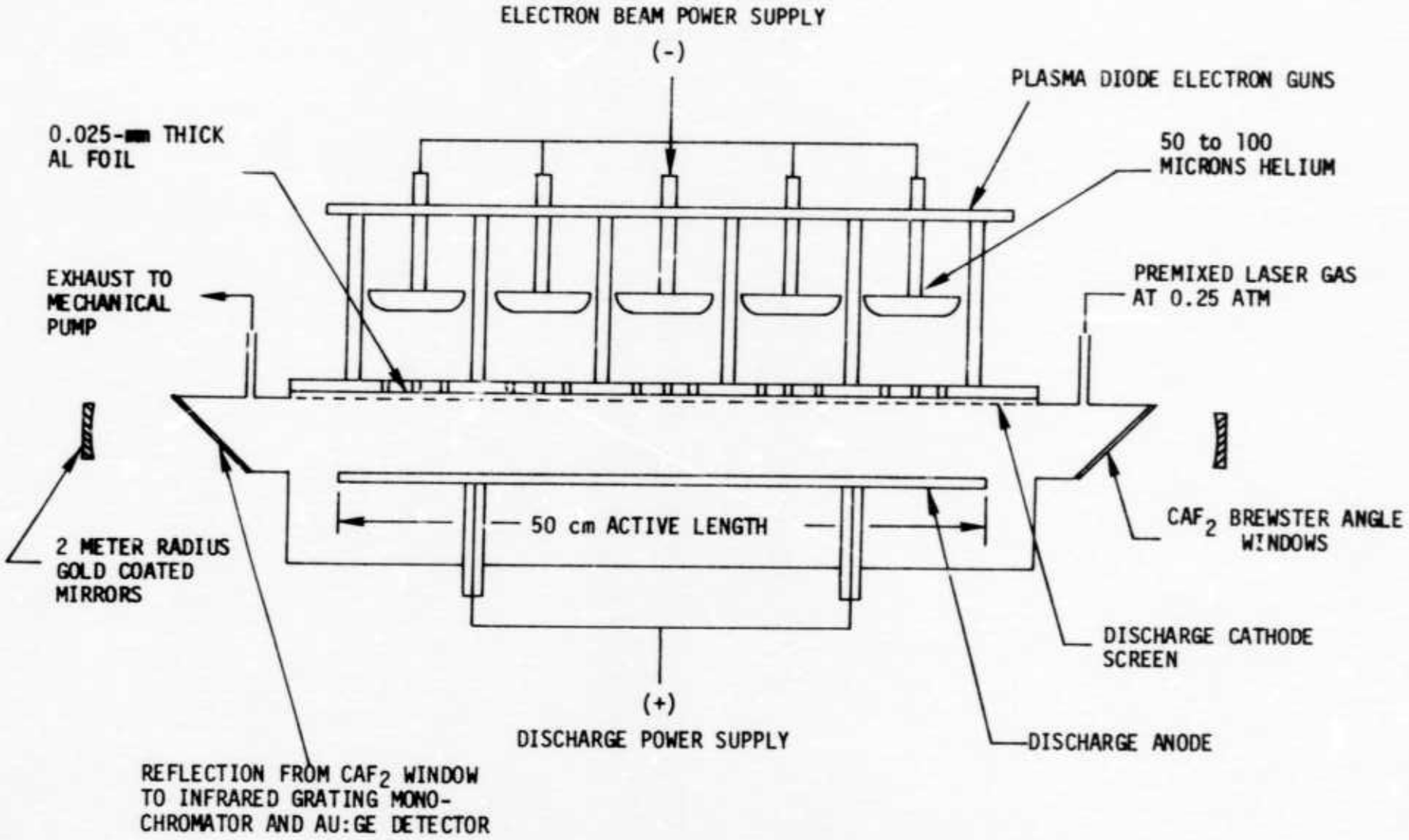

Figure A-2. Schematic of Five Tube Plasma Diode Electron-Beam-Stabilized Electric Discharge Cell and Laser Cavity. The anode-cathode spacing in the laser discharge cavity was 2.5 cm.

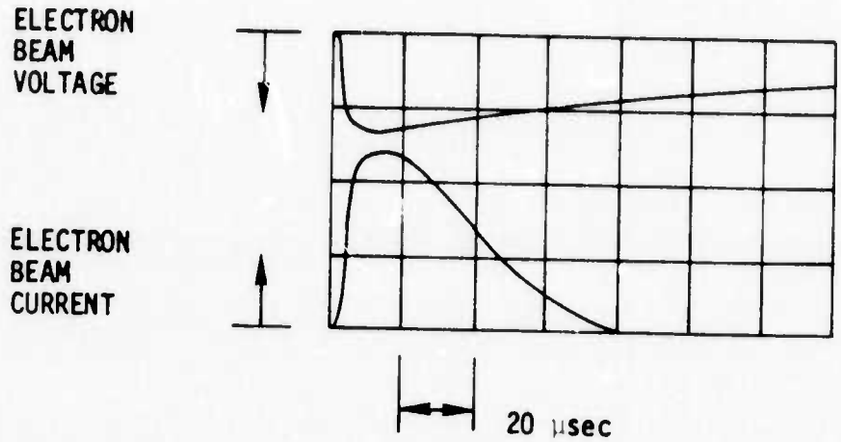

Figure A-3. Typical Electron Beam Voltage and Current Versus Time; Peak Electron Beam Voltage 110 kV; Peak Electron Beam Current Density 100 ma/cm^2 Measured 2 cm from the 0.012-mm Thick Titanium Foil; Helium Pressure was 95 Microns.

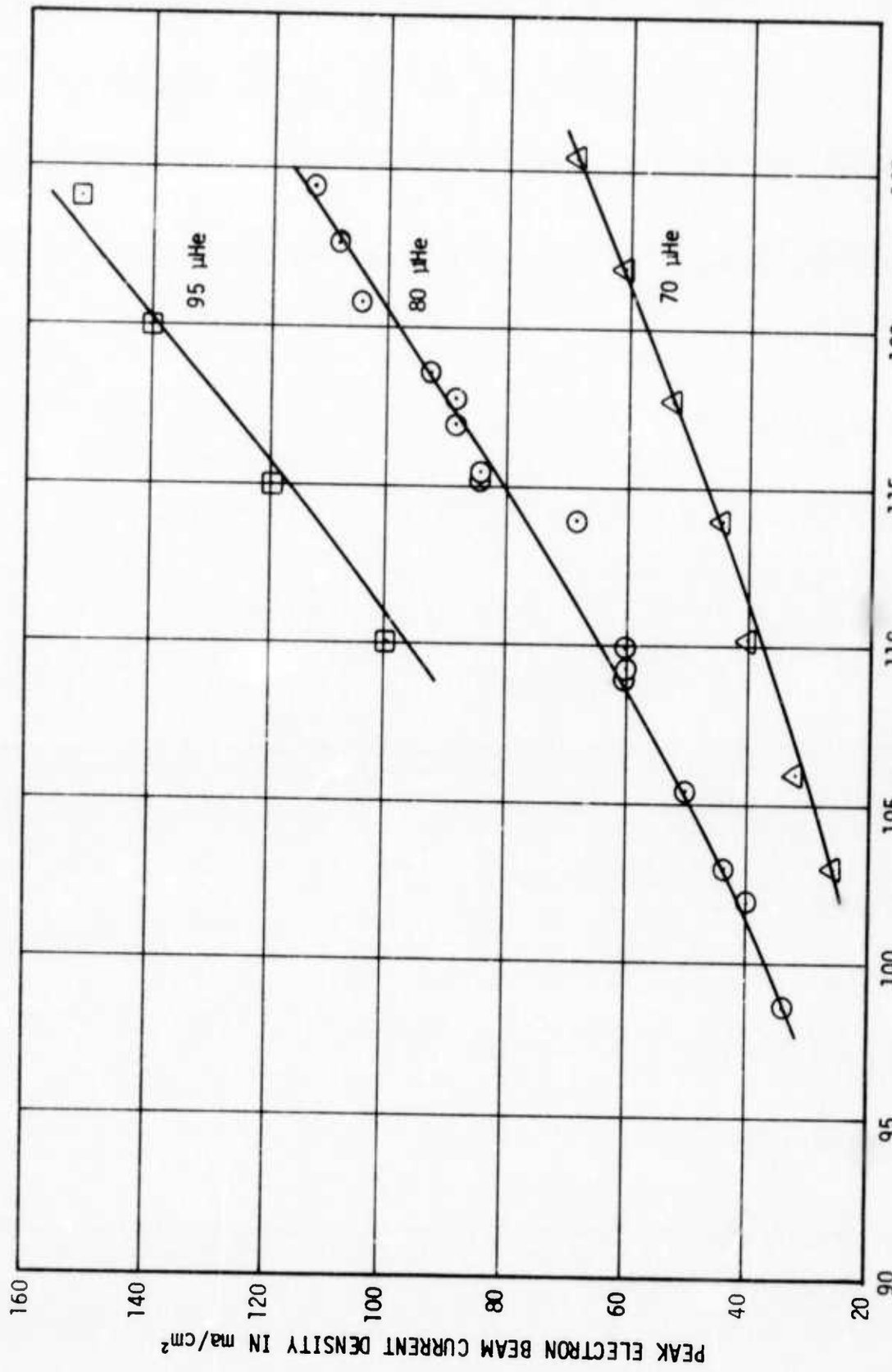

Figure A-4. Peak Electron Beam Current Density at a Distance 2 cm from a 0.012-mm Thick Titanium Foil

arcing. The maximum current density through a 0.0012-cm titanium foil at the center of the diode was 150 ma/cm^2. The diode was generally operated under conditions which provided an average current density of 25 to 50 ma/cm^2 for a time interval of about 30 μsec.

The successful operation of the single plasma diode electron gun as part of the MSNW IR&D Program led to the design and construction of a 5- x 50-cm apparatus utilizing the plasma diode electron beam to stabilize the electrical discharge. The most expeditious approach to building the larger system was to use the unit already developed as a module and place five cylindrical units side-by-side on a common base (Figure A-2). This led to a minimum development time before proceeding with our laser objectives. However, with this geometry, a certain amount of beam nonuniformity had to be accepted.

Electron beam current density measurements were made to ascertain the severity of the problem with a five element (1 cm^2 each) Faraday cup array at several vertical positions below the discharge screen cathode. The Faraday cup array could also be moved horizontally along the 50-cm path inside the discharge chamber. The discharge chamber was filled with 90 torr of SF_6 for these experiments. SF_6 has a large electron attachment capability and captures unwanted secondary electrons. In the presence of SF_6 low energy electrons produced in the discharge chamber therefore have a minimum effect on the Faraday cup measurement of high energy electrons.

Figure A-5 shows centerline electron beam current density versus distance along the 50-cm horizontal path. The vertical position, 2.3 cm below the discharge cathode screen, is the approximate normal location of the 5-cm x 50-cm discharge anode. Raising the Faraday cup until it is 1.3 cm from the discharge screen increases the peak current density by 40% with little effect on the minimum current density measured between the diode tubes. The large nonuniformities in the electron beam current density profile shown here limit the laser performance that can be achieved, and also cloud the interpretation of the absorption measurements used to obtain information on the excited state populations. A uniform plasma diode gun, 50 cm long, was therefore constructed.

A.3. Ceramic Plasma Diode Electron Gun

To provide a uniform plasma diode electron gun over a 50-cm path, a single piece of cast alumina was used as the plasma diode chamber instead of five glass tubes. The alumina ceramic is 2.5 cm thick to support the vacuum, and is 50 cm long, 10 cm wide, and 25 cm high. The ends of the vessel are rounded using a 5-cm radius. An aluminum cathode was machined to fit inside the alumina chamber with a 1-mm gap. It was spaced 12 cm from a 70 percent transmission stainless steel anode screen. Just as with the five-tube plasma diode, a low flow of high purity helium was passed through the ceramic chamber to reduce the problem of impurities which could cause undesirable glow to arc transition at high voltage. The overall configuration of the electron gun and discharge chamber are shown in Figure A-6.

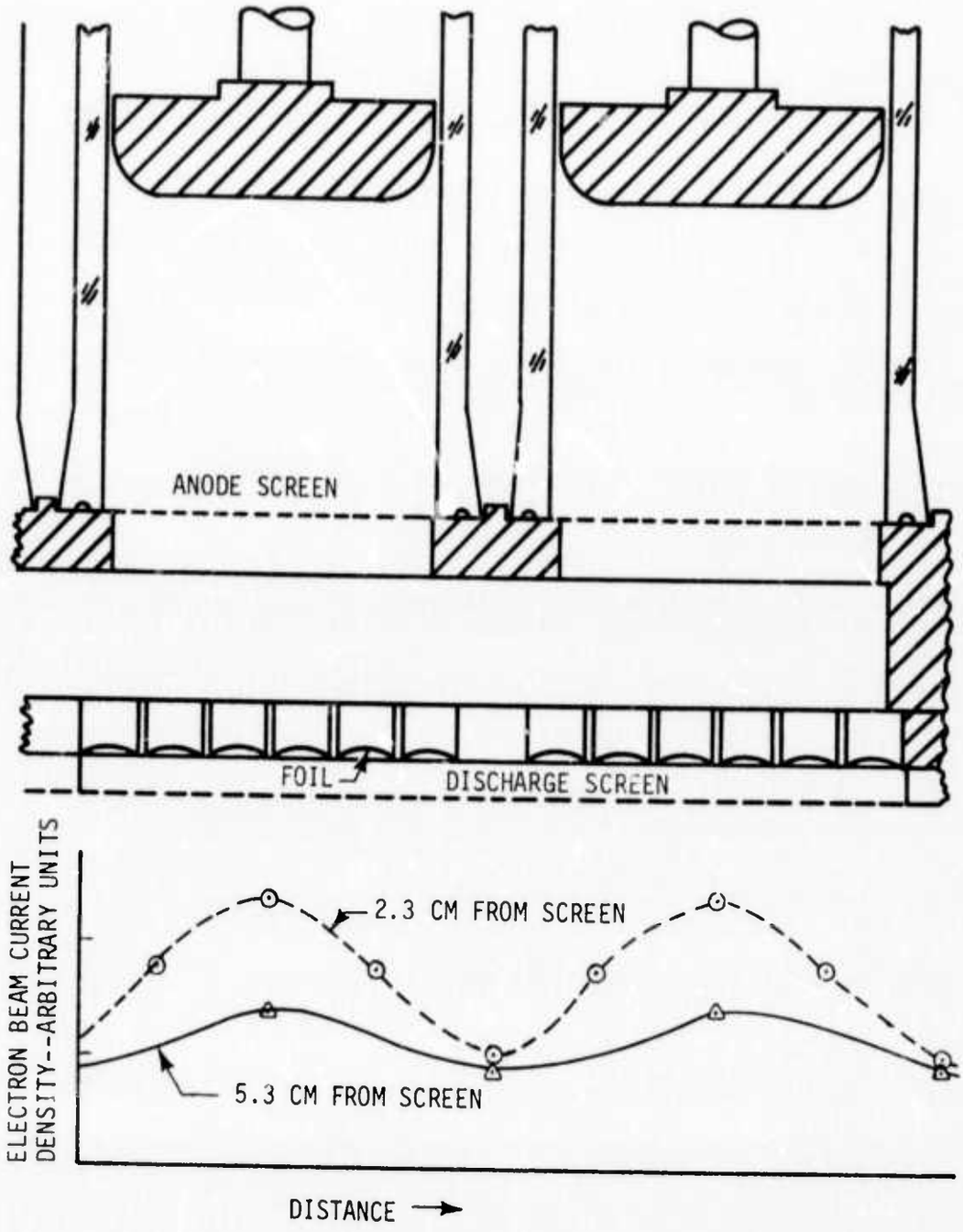

Figure A-5. Electron Beam Nonuniformities Measured Below the Foil and Screen of the 5-Tube Plasma Diode Electron Gun

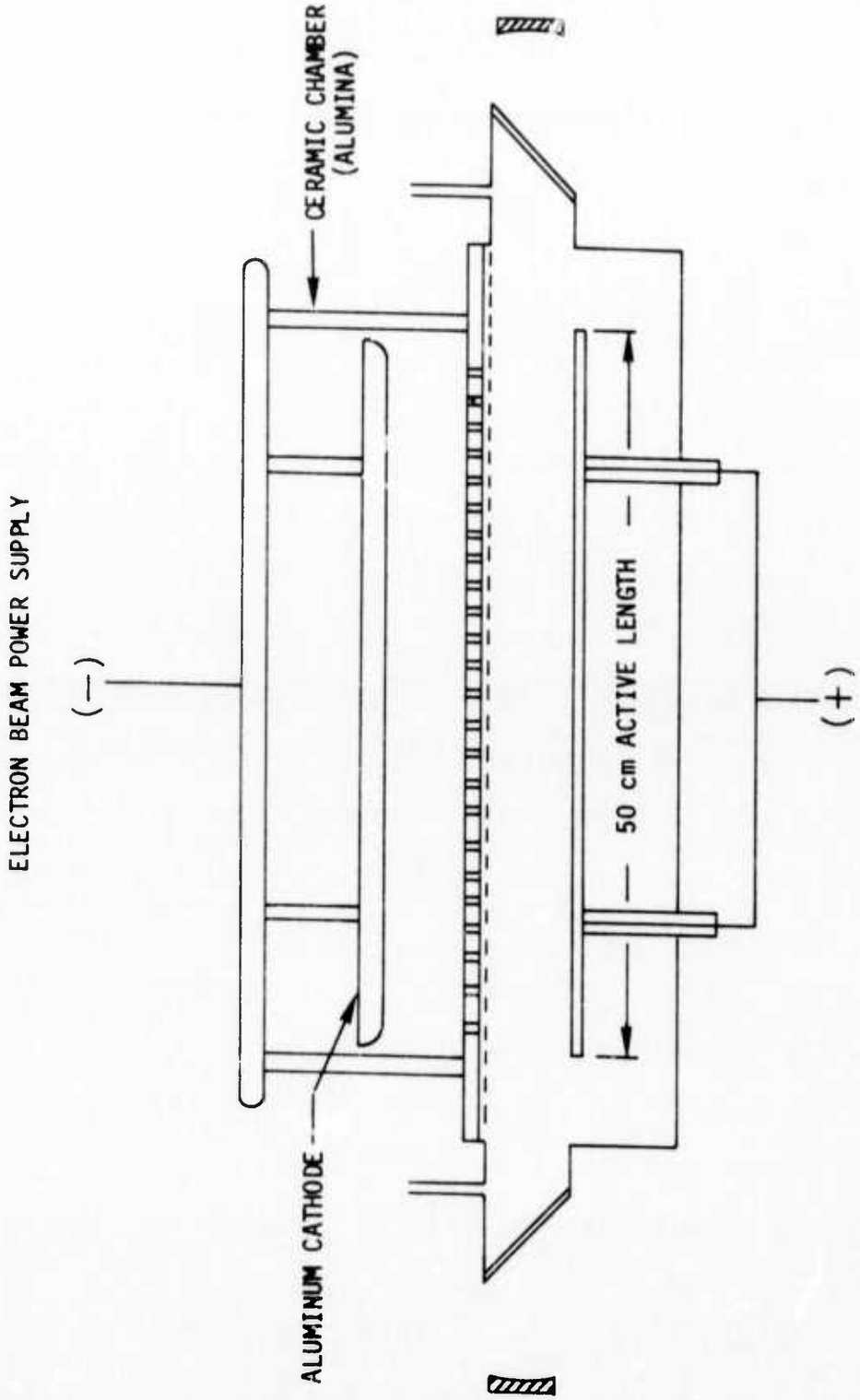

Figure A-6. Schematic of Single Electrode Ceramic Plasma Diode and Electric Discharge Cell

Conditioning the continuous electrode plasma diode was more difficult than with the five-tube diode. With essentially the same Marx bank and other electrical components used for both devices, aluminum vapor during an arc would deposit as a spot on the alumina insulator near the cathode. Once this spot had developed, glow to arc transition occurred repeatedly with this point as a nucleus. This pattern continued until the apparatus was disassembled and cleaned.

Because of the glow to arc transition problems, it was decided to limit operation of the ceramic diode below 120 kV as a precautionary measure. This resulted in a lower average electron beam current density through the 0.025 mm foil, about 30 ma/cm^2 compared to a typical figure of 50 ma/cm^2 for the five-tube diode. A typical oscillogram is shown in Figure A-7. Fifteen percent of the current delivered to the diode appears through the foil with the probe 1.5 cm away. This e-beam current was collected with an aluminum plate having the same area (480 cm^2) as the foil.

The main purpose in the design and construction of the single cathode ceramic body plasma diode was to achieve a uniform profile of electron beam current density along the 50-cm dimension of the cell. Profile measurements were taken 1.5 cm away from the foil in air using an array of graphite Faraday cups which had an area of 0.5 cm^2 and were spaced 2 cm apart. The longitudinal profiles were flat within a few percent throughout the 48 cm length until a point about 2 cm from the end of the foil where the current density began to fall toward zero. The window support structure would cause some electron scattering

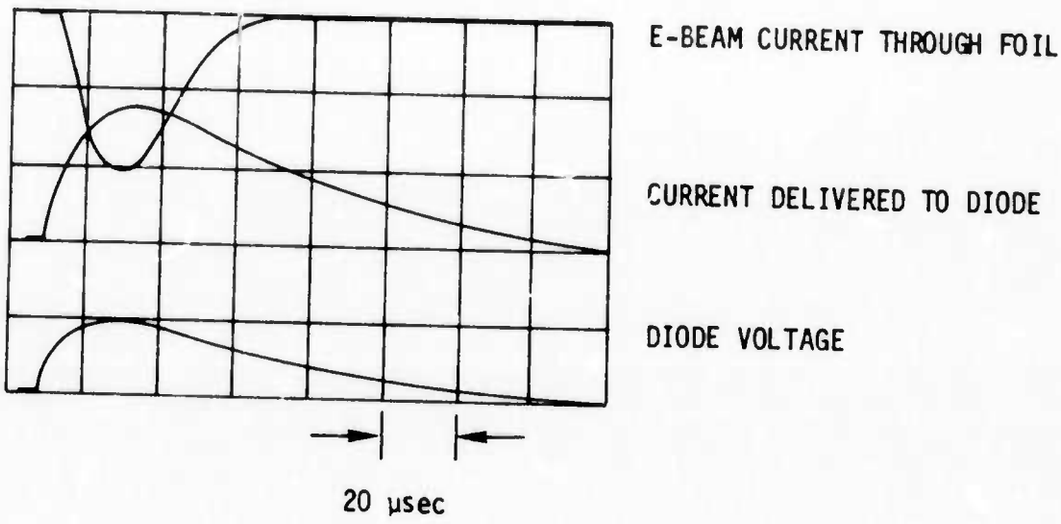

Figure A-7. Oscilloscope Trace Showing Ceramic Plasma Diode Performance. Trace Sensitivities are as Follows. The E-Beam Current Through the 0.025-mm Aluminum Foil is 5 A/Div and the Total Current to the Diode is 35.5 A/Div. Diode Voltage Sensitivity is 110 kV/Div. Foil Area is 480 cm^2.

since it was a ladder structure with ribs 1.8 mm thick and spaced 1.25 cm apart. This uniform longitudinal profile about 46 cm long was considered to be satisfactory for kinetic modeling. A transverse profile scan is shown in Figure A-8. The width of the anode used in the laser discharge cell was 5 cm, and the optical diameter was 2.5 cm which fall within the region of relatively uniform e-beam current density.

Measurements were taken of the current density falloff with distance from the foil in air at one atmosphere pressure, and are shown in Figure A-9. The foil and the high density air cause a comparable scattering half angle, about 1/2 radian at 120 kV. In laser experiments the distance between the anode and the cathode in the discharge chamber was 2.5 cm and the gas mixture was predominantly argon at 1/4 atmosphere. These factors yield satisfactory uniformity in the e-beam current density throughout the volume covered by the 2.5-cm diameter optics.

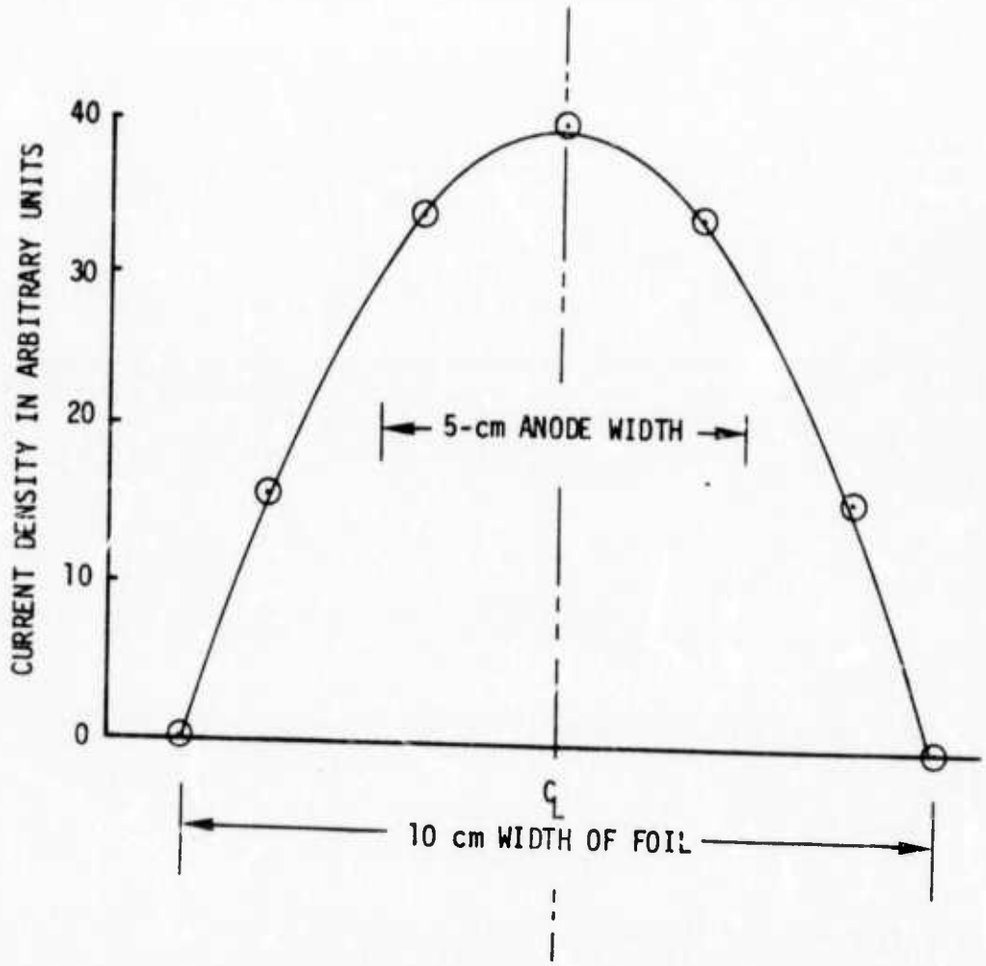

Figure A-8. Transverse Current Density Profile in Ceramic Plasma Diode Electron Gun

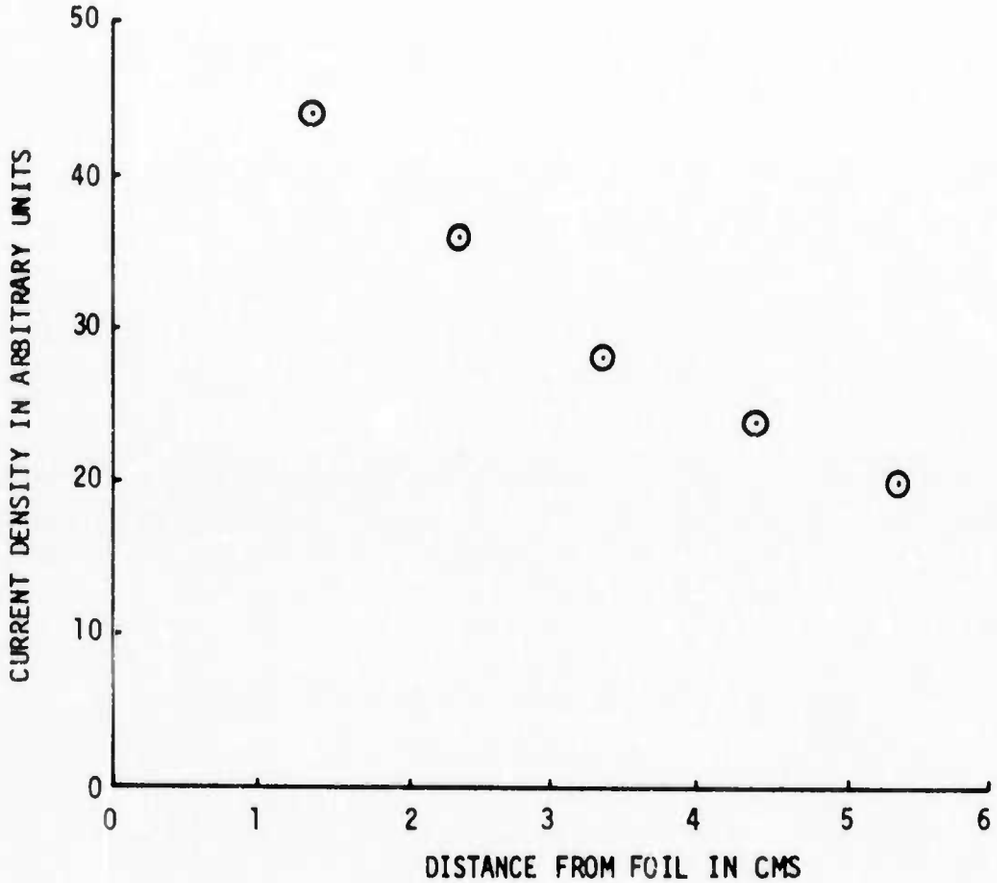

Figure A-9. Current Density Profile in Air Versus Distance from the Foil

REFERENCES

1. C. A. Fenstermacher, M. Nutter, W. Leland, and K. Boyer, Appl. Phys. Lett. 20, 56(1972).

2. J. D. Daugherty, E. R. Pugh, and D. H. Douglas-Hamilton, Bull. Amer. Phys. Soc. 17, 399 (1972).

3. M. M. Mann, W. B. Lacina, and M. L. Bhaumik, IEEE J. Quant. Elect. 8, 617(1972).

4. K. L. Kompa, J. H. Parker, and G. C. Pimentel, J. Chem. Phys. 49, 1257 (1968).

5. J. H. Parker and G. C. Pimentel, J. Chem. Phys. 51, 91 (1969).

6. S. R. Byron, L. Y. Nelson, and G. J. Mullaney, Appl. Phys. Lett. 23, 10 (1973).

7. S. R. Byron, et al., Semi-Annual Technical Report No. 1, Electron Beam Molecular Lasers, MSNW Report No. 72-105-1, November 1972.

8. L. Y. Nelson, G. J. Mullaney, and S. R. Byron, Appl. Phys. Lett. 22, 2, 15 January 1973.

9. R. E. Center and G. E. Caledonia, Appl. Phys. Lett. 19, 211 (1971); G. E. Caledonia and R. E. Center, J. Chem. Phys. 55, 552 (1971).

10. M. L. Bhaumik, W. B. Lacina, and M. Mann, IEEE J. Quant. Electron, QE-6, 576 (1970).

11. R. C. Millikan and D. R. White, J. Chem. Phys. 39, 3209 (1963).

12. J. Bott, J. Chem. Phys. 57, 96 (1972).

13. J. H. Hinchen, United Aircraft Report UAR-L127, July 1972.

14. H. L. Chen and C. B. Moore, J. Chem. Phys. 54, 4072 (1971).

15. P. F. Zittel and C. B. Moore, "V-T, R and V-V Relaxation in DCl Systems," to be published in J. Chem. Phys.

16. F. Linder and H. Schmidt, Zeitschrift fur Naturforschung, Band 26a, Heft 10, 1064 (1971).

17. G. J. Schulz, Phys. Rev. A135, 988 (1964).

18. H. S. W. Massey, Electronic and Ionic Impact Phenomena, Vol. II (Oxford University Press, Clarendon, 1969), p. 888.

19. H. S. W. Massey, loc. cit. p. 1063.

20. A. G. Englehardt and A. V. Phelps, Phys. Rev. 133, A375 (1964).

21. A. G. Englehardt and A. V. Phelps, Phys. Rev. 131, 2115 (1963).

22. R. M. Osgood, Jr., P. B. Sackett, and A. Javan, J. Chem. Phys. 60, 1468 (1974).

23. J. K. Hancock and W. H. Green, J. Chem. Phys. 57, 4515 (1972).

24. M. A. Kovacs and M. E. Mack, Appl. Phys. Lett. 20, 487 (1972).

25. J. L. Stewart and E. S. Stewart, J. Acoust. Soc. Amer. 24, 199 (1952).

26. R. E. Meredith and F. G. Smith, Investigations of Fundamental Laser Processes, Vol. II, Willow Run Laboratories, 84130-39-T(11), (1971).

27. R. J. Lovell and W. F. Herget, J. Opt. Soc. Am. 52, 1374 (1962).

28. D. F. Smith, Molecular Properties of Hydrogen Fluoride, 2nd U. N. Geneva Conference, Pergammon Press, London.

29. B. Oksengorn, Spectrochimica Acta, Vol. 19, 541 (1963).

30. V. Bondybey, P. K. Pearson and H. F. Schaefer III, J. Chem. Phys. 57, 1123 (1972).

31. R. E. Center and Hao-Lin Chen, J. Chem. Phys. 61, 3785 (1974).

32. S. N. Suchard, Appl. Phys. Lett. 23, 68 (1973).

33. M. C. Lin and W. H. Green, J. Chem. Phys. 53, 3383 (1970).

34. J. W. Dreyer and D. Perner, J. Chem. Phys. 58, 1195 (1973).

35. R. A. Young, G. Black and T. G. Slanger, J. Chem. Phys. 50, 303 (1969).

36. P. Millet, Y. Salamero, H. Brunet, J. Galy, D. Blanc, and J. L. Teyssier, J. Chem. Phys. 58, 5839 (1973).

37. J. W. Dreyer and D. Perner, Chem. Phys. Lett. 16, 169 (1972).

38. F. J. Comes and E. H. Fink, Z. Naturforsch. 28a, 717 (1973).

39. E. H. Fink and F. J. Comes, Chem. Phys. Lett. 25, 190(1974).

40. G. H. Dieke and T. M. Donahue, Phys. Rev. 81, 248 (1951).

41. D. H. Douglas-Hamilton and S. A. Mani, Appl. Phys. Lett. 23, 508 (1973).

42. J. LeCalvé and M. Bourène, J. Chem. Phys. 58, 1446 (1973).

43. G. N. Hays and H. J. Oskam, J. Chem. Phys. 59, 6088 (1973).

44. D. W. Setser, D. H. Stedman, and J. A. Coxon, J. Chem. Phys. 53, 1004 (1970).

45. S. R. Byron, et al., Semi-Annual Technical Report No. 2, Molecular Lasers in E-Beam Stabilized Discharges, MSNW Report No. 74-105-2, August 1973.

46. S. R. Byron, et al., Semi-Annual Technical Report No. 3, Molecular Lasers in E-Beam Stabilized Discharges, MSNW Report No. 74-105-3, June 1974.

47. B. B. O'Brien, Jr , Appl. Phys. Lett. 22, 503 (1973).